PREDICTING HORIZONTAL PRESSURE IN 2-STAGE MSE STRUCTURES

by

THOMAS PATRICK TAYLOR

Presented to the Faculty of the Graduate School of

The University of Texas at Arlington in Partial Fulfillment

of the Requirements

for the Degree of

MASTER OF SCIENCE IN CIVIL ENGINEERING

THE UNIVERSITY OF TEXAS AT ARLINGTON

May 2015

ACKNOWLEDGEMENTS

ABSTRACT

PREDICTING HORIZONTAL PRESSURE IN 2-STAGE MSE STRUCTURES

Thomas P Taylor, M.S.

The University of Texas at Arlington, 2015

Supervising Professor: Anand J. Puppala

Mechanically Stabilized Earth (MSE) structures have been successfully used in the United States as embankment support structures for heavy highway transportation projects since 1972. On project sites that have poor foundations and where large settlements are predicated a variation of MSE called 2-Stage MSE is utilized. As the name suggests, 2-Stage structures are constructed in two stages. Stage-1 consists of constructing a flexible faced MSE structure and Stage-2 consists of attaching a veneer to the face of the Stage-1 structure. The Stage-1 and Stage-2 structures are separated by a short distance forming a cavity that is filled with granular material. The foundation may be improved before construction of the Stage-1 structure. After construction of the Stage-1 structure and before construction of the Stage-2 structure the foundation is allowed to consolidate.

The 2-Stage engineering process includes design and analysis of the foundation, the Stage-1 MSE and the Stage-2 Veneer including the connection element. The design of the connection element requires that the horizontal pressure in the cavity between the Stage-1 and Stage-2 structure be determined. There are no published standard specifications that outline how to determine the horizontal pressure in the

cavity for 2-Stage MSE structures. Designs of 2-Stage MSE have been known to use the theory of soil arching to predict the horizontal pressure in the cavity.

The main objective of this study is to predict the horizontal pressure in the cavity of the 2-Stage structure through numerical modelling. The study will first determine if soil arching is occurring in the cavity by construction of a base-line model of the Stage-1 and Stage-2 structure by assuming each facing are non-yielding rigid structures. The base-line model numerical results will be compared with the classic silo pressure equation. Parametric studies of the base-line model are conducted through varying the internal frictional angle of the cavity material and the interface friction angle of the facing. A final parametric a study is conducted by changing the Stage-1 facing into a yielding structure by prescribing internal settlement in the control model. The parametric study results are compared to the base-line model results to establish the effect the variation of the properties have on the magnitude of the horizontal pressure in the cavity.

Table of Contents

List of Figures

List of Tables

Chapter 1

Introduction

1.1   General

Mechanically Stabilized Earth (MSE) is a technology used to construct retaining walls and steep slopes (Anderson 2012, Collin 1986, NCHRP 1987, NHI 2009). MSE is a composite structure consisting of tensile resisting inclusions and compacted soil (Figure 1-1). MSE is considered a fill structure that uses the bottom up construction method. In this method the compacted backfill, soil reinforcing, and facing elements are placed in a repetitive manner that progresses from the foundation to the top of surcharge.

MSE that is used as commercial technology was invented by Henri Vidal in 1963 and was introduced in the United States by the Reinforced Earth Company (RECo) in 1971. The first commercial use of MSE technology in the Unites States was on a transportation project for the California Department of Transportation (Caltran) along Highway 39 in the San Gabriel Mountains (NCHRP 1987). For this project RECo used smooth steel strips that were mechanically attached to a segmental, elliptical, steel panel (SSP). The steel strips reinforced the soil while the SSP prevented the soil between the steel strips from eroding and raveling at the face of the structure. Since 1971 various competing proprietary MSE systems have been developed that utilize both steel and polymer soil reinforcing elements that are attached to concrete panels, steel panels, mesh panels and modular concrete block facings. It has been estimated that every Department of Transportation in the United States has constructed an MSE retaining wall (NHI 2009).
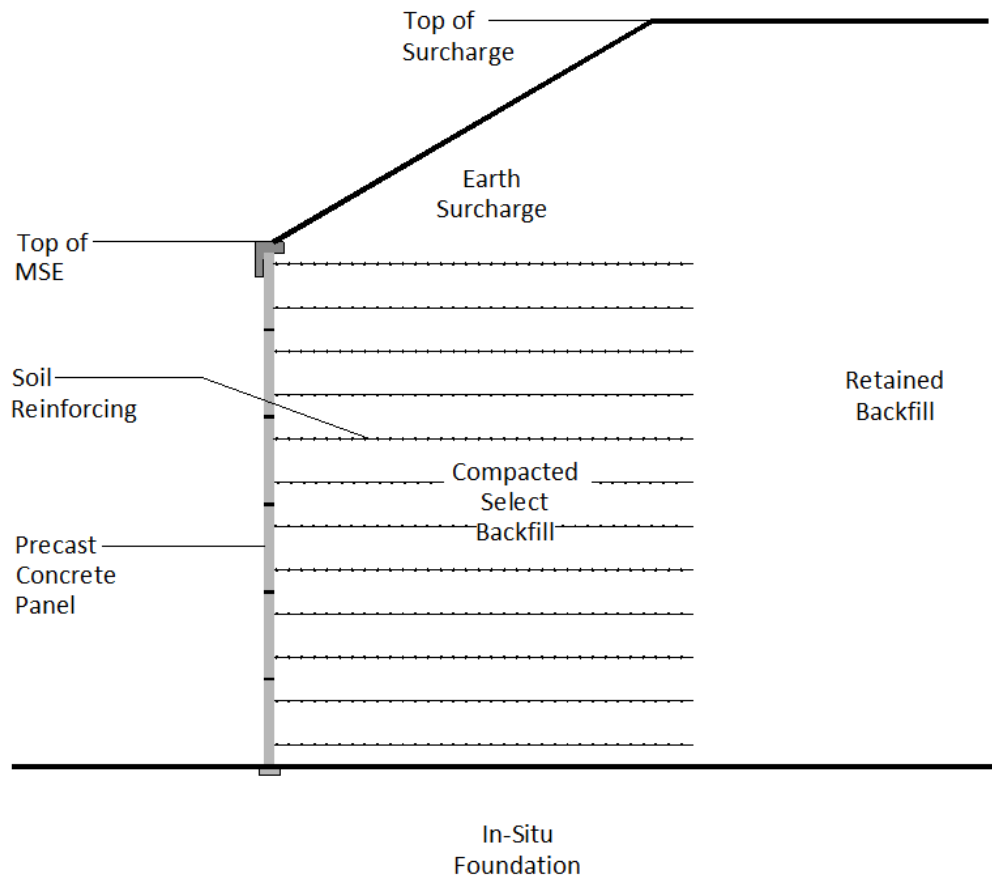
Figure 1-1 Typical MSE structure

Figure 1-2 First reinforced earth wall constructed in United States (NCHRP 1987)

When compared to the traditional cast-in-place (CIP) concrete retaining structure the MSE structure is a cost effective means of constructing retaining structures (Christopher 1990). MSE is now routinely used as the abutment approach ramp and as grade separations in most United State transportation structures. In the abutment application the MSE may, or may not, support the bridge superstructure (Anderson 2005). In either case the MSE typically will support a traffic live load.

By introducing a slight design modification the MSE can also be used in areas where there is limited space for the placement of the soil reinforcing, e.g. mountainous regions. Technology that is used in a confined space is called Shored MSE (Figure 1-3) (Morrison et.al. 2009).
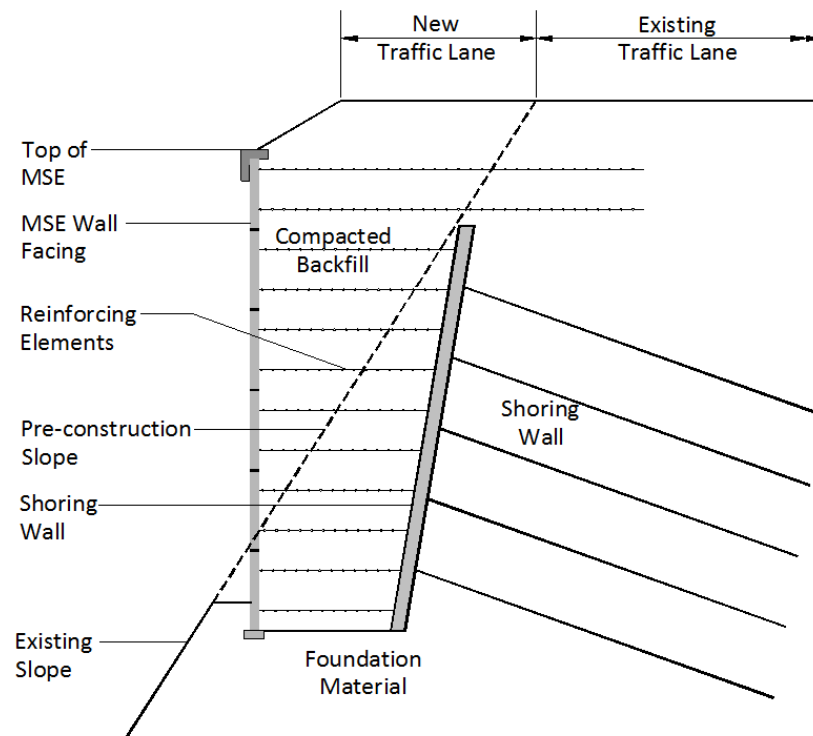
Figure 1-3 Typical shore MSE

MSE is considered to be a flexible structure that is capable of tolerating substantial differential settlement of the foundation soils that it is placed on (Collin 1986, Morrison 2009). Because of the flexibility of the structure MSE it is commonly used in areas where the foundation soils are of poor quality. This has led to the use of MSE as a preload structure that is then faced with a veneer (Bloomfield 2001). The technology that applies a veneer to the MSE structure is called a 2-Stage structure (Figure 1-4).
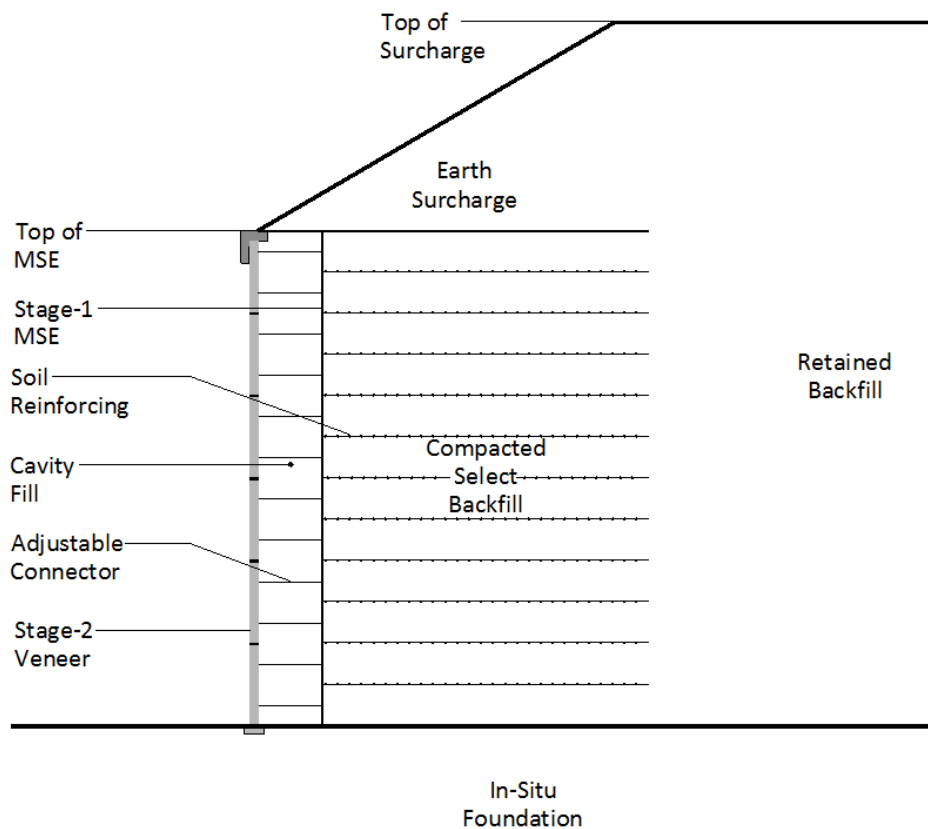
Figure 1-4 Typical 2-Stage MSE structure

The name, 2-Stage, is indicative of the construction sequence. In the 2-Stage application the MSE structure is constructed in Stage-1, the foundation is allowed to consolidate, than in Stage-2 the MSE structure is faced with an architectural veneer panel. The veneer facing is attached to the MSE facing using an adjustable connection

element (Crigler 1999, Taylor 2000, Timmons 2004, Taylor 2011, Taylor 2013). As described earlier, the MSE functions as both a preload structure and the final grade separation structure. Using the MSE as a preload structure decreases the time for settlement of the compressible foundation soils while facing the MSE with a veneer panel decreases the construction time associated with the project.

The lack of understanding of the 2-Stage MSE concept has led to several poor performing structures. Problems with these structures occur after the Veneer facing has been applied (Figure 1-5). These problems have been attributed to improper prediction of the time rate of foundation settlement, internal settlement of the MSE structure after placement of the Veneer Panel, and improper tightening of the adjustable connection element that joins the Veneer facing to the MSE facing (Gerber 2011).

Figure 1-5   Buckling of wall panels in 2-Stage MSE wall (Gerber 2011)

When MSE is used in locations where there are poor foundation soils it is essential to fully understand the magnitude of the expected settlements and the time for

complete settlement of the supporting foundation soils to occur. The Veneer face is expected to be attached to the Stage-1 MSE structure after all anticipated settlement is complete; therefore, the prediction and monitoring of the time rate of settlement is vital to the performance of the 2-Stage MSE structure. Excessive settlement after the attachment of the Veneer facing can cause cracking, spalling, and distortion of the segmental concrete panels (SCP).

There is a limit to the differential settlement that the SCP can tolerate. The tolerance is a direct function of the facing system that is being used (NHI 2009, AASHTO 2012). The magnitude of differential settlement that SCP can tolerate is a function of the length of the panel and the opening of the joints that are located at the interface of successive panels. The joint configurations of most DOT approved SCP MSE systems creates a 19mm gap between adjacent panels limiting the differential settlement to 1%, e.g. 1 meter in 100 meters (NHI 2009, AASHTO 2012). In this condition, differential settlement is defined as being parallel to the face of the MSE structure.

To limit post construction settlement of the face of the Stage-1 MSE the MSE structure details, construction inspection and control of ground water are critical to the successful performance. In known design methods the face of the MSE and the face of the Veneer are modeled as rigid structures; therefore, the MSE structure must be designed and constructed to limit movement of the face after attachment of the Veneer. The Stage-1 MSE structure must be ridged enough to properly attach the Veneer facing panels and must maintain its rigidity for the duration of the design life. The MSE face movement and distortion can be limited by placing a free draining rock at the back face

of the MSE facing, placing and compacting the backfill in shallow lifts in controlled

densities and controlling the ground water at the top of the MSE.

The 2-Stage MSE connector is typically a slender, adjustable, steel element that

is hooked to the respective facings (Crigler 1999, Taylor 2000, Timmons 2004, Taylor

2011, Taylor 2013). The connector can be fixed to the Stage-1 MSE or attached in a

manner that allows for some settlement to occur (Taylor 2011, Taylor 2013). The space,

or cavity, between the facing is typically filled with a free draining granular soil. Any

settlement of the foundation or the Stage-1 MSE can cause the Stage-2 facing to distort.

When the settlement is small the distortion is typically a cosmetic issue where the panel

edges may protrude outward. However, if the settlement is large it is possible for the

Veneer facing system to fail by overstress at the connection.

Based on the above discussion, the successful performances of 2-Stage MSE

structures can be increased by decreasing the uncertainties associated with the design

process including:

1.   Placement of the Stage-2 Veneer after the foundation has settled.

2.   Proper construction of the Stage-1 MSE system.

3.   Understanding the limitations of the 2-Stage MSE system.

1.2   Research Objectives

The objective of the research study is to investigate the horizontal pressure

within the cavity of the 2-Stage MSE and the forces that develop in the connection

element using numerical modelling. Another objective is to investigate the connector in a

large scale, single panel application, to determine the effect that vertical settlement has on the connection at the face of the Stage-1 wall system. The final objective is the development of a design procedure for the connection of 2-Stage MSE structures. These objectives will be achieved by executing the following:

1. Investigate by using a large scale structure the amount of settlement that can be tolerated by an adjustable 2-Stage connector.

2. Develop 2D and 3D numerical models to predict the horizontal pressure in the 2-Stage cavity and the subsequent forces on the 2-Stage connector.

3. Investigate the effects of post construction internal settlement of the MSE Stage-1 on the horizontal pressure in the cavity and the subsequent forces on the 2-Stage connector.

4. Investigate the effects of fixing the connector and/or allowing the connector to move in the vertical direction at the Stage-1 facing.

5. Develop a procedure for the design 2-Stage structures using the Arching theory MSE.

1.3   Thesis Organization

Chapter 1 introduces Mechanically Stabilized Earth (MSE) and various hybrid MSE systems. The 2-Stage MSE is introduced and described. Further, the objective of the research project is described.

Chapter 2 presents a review of the literature and is subdivided into five sections. The first subsection presents earth retaining structures, the development of the conventional MSE, the development of Shored MSE and the development of 2-Stage

MSE. The second subsection presents general earth pressure theories and how they influenced the development of MSE internal design methodologies including the application to 2-Stage MSE structures. The third subsection presents soil arching theories and how they have been used to determine the forces in narrow spaced retaining structures. The forth subsection presents a review of experimental programs that have been conducted on retaining structures in confined spaces. The fifth and final subsection presents a review of numerical modeling that has been conducted on MSE structures in confined spaces.

Chapter 3 presents the large-scale testing that was performed on a 2-Stage structure, the observations and the conclusions. The testing was carried out to determine the ability of the connection element to move during settlement of the Stage-1 MSE and if there was a limit to the movement the connector could tolerate without compromise to the connection point.

Chapter 4 presents and discusses the finite element numerical modelling studies that were conducted on hypothetical 2-Stage scenarios. The study will first determine if soil arching is occurring in the cavity by construction a base-line model of the Stage-1 and Stage-2 structure by assuming each facing are non-yielding rigid structures. The base-line model numerical results will be compared with the classic Janssen silo pressure equation. Parametric studies of the base-line model will then be conducted through varying the internal frictional angle of the cavity material and the interface friction angle of the facing. A final parametric a study will be conducted by changing the Stage-1 facing into a yielding structure by prescribing internal settlement in the control model. The parametric study results will be compared to the base-line model results to establish

the effect the variation of the properties have on the magnitude of the horizontal

pressure in the cavity.

Chapter 5 presents the summary of the research, conclusions, and

recommendations for future research are presented.

Chapter 2

Literature Review

2.1   Introduction

The 2-Stage structure consists of an MSE structure and a Veneer that is separated by a cavity and that is filled with a granular material. In order to design the 2-Stage structure the designer needs to be familiar with retaining wall design including external, internal and global modes of failure. Therefore, it is important that the designer understand earth pressure theories and how they are applied to the design of the MSE as well as the cavity separating the two facings.

A literature review was conducted on retaining structures, earth pressure theories, soil arching, experimental models of retaining structures in confined spaces and numerical modelling of retaining structures in confined spaces. The literature review for this chapter is organized in to five subsections. The first subsection provides general information on the different types of retaining structures and the common modes of failure. The second subsection provides general information on earth pressure theories and their influence on the design of MSE Structures. The third subsection reviews the theory of soil arching and how it is applied to structures constructed in confined spaces. The fourth subsection provides information on two experimental models that used centrifuge models to measure the lateral earth pressures behind retaining walls that are constructed in confined spaces. The fifth and final subsection reviews the numerical modelling of structures that are constructed in confined spaces.

2.2 Retaining Structures

2.2.1 Introduction

As the name implies, retaining structures are structures that retain a soil or rock mass and are used when a substantial grade change is required. The retaining structure can originate from an excavation in a soil or rock mass or by the method of backfilling that originates at the ground surface. The method of constructing the retaining structure may also be the combination of both type excavation and fill. Typical retaining structures include gravity, semi-gravity, and anchored (Handy et. al., 2007, Bowels 1996, Hunt 1985). Each of these structures is designed to assure they are stable against external failures, internal failures, and global failures.

2.2.2 Stability

As is defined in most Foundation Engineering and Geotechnical Engineering text books, external stability assumes that the retaining structure is a coherent gravity mass and that failure occurs in the soil mass the structure is supporting. Externally the retaining structure must be stable against sliding failures (Figure 2-1), overturning failures (Figure 2-2), and bearing capacity failures (Figure 2-3). In addition, and as a serviceability requirement, the structure settlement is limited to an acceptable magnitude so the structure can still perform its intended purpose.
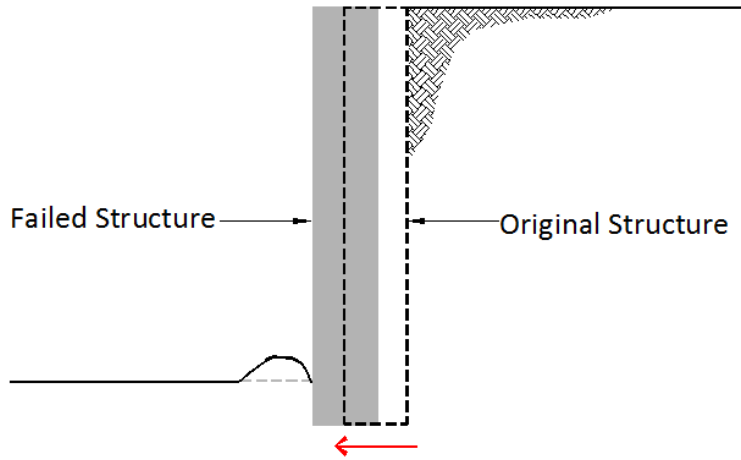
Figure 2-1 External sliding failure mode
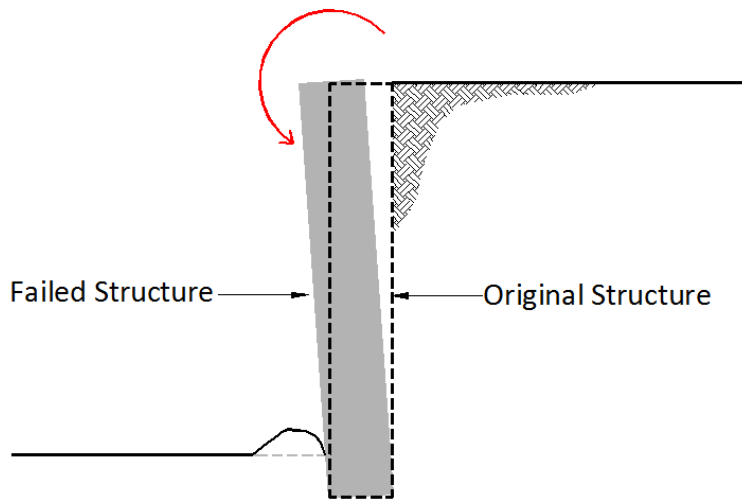
Figure 2-2 External overturning failure mode
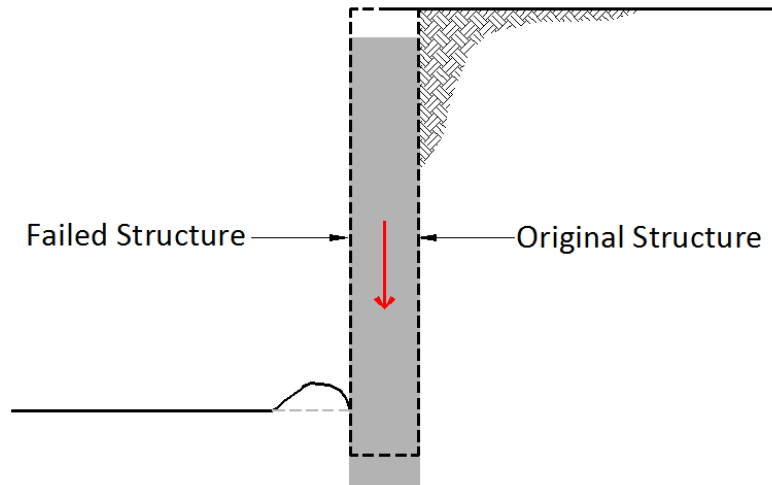
Figure 2-3 External bearing failure mode

Internal stability failure modes are a function of the type of retaining structure that is being used. Internal stability investigations assures that the coherent structural mass can withstand all externally and internally applied loading including deflection, shear, bond, thermal forces, dynamic forces, etc.

Global stability of the structure occurs over a larger soil area that encompasses the in-situ foundation and the retained soil mass and investigations include rotational failure (Figure 2-4) and block failure (Figure 2-5) modes (Clayton et. al., 2013, Macnab 2002).
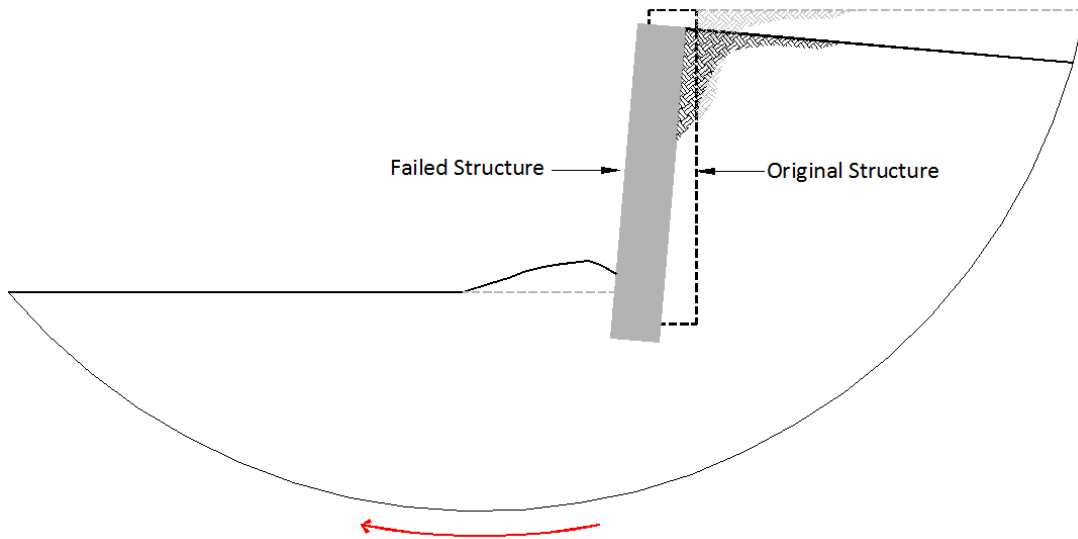
Figure 2-4   Global rotational failure mode
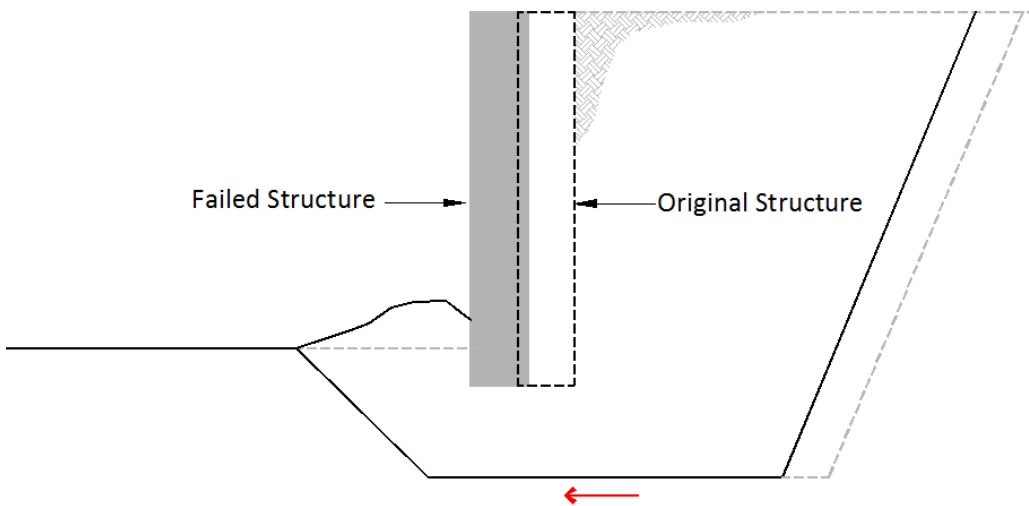
Figure 2-5   Global block failure mode

2.2.3   *Gravity Retaining Structures*

Gravity and semi-gravity retaining structures depend on the mass of the structure to resist the applied soil pressure. As the height of soil retention increases the mass of

the structure increases. Gravity structures consists of a mass of plain concrete or rock,

whereas semi-gravity structures consist of a mass of concrete that is lightly reinforced

with steel and include cantilever structures consisting of a slender vertical stem of

concrete that incorporates a slab and where the stem and slab is heavily reinforced with

steel (Clayton 2103). A gravity structure cannot support bending while semi-gravity

structures can support bending and is a function of the structure thickness and quantity

of reinforcing. Gravity and semi-gravity structures are designed so the weight of the

structural mass is sufficient to resist the forces acted on the soil mass it retains. Each of

these structures is typically wide at their base, tapering in width as the height increases.

| Gravity | Semi-Gravity | Semi-Gravity cantilever |
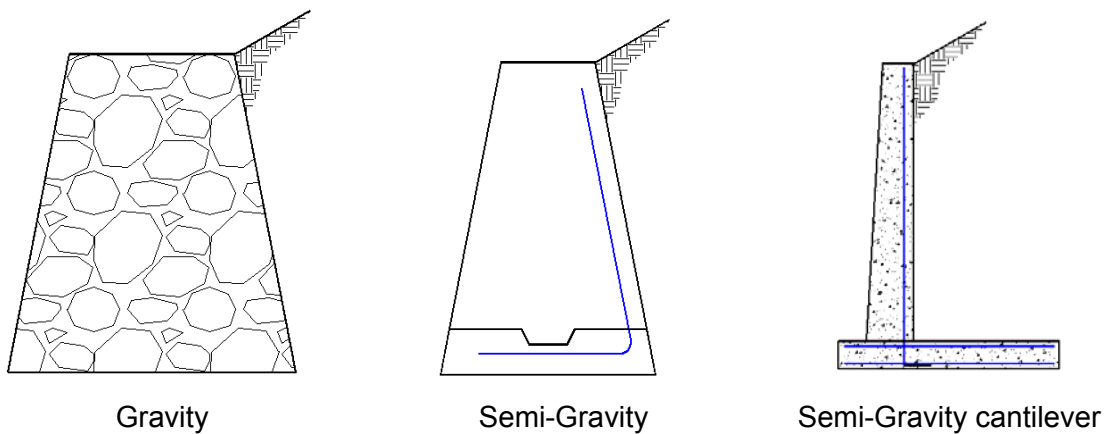
Figure 2-6   Gravity retaining walls

2.2.4   Anchored Retaining Structures

Anchored retaining structures typically are used in locations where the soil is

required to be excavated or cut from a soil or rock mass. The anchored structure, as the

name implies, comprises a series of horizontally spaced anchors that extend into the soil

and at a distance past the predicted failure surface. One or more rows of anchors may

be used. The anchors are structurally attached to a thin facing element that typically

consists of steel or concrete (Figure 2-7). Examples of anchored retaining structures

include steel sheet piles and soil nailed structures. These structures are advantageous in deep cuts where a high retention capacity is required (Hunt 1986). Internal stability of the anchored retaining structure requires that the anchor be designed to resist failure by rupture and pull-out from the soil. In addition, the proximal end of the anchor that attaches to the facing must be able to transfer tension forces that develop in the anchor into the face element. Structures that use a structural facing element, such as sheet piling, also rely on the bending capacity of the facing element for stability (Das and Shukla 2013, Xanthakos 1991).
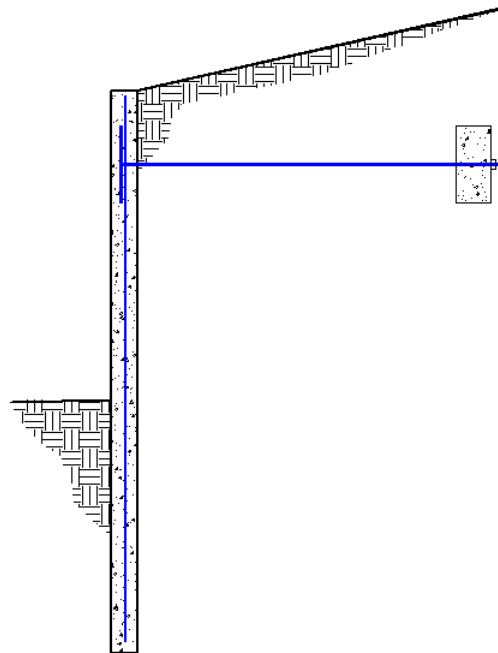
Figure 2-7   Anchored retaining structure

2.2.5   Reinforced Soil Structures

Reinforced soil structures are also known as MSE structures (Figure 2-8) and are a type of anchored structure. As described in the introduction, MSE was first introduced commercially in the United States in the transportation sector in 1971 by RECo

(Anderson 2010). Most MSE systems that have been developed have been done so by private industry and therefore are considered to be proprietary. The proprietary component of the system is usually restricted to the method that is used to connect the soil reinforcing element to the facing element or to the physical attributes of the soil reinforcing such as its shape, surface area, surface configuration, material, etc. Because of this, most proprietary systems have United States and Foreign Patents that protect the technology (Christopher 1990). Some of the patented systems that are in use today have had their patents expire and are now considered to be part of the public domain.
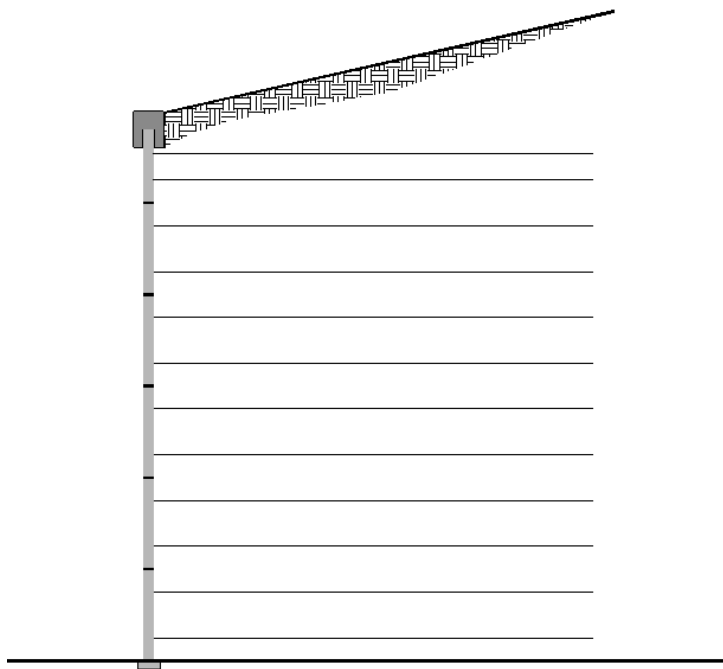
Figure 2-8   MSE retaining structure

MSE structures are designed in a similar manner as both gravity retaining structures and anchored retaining structures. MSE structures are designed to be stable against external, internal, and global forces. External and global stability consider that the combined wall facing and the reinforced soil mass is a rigid block that functions as a

coherent gravity mass. External modes of failure of the coherent gravity mass include sliding, overturning, and bearing (Figure 2-1 to Figure 2-3). Global modes of failure of the rigid block include deep seated rotation and block shear (Figure 2-4 to Figure 2-5) (AASHTO 2012, NHI 2009, NHCRP 1987).

The difference in the design procedures between gravity retaining structures, anchored retaining structures and MSE structures is in the internal modes of failure. In the internal stability design of gravity structures, such as the CIP concrete, the concrete elements are reinforced with steel bars. The stem and base slab of the structure are designed to assure that the combined concrete and steel reinforcing is capable of preventing tensile and bond failures (Bowels 1996). For an MSE structure the internal modes of failure are similar to the anchored retaining structure and include tensile failure of the soil reinforcing (Figure 2-9), bond failure, also known as pull-out failure, of the soil reinforcing from within the compacted soil mass (Figure 2-9), and the connection failure between the soil reinforcing and the facing element (Figure 2-11) (AASHTO 2012, NHI 2009, Christopher 1990, NCHRP 1987, Collin 1986).
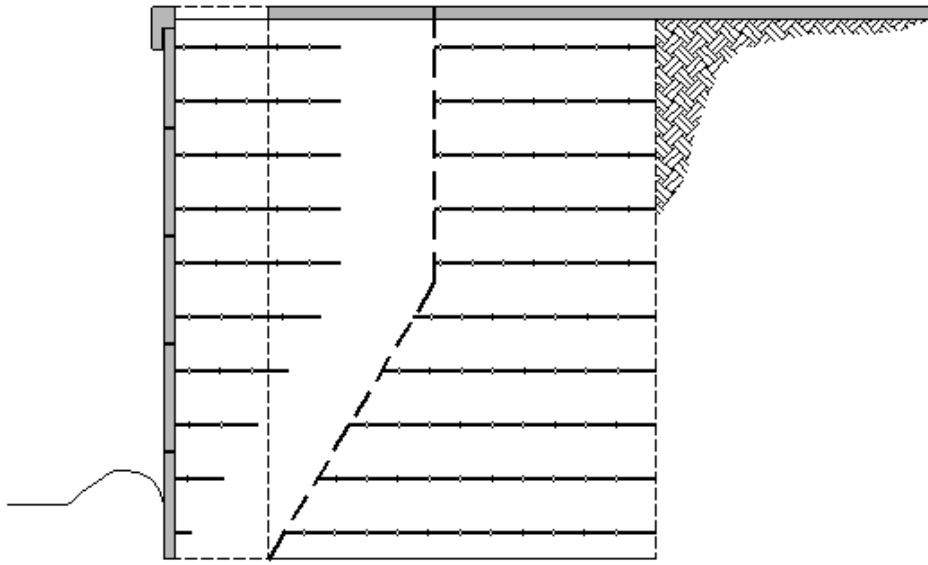
Figure 2-9   Tensile failure of soil reinforcing
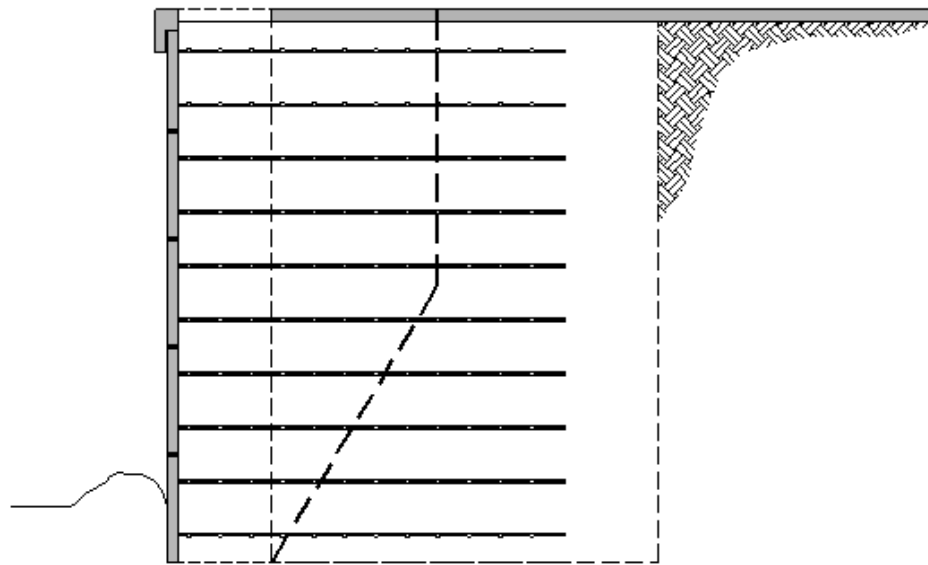
Figure 2-10   Pull-Out failure of soil reinforcing
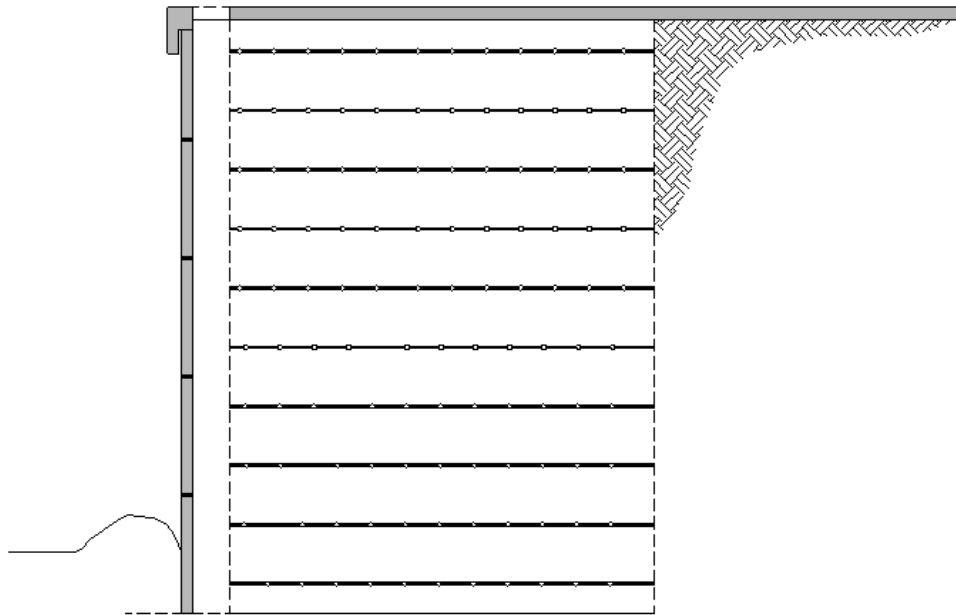
Figure 2-11   Connection failure of soil reinforcing

2.2.5.1   Conventional MSE Structures

The conventional MSE structure is considered to be a composite structure.

Standard MSE components that make up the composite MSE structure include

compacted soil, a soil reinforcing element, a facing unit, and a means to structurally

connect the soil reinforcing to the facing elements (Figure 2-12). The soil reinforcing

element may consist of discrete steel strips, discrete steel mesh, wide steel mesh,

discrete polymer strips or wide polymer geogrids. The MSE soil reinforcing system is

classified according to the extensibility of the soil reinforcing element. Soil reinforcing

elements that have mobilized strains that are less than the strain of the compacted soil

are classified as inextensible. Soil reinforcing elements with mobilized strains that are

greater than the strain of the compacted soil are classified as extensible (NHI 2009).

Based on this classification steel soil reinforcing elements are typically categorized as

inextensible whereas polymer soil reinforcing elements are typically categorized as extensible.
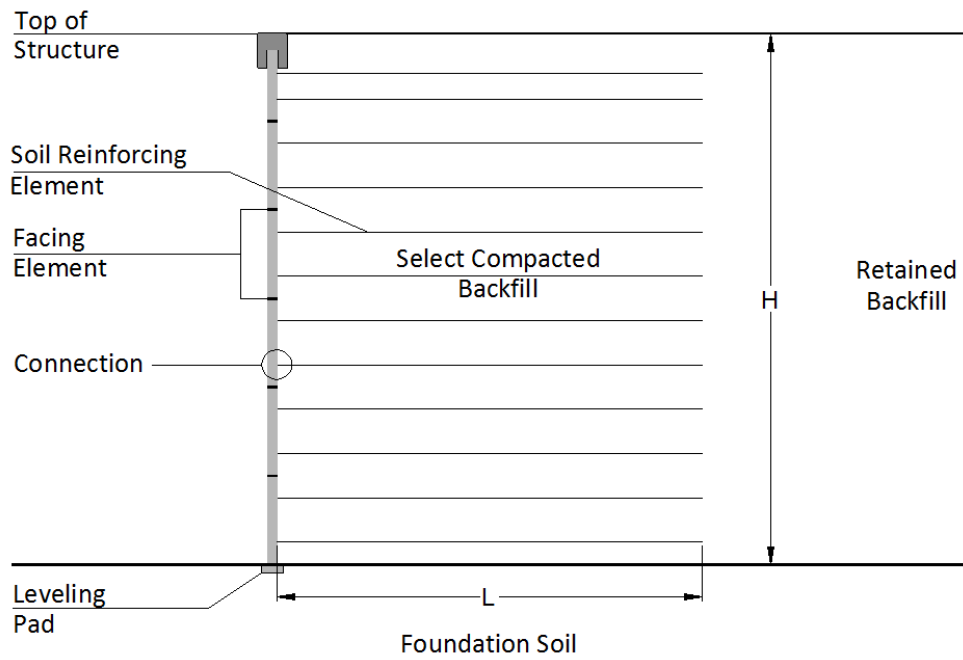
Figure 2-12   Cross section of conventional MSE structure

Based on design specifications the conventional MSE structure is typically required to have a soil reinforcing length (L) to structure height (H) ratio that is greater than, or equal to, 70% (AASHTO 2012). The value of 70% is an arbitrary value that has been selected based on experience with, and success of, structures that are in service today. The 70% rule typically yields structures that satisfy all external, internal and global stability requirements. The length to height ratio is also known as the aspect ratio (L/H). It should be noted that structures have been successfully constructed with aspect ratios less than 70% (AASHTO 2012, Anderson 2010, NHI 2009).

To determine the internal stability of an MSE structure the design methodologies typically use a limit equilibrium (LE) analysis that satisfies the Mohr-Coulomb failure

criteria where yielding coincides with failure. The LE method uses classical earth pressure theories such as Rankine and Coulomb to determine the forces in the soil reinforcing. The MSE design methodologies are an over-simplification of actual soil interaction. The methods are used because they allow for quick and easy modelling, with, or without the aid of a computer (Christopher 1990, Collin 1986).

Several recognized design specifications dictate the analysis requirements. These specifications include, but are not limited to, the American Association of State Highway and Transportation Officials (AASHTO) Load and Resistance Factored Design (LRFD) Bridge Specification (AASHTO 2012) and the Federal Highway Administration (FHWA) NHI-10-024 Mechanically Stabilized Earth and Reinforced Slope Design Manual (NHI 2009). These two references are recognized as being the most comprehensive and authoritative. The computer software program MSEW developed by Adama Engineering follows the AASHTO and FHWA design specifications and can be used as a quick and efficient method to analysis and design MSE structures.

2.2.5.2   Shored MSE Structures

A recent augmentation in MSE technology occurred in mountainous regions where roadways were being constructed in areas where there was limited right of way and where the 70% rule that was described in Section 2.2.5.1 could not be followed (Figure 2-13). A modification to the MSE design methodology was necessary because of the limited right of way that was available to keep traffic on the existing roadway operational. The need to maintain traffic flow created a condition where the design of MSE following the 70% rule was not possible. The additional cost of excavation, disposal of the existing slope material, and the maintenance of traffic made MSE technology not

23

an economical option. This led to the development of the design methodology for Shored Mechanically Stabilized Earth (SMSE) (Morrison 2009).
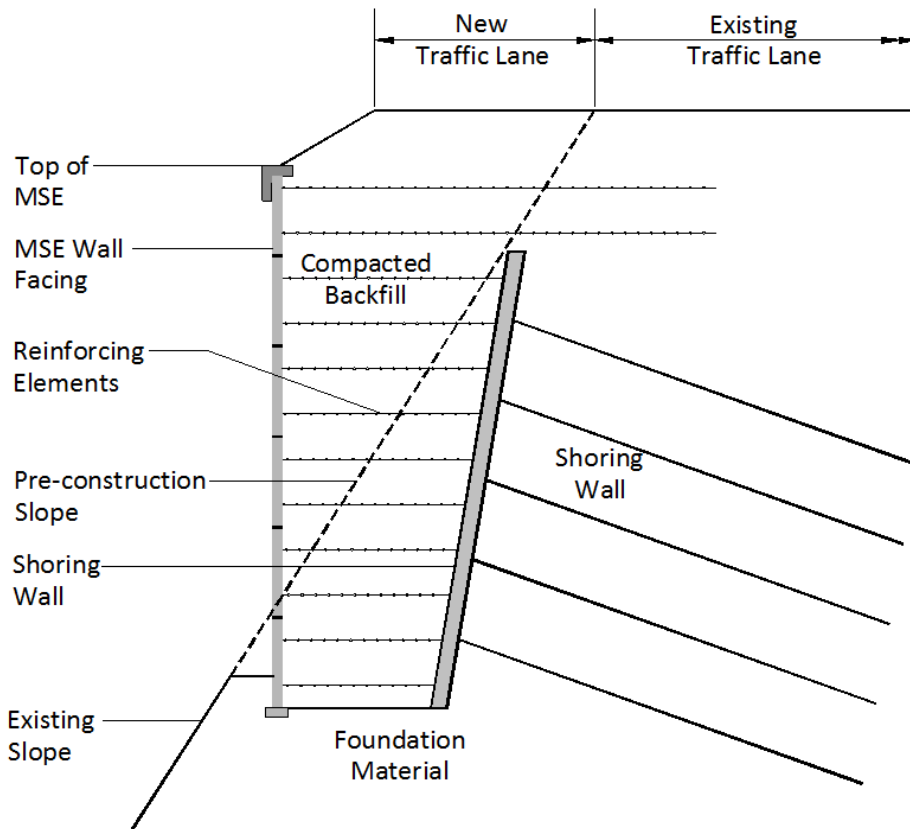
Figure 2-13   Section through shored MSE structure

SMSE draws on the principles of standard MSE design methodologies with modifications that account for the decreased area that is available for the soil reinforcing in the confined space between the shoring wall and the face of the new wall. The distance of the confined space between the MSE and Shoring facing typically has an aspect ratio equal to approximately 30%. As is the case with MSE, the space between the MSE facing and the Shoring facing is reinforced using soil reinforcing elements that are mechanically attached to the MSE facing element. The soil reinforcing is typically not attached to the shoring wall; however, it has been known to be attached (Morrison

2009). In addition, and to add stability to the structure, the top one or two rows of the soil reinforcing may extend a distance greater than 70% of the height of the structure (Figure 2-13). The increase in the length of the soil reinforcing at the top of the structure helps to integrate the structure with the shoring wall (Morrison 2009).

The shoring wall is designed to be stable and therefore can be considered a rigid structure. Because the shoring wall is assumed to be rigid and the structure is typically founded on competent rock formations, external stability and global stability will usually not be a concern and are omitted from the SMSE analysis. Therefore, internal stability of the reinforced space will govern the design. The force that develops in the space bound by the rigid structure and the face of the MSE is modeled using the theory of soil arching that was developed by Handy and Spangler (Handy 1985, Kniss 2007, Tanyu 2007, Morrison 2009). The theory recognizes that the earth pressure cannot fully develop in the narrow space because it is flanked by rigid interfaces, e.g., MSE facing and Shoring facing. Because of the confined space the classical earth pressure methods that are used to determine the horizontal force, such as Rankine and Coulomb, do not apply.

2.2.5.3   2-Stage MSE

Another variation of MSE and a variation of SMSE technology are used in areas where the length to height ratio is less than 30%. These structures are considered Fascia Walls or Veneer structures (Handy 2007). Veneer will be referenced herein. As is the case with an SMSE structure the narrow space is bound by two rigid structures. In the case of these structures the Veneer is always structurally attached to the flanking rigid structure. The method of attachment is typically adjustable to account for irregularities between the rigid structure and the Veneer structure. The narrow space that is bound by the interface between the rigid structure and the Veneer structure is

25

called the cavity. The cavity is filled with self-compacting fill material that may be granular or cementitious and varies among geographical regions and specifications.

The technique that uses an MSE structure that is then faced with a veneer is called a 2-Stage MSE. Stage-1 consists of building the MSE structure and Stage-2 consist of facing the Stage-1 MSE with the Veneer. This type of structures is used in locations where the in-situ foundation soils are of poor quality, where large settlements are anticipated, and where the MSE structure is being used as a surcharge to preload the foundation (Bloomfield 2001).
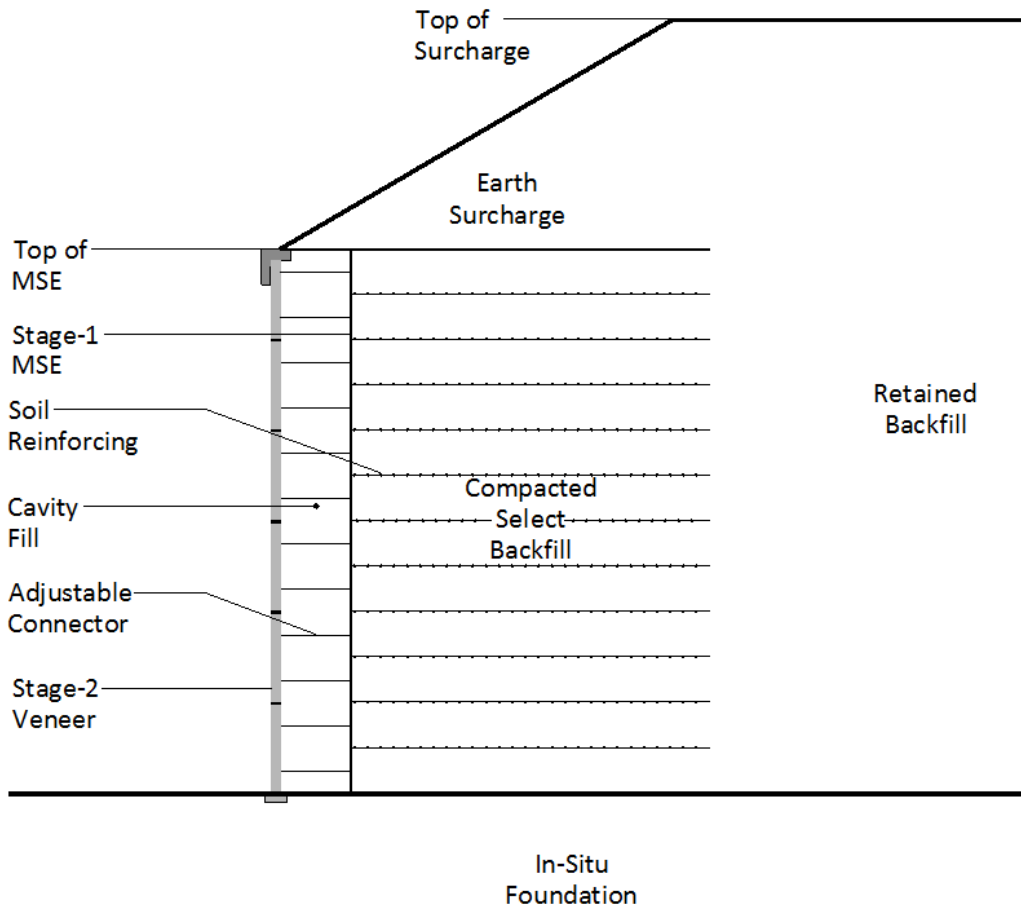
Figure 2-14   Section through 2-stage MSE structure

The Stage-1 MSE structure typically consists of a system that uses a flexible facing element in lieu of the standard SCP MSE system (Figure 2-15). The flexible facing is typically fabricated from steel welded wire reinforcing sheets that are formed into the shape of an "L". The soil reinforcing can be either extensible or inextensible. It should not be assumed that because the face is described as being flexible, that the final Stage-1 MSE is not a rigid structure. The composite system that consists of the flexible facing, soil reinforcing and compacted backfill is considered the rigid structure. Because the in-situ foundation soils are expected to settle differentially the MSE facing is required to be flexible. Flexible faced welded wire MSE has been used on projects where the foundation has settled more than 1 meter (Bloomfield et al. 2001). A rigid facing such as the SCP would not be able to tolerate this magnitude of settlement without sever distress and possible failure of the connection that joins the soil reinforcing to the SCP.

Figure 2-15   Stage-1 flexible faced MSE structure

The Stage-2 structure consists of a concrete facing element that can be full height or segmental, such as SCP (Figure 2-16 and Figure 2-18) or modular concrete blocks. The Stage-2 facing is not attached to the Stage-1 structure until all anticipated primary settlement has occurred in the foundation. The element that attaches the Veneer to the flexible faced MSE consists of an adjustable component that is connected to both faces at predetermined connection points. Because the Stage-1 structure is expected to settle the connectors may not be placed in a horizontal plane (Figure 2-16) but may be skewed in both the vertical (Figure 2-17) and horizontal direction. The orientation of the connection elements are a function of the elevation of the connection on the Stage-2 facing, the elevation of the Stage-1 facing connection, and the final overall settlement. Therefore, the connection element must be adjustable in length in order to account for the possibility that the connector will be skewed at an angle (Crigler 1999, Taylor 2000, Timmons 2004, Taylor 2011, Taylor 2013).

Figure 2-16   Stage-2 horizontal connection elements

Figure 2-17   Stage-2 skewed connection element (Bloomfield, *et al.* 2001)

Figure 2-18   Stage-2 SCP facing applied to Stage-1 flexible face

Figure 2-19   Completed 2-Stage MSE structure

2.3   Earth Pressure

2.3.1   Introduction

A 2-Stage MSE structure requires the design of the MSE structure, the Veneer structure and the connection element. As discussed earlier the external stability of the MSE structure follows classical design methods used for gravity retaining wall structures and is straight forward and is covered in most principle of foundation engineering books and manuals (Clayton 2013, Macnab 2002, Bowels 1996), therefore, it is not presented in this thesis. The internal stability of the MSE structure and the Veneer structure requires that the state of stress that develops within the reinforced soil mass and within the cavity be determined. This requires knowledge of earth pressure theories.

Based on the literature review it can be demonstrated that the basic principle of earth pressure on retaining walls was first introduced by Coulomb in 1776 and refined by Rankine in 1857 (Terzaghi 1943). All presently used retaining wall theory is an extension of these two classical concepts.

2.3.2   *Lateral Earth Pressure Coefficient*

The fundamental principle of earth pressure theory is that the horizontal earth pressure, σ_h, is a function of the vertical earth pressure, σ_v. To determine the horizontal earth pressure the vertical earth pressure is multiplied by a coefficient, K (Equation 2-1).

$$\sigma_h = K \cdot \sigma_v$$ Equation 2-1

Based on this relationship, the factor K is known as the coefficient of lateral earth pressure and is the ratio of the horizontal pressure to the vertical pressure (Equation 2-2).

$$K = \frac{\sigma_h}{\sigma_v}$$ Equation 2-2

The magnitude of the coefficient K is a function of the state of stress of the soil. If the soil is under natural conditions, with no movement, the soil is said to be at-rest. Under these conditions K is called the at-rest coefficient and is denoted by the variable K_o. If on the application of a vertical load to the surface of a retaining structure, the soil behind the structure moves reaching a state of equilibrium the state of stress in the soil changes. If the soil expands laterally the coefficient K is known as the active coefficient and is denoted by the variable K_a. If the soil contracts laterally the coefficient K is known as the passive coefficient and is denoted by the variable K_p. The at-rest, active, and

passive, cases are the three fundamental states of stress that can occur within a soil mass.

For an earth retaining structure, when the face of the structure moves away from the retained soil the soil is in the active state of stress. In this case the vertical stress remains unchanged but the horizontal stress decreases, $\sigma_h < \sigma_v$. The active case represents a state of minimum horizontal stress. When the face of the retaining structure moves toward the retained soil, the soil is in a state of passive stress. In this case, and as in the active case, the vertical stress remains unchanged, whereas the horizontal stress increases, $\sigma_h > \sigma_v$. The passive case represents a state of maximum horizontal stress.

The at-rest coefficient K_o for cohesionless soil is estimated according to Jacky equation that is shown in Equation 2-3 (Jaky 1944).

$$K_o = 1.0 - \sin(\phi')$$

Equation 2-3

Where: K_o =   at-rest earth pressure coefficient (dim)

              ϕ' =   the effective friction angle of the soil (deg)

As the friction angle decreases the at-rest coefficient increases. Typical values of the at-rest coefficient for soil used as backfill in earth retaining structures ranges between the value of 0.35 and the value of 0.50 and equates to soil friction angles of 40 degrees to 30 degrees respectively (Adib 1988). For earth retaining structures it has been shown that the act of compacting soil near the face changes the at-rest state of stress to values greater than the Jaky at-rest state of stress and can approach values as large as 1.50 (Duncan 1984). This is similar in concept to an over-consolidated soil.

The passive pressure coefficient (Equation 2-4) and active pressure coefficient (Equation 2-5) is a function of the effective internal friction angle of the soil, ϕ'. For a level surcharge the coefficients are determined using the Rankine stress state.

$$K_p = \tan^2\left(45° + \frac{\phi'}{2}\right) = \frac{1 + \sin(\phi')}{1 - \sin(\phi')} \qquad \text{Equation 2-4}$$

$$K_a = \tan^2\left(45° - \frac{\phi'}{2}\right) = \frac{1 - \sin(\phi')}{1 + \sin(\phi')} \qquad \text{Equation 2-5}$$

The passive resistance increases with decreasing ϕ' and the active resistance decreases with an increasing ϕ'.

2.3.3   Coulomb Theory

Coulomb in 1776 developed a method for the analysis of forces on retaining walls. In this method Coulomb assumed a soil wedge that was bounded by the face of the retaining wall and by a failure surface that originated at the base of the wall (Ketchum 1919). This is known as the sliding wedge method of analysis. The lateral earth pressure coefficient was determined by Equation 2-6 and is a function of the internal friction angle of the soil, the slope at the top of the structure, the slope angle of the structures backs face and the interface shear that develops between the soil and the structure (Coulomb 1776).

$$K_a = \frac{\cos^2(\phi - \alpha)}{\cos^2(\alpha) \cdot \cos(\alpha + \delta) \cdot \left(1 + \sqrt{\frac{\sin(\phi + \delta) \cdot \sin(\phi - \beta)}{\cos(\alpha + \delta) \cdot \cos(\alpha - \beta)}}\right)^2} \qquad \text{Equation 2-6}$$

Where: ϕ =   internal friction angle of the soil (deg)

$$\delta \quad = \quad \text{interface friction angle of the soil and structure (deg)}$$

$$\beta \quad = \quad \text{slope of surcharge at top of structure (deg)}$$

$$\alpha \quad = \quad \text{slope of back face of structure from vertical (deg)}$$

The lateral earth pressure can then be determined using Equation 2-7. Note that in Equation 2-6 that the earth pressure coefficient for a level back slope, no interface friction, and when the back face of the structure is vertical reduces to the Rankine earth pressure coefficient determined in Equation 2-5.

$$\sigma_H = \gamma \cdot h \cdot K_a \qquad \text{Equation 2-7}$$

Where: $\quad \sigma_H \quad = \quad$ horizontal earth pressure (kPa)

$\quad$ h $\quad = \quad$ height of the retaining structure (m)

$\quad \gamma \quad = \quad$ unit weight of backfill (kN/m^3)

$\quad K_a \quad = \quad$ active earth pressure coefficient (dim)

2.3.4   Rankine Theory

Rankine in 1875 (Terzaghi 1996) developed an equation to determine the horizontal pressure on a retaining wall for an incompressible, cohesionless, granular mass of soil with and assumed indefinite extent. Rankine defined two equations, one for the active case (Equation 2-8) and one for the passive case (Equation 2-9). These equations are based on the pressure coefficients as defined in Equation 2-4 and Equation 2-5, respectively.

$$\sigma_H = \gamma \cdot h \cdot \left[\frac{1 - \sin\phi}{1 + \sin\phi} \right] = K_a \cdot \sigma_v \qquad \text{Equation 2-8}$$

$$\sigma_H = \gamma \cdot h \cdot \left[\frac{1 + \sin\phi}{1 - \sin\phi} \right] = K_p \cdot \sigma_v \qquad\qquad \text{Equation 2-9}$$

2.3.5 Failure Surface

Both Coulomb and Rankine assumed that the retaining wall was able to rotate about its base and therefore the top could translate into or away from the soil mass. They demonstrated that the failure of the soil mass occurred along a slip line that was the dividing boundary of the unstable soil mass to the stable soil mass. The shape of the boundary is based on empirical assumptions. Coulomb recognized that the surface of failure was slightly curved but simplified it to a linear surface noting that the error to do so was negligibly small (Clayton 2013, Huntington 1957). It is typical in practice to backfill retaining walls with a well- graded, granular material that contains less than 10% fine material (AASHTO 2012, NHI 2009, Christopher, 1990, NCHRP 1987, Collin 1986). Based on this soil type the slip line failure surface can be assumed to be equal to the Rankine failure surface originating at the bottom back face of the retaining structure propagating at an angle of $45° + \frac{\phi'}{2}$ as shown in Figure 2-20.
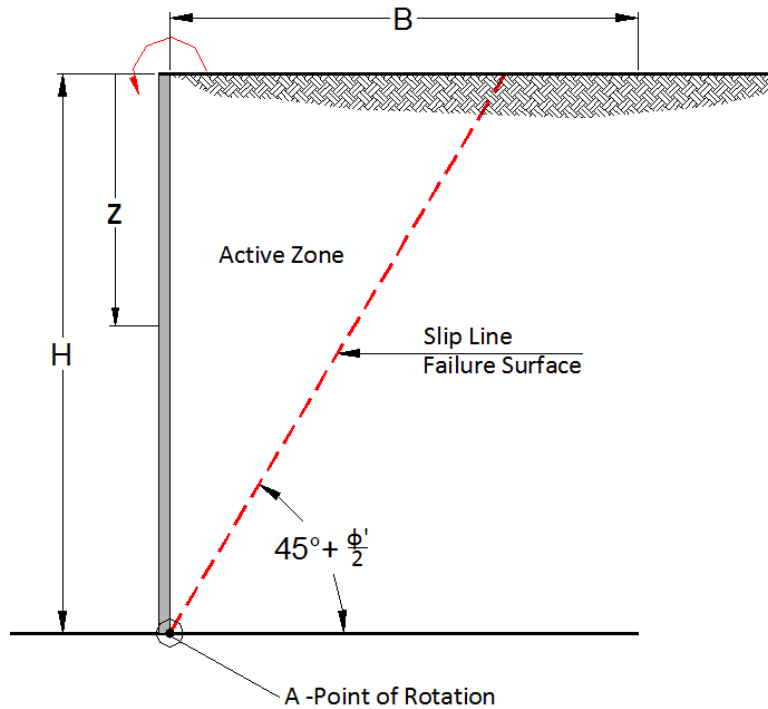
Figure 2-20   Location of active wedge in retaining wall

The magnitude of the lateral earth pressure at any depth on the back face of the retaining structure can be expressed as the product of the unit weight of the backfill multiplied by the depth and then multiplied by the active earth pressure as demonstrated in Equation 2-10 (AASHTO 2012).

$$\sigma_h = K_a \cdot \gamma \cdot z$$

Equation 2-10

Where:

σ_h = horizontal earth pressure (kPa)

K_a = active earth pressure coefficient (dim)

γ = unit weight of backfill (kN/m^3)

z = depth (m)

To activate the active state the retaining structure facing is assumed to rotate about the base a very small amount. As the wall rotates away from the soil, the soil

strains until it reaches the active state creating the wedge of soil at the boundary of the slip line. The retaining wall must be able to counter balance the horizontal force in order to prevent failure.

2.3.6 MSE Internal Design Methodology

The internal design methodology used for MSE has evolved since the technology was first introduced in the United States (NHI 2009, Erlich et. al. 1994, Christopher 1990, NCHRP 1987, Collin 1986, Anderson et. al. 1985, Juran, 1985, Juran et. al. 1978). Reinforced soil structures behavior has been described as being analogous to the behavior of reinforced concrete structures with the basis being on the bond of the reinforcement in each structure, e.g., reinforcement to soil bond for MSE and reinforcement to concrete bond for reinforced concrete (Jones 1985, Schlosser 1978). The tensile forces in a reinforced concrete element are resisted completely by the reinforcing. In MSE structures the internal tensile force is resisted by a combination of the soil reinforcing and the soil. The soil reinforcing element anisotropically reduces the normal strain rate in the soil mass in the direction of the element (Jewell 1984). This phenomenon was explained by Vidal as being equal to adding cohesion to the soil reinforcing system. It is therefore possible for a complete compressive state to exist in MSE (Juran 1978, Duncan 1984, Jones 1985).

On the introduction of MSE into the United States the proprietors of the MSE system developed unique design methodologies that were used to design their MSE system (Collin 1986). These design methodologies were based on empirically derived equations that can be traced back to the fundamental earth pressure theory.

37

MSE design consists of determining the geometric and reinforcement

requirements to prevent external and internal failure and uses a limit equilibrium (LE)

method of analysis (Christopher 1993). The required soil reinforcing geometric

parameters for all MSE structures include the length, vertical spacing, and horizontal

spacing of the soil reinforcing. As shown in Figure 2-12 MSE consists of alternating rows

of soil reinforcing and compacted soil. When a MSE structure is constructed using

proper construction procedures it forms a coherent, rigid mass. The soil reinforcement is

required to be strong enough to prevent rupture at the critical failure surface that passes

through the reinforced mass of soil and long enough beyond that critical surface to

prevent pullout of the element (Jewel 1984).

In order to solve the internal stability of an MSE structure the first requirement is

to define the location of the critical failure surface. The choice of the location of the

critical surface was initially based on classical earth pressure theories that were used for

slope stability problems including wedge, circular, logarithmic spirals, 2-part wedge and

3-part wedge analysis (Collin 1986).   As the technology matured full height

instrumented structures were used to determine and verify the location of the failure

surface for different reinforcing systems, e.g. discrete steel strips, wide steel mesh,

geogrid, etc. In order to determine the stress pattern in the soil reinforcing a series of

strain gauges was positioned at intervals along on the soil reinforcing element (Sampaco

1994, Simac et. al. 1990, Bastick et. al. 1993, Christopher et. al. 1990, Anderson et. al.

1985, Bishop 1980). As the name implies, the strain gauges were used to measure the

strain in the reinforcing at working stress conditions. From the maximum strain the

maximum tension in the soil reinforcing could be back-calculated. The critical surface

was defined as the location of the maximum tension in the soil reinforcing. The critical

surface divides the reinforced mass into two zones consisting of an active zone and a passive zone. The active zone is moving toward the face of the wall and the passive zone is stationary.

It was demonstrated that the location of the failure surface that developed in the reinforced soil mass was a function of the stiffness of the soil reinforcing system. Therefore, the failure surface for an inextensible soil reinforcing system was different than the failure surface of an extensible soil reinforcing system. The failure surface for both inextensible and extensible soil reinforcing is shown in Figure 2-21.

Inextensible soil reinforcing   Extensible soil reinforcing
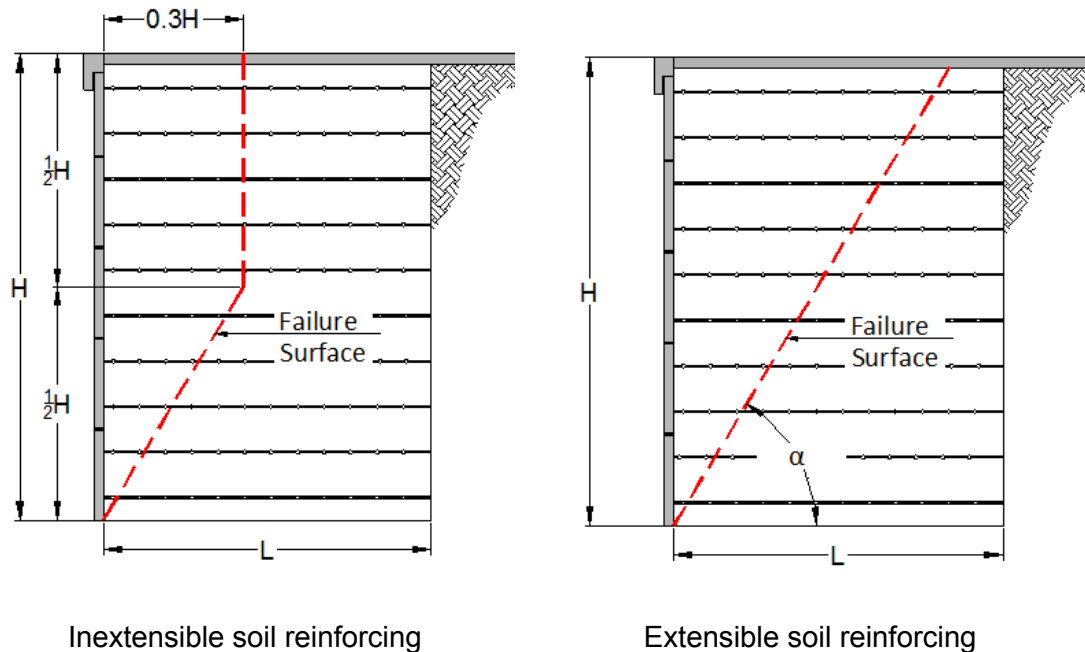
Figure 2-21 Internal failure surface of MSE structures

Based on instrumented structures using inextensible soil reinforcing it was shown that the maximum strain location formed a logarithmic spiral. For simplicity the logarithmic spiral was idealized into a bi-linear orientation as shown in Figure 2-21 (Juran 1978). The bilinear failure surface was determined to occur because the soil

reinforcing systems stiffness is greater than the soil it reinforces. In contrast and also based on instrumentation the extensible soil reinforcing systems failure surface was shown to be linear and to closely follow the Rankine failure surface at or near failure. The linear failure surface occurred because the extensible soil reinforcing stiffness is less than the soil it reinforces allowing the reinforced mass to move to the active case.

For a structure with a horizontal back-slope the bi-linear failure surface intersects the top of the reinforced mass at a distance that is approximately equal to 30% of the height of the structure. At a depth that is approximately equal to 50% of the height of the structure the failure surface propagates toward the face of the structure intersecting the structure face at the base of the wall. The angle of propagation (α) of the failure surface for extensible soil reinforcing is nearly equal to Rankine failure surface as defined in Equation 2-11.

$$\alpha = 45° + \frac{\phi}{2}$$
Equation 2-11

Where: α = Angle of failure surface (deg)

ϕ = Internal friction angle of soil (deg)

Once the failure surface is determined the internal stability of the MSE may be solved.

2.3.7 Bond Effect of Soil Reinforcing

When a vertical load is applied to a non-reinforced soil mass it strains both axially and laterally. In the axial direction the soil is contracting and in the lateral direction the soil is extending. The lateral extension in a non-reinforced soil mass is not restricted. When a soil reinforcing element is placed horizontally in the soil mass and the vertical load is applied to the soil surface the soil reinforcing restricts the lateral deformation

through bond as if acted on by a lateral force (Jewel 1984). If full restriction of movement is provided the lateral force is considered equivalent to the at-rest soil condition, $\kappa_o \cdot \sigma_v$. Likewise, if the soil reinforcing allows for some lateral extension of the soil than the lateral force is considered equivalent to the active soil condition $K_a \cdot \sigma_v$ (Adib 1988).

$$\sigma_h = K_a\sigma_v$$

Unrestrained laterally

$$\sigma_h = K_o\sigma_v$$

Restrained laterally
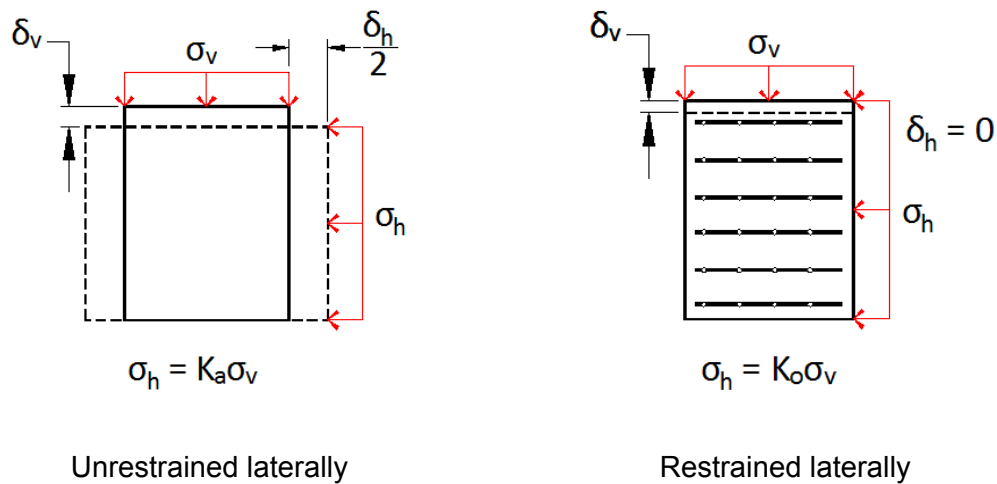
Figure 2-22   Lateral strain in soil element (Jones 1985)

The amount of restraint that is provided by the soil reinforcing has been directly correlated to the stiffness of the soil reinforcing (Collin 1986, Mitchel 1987, Bounaparte et al., 1987, Adib 1988, Christopher 1993, Allen et al., 2001). Consequently, the internal earth pressure coefficient in an MSE structure is a function of the stiffness of the soil reinforcing.

2.3.8   Soil Reinforcing Stiffness

The stiffness of the soil reinforcing is an extremely important parameter in the design of MSE structures. The stiffer the soil reinforcing element is the lower the soil strain will be and the higher the stress in the soil reinforcing. The stiffness of the soil

41

reinforcing dictates the internal forces that occur in the reinforced soil mass and therefore the internal earth coefficient.

A research project sponsored by the FHWA from 1983 through 1989 unified the design methodology for both inextensible and extensible soil reinforcing into what is known as the Stiffness Design Method as documented in the *FWHA-RD-89-043 Reinforced Soil Structures Design and Construction Guidelines* manual (Christopher et al., 1989). This methodology was developed as the result of full scale instrumented MSE structures. The research project combined case studies, numerical models (Adib 1988 and Schmertmann et al., 1989), analytical models, pullout tests (Bonczkiewicz 1990), small scale models (Juran 1985 and 1986), centrifuge models (Jabar 1989) and instrumented full scale walls (Christopher and Bonczkiewicz 1989) built specifically for the research project. Many other researchers contributed to this effort including an earlier NCHRP literature review performed by Mitchell and Villet 1987 along with supporting work by Collin (1988). A summary of the research program is contained in Volume II of Christopher et al. (1989) and a detailed description of the research and results in relation to the development of a global stiffness factor is provided by Christopher (1993). This design method is similar to the Tieback Wedge Method but used the stiffness of soil reinforcing system to calculate both the lateral earth pressure coefficient and the location of the failure surface as was previously discussed. The Stiffness Design Method required iteration and knowledge of the reinforcing system that was being used.

The global stiffness of the soil reinforcing system was calculated using the following relationship (Christopher 1993):

$$S_r = \frac{E_r \cdot A_r}{\left(\dfrac{H}{n}\right)}$$

Equation 2-12

Where:
    S_r =   Global Stiffness (kPa)

    E_r =   Modulus of reinforcement (kPa)

    A_r =   Area of reinforcement (m^2)

    H   =   Height of the MSE structure (m)

    n   =   Number of rows of soil reinforcing (dim)

The lateral earth pressure coefficient was calculated using the following relationships:

$$K_r = K_a\left(\Omega_1\left(1 + 0.4\frac{S_r}{47880\,(kPa)}\right)\left(1 - \frac{Z}{6\,(m)}\right) + \Omega_2\frac{Z}{6\,(m)}\right) \quad \text{if} \quad Z \le 6\ m$$

Equation 2-13

$$K_r = K_a\Omega_2 \quad \text{if} \quad Z > 6\ m$$

Equation 2-14

Where:
    K_a =   Coefficient of active earth pressure (dim)

    Ω_1 =   1.0 for strips and polymer sheet reinforcement (dim)

                  1.5 for bar mats and welded wire mesh (dim)

    Ω_2 =   1.0 if $S_r \le$ 47880 kPa

                  Ω_1 if $S_r >$ 47880 kPa

    Z   =   Depth from top of structure to soil reinforcing (m)

As previously indicated, the development of this method was based on numerous full scale test structures and was verified through numerical modelling. The method was included in the 1994 AASHTO Specifications for Bridges. Experience with MSE structures in use today demonstrate that when MSE is designed as outlined above and

constructed following state of practice specifications they can be considered a rigid structure.

2.4   Soil Arching
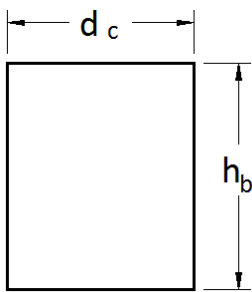
2.4.1   Introduction

Arching in a soil mass can be defined as the redistribution of stresses by the transfer of force to the sides of an adjoining rigid structure from a yielding mass (Moradi 2013). Shearing resistance on the adjoining rigid structure keeps the yielding mass in its original location and changes the pressure distribution on the side supports and the adjoining parts of the soil. The transfer of pressure from a yielding mass of soil onto the adjoining stationary support is commonly called the arching effect, and the soil is said to arch over the yielding part of the support (Terzaghi 1943). Terzaghi anticipated that the intensity of the arching effect under static forces would be reduced or changed by any external influence that would cause a supplementary settlement of a footing or the additional outward movement of the retaining wall.

Depending on the movement of the yielding mass or the supporting structures the shearing resistance can be in the upward direction or downward direction. If the yielding mass moves downward the shear resistance acts in the upward direction and the stress at the base decreases (Marston 1930). If the support structure moves upward the shear resistance acts in the downward direction and the stress at the base increases. The theory of arching is used in the design of many engineered structures such as silos, tunnels, underground conduits, mining stopes, shored MSE walls, fascia walls, column supported embankments, and in the connection design of geogrid reinforced soil (GRS) structures.

The arching theory used in soil mechanics originates from the design of silo structures. From the time of the late 19th century an assortment of arching theories have been developed and used to determine the pressures that occur on silo walls (Moradi et. al. 2013, Wu 1990). A silo is defined as a bulk storage structure with a height that is substantially greater than the width. The Australian Standards (AS 3774) has categorized bulk storage containers based on their height to width ratio (Table 2-1).

Table 2-1　Container geometry AS-3774

Type	Class	Ratio	
A1	Squat	$h_b / d_c < 1.0$	
A2	Medium	$1.0 \leq h_b / d_c \leq 3.0$	
A3	Tall	$h_b / d_c > 3.0$	

Where:　　h_b　　=　　Height t of container (m)

　　　　　d_c　　=　　Width of container (m)

Based on AS-3774 a silo would be considered a Type-A3 where the height to width ratio is greater than 3 and would be consistent with the shored MSE ratio of 30%. 2-Stage Walls typically have a cavity width that is 305mm when cementitious fill material is used and between 400mm and 1000mm when granular fill is used. Therefore, 2-Stage structures would also be classified as A3.

2.4.2　　French Military Silo Theory

While constructing magazine silos in the early 1800's French military engineers established that the base of the silo only supported a fraction of the total weight of the material above it and that the side walls carried far more weight than expected.

Experimentally they demonstrated that if a small section of the silo base was detached and lowered, the resulting load that the detached section experienced was independent of the height of the material in the silo. They theorized that an arch had occurred above the section (Moradi 2013, Tein 1996, Singh et. al. 1985). The theories that are used in the design of soil structures today are a direct result of the arching theories that were developed from the design of military silo structures.

2.4.3   Janssen Silo Theory

The fundamental theory of soil arching can be attributed to work performed by Janssen on grain bins. Janssen recognized that the calculation of the pressure on the walls of grain bins was similar to finding the pressure on a retaining wall (Wright 1994, Ketchum 1919, Janssen 1895). For shallow bins of wide widths he noted that the classical Rankine failure surface of rupture cuts through the grain and propagated out the top of the grain mass. In contrast, for deep bins with narrow widths, the Rankine failure surface could not fully cut through the grain but intersected the bin side wall. It should be understood that the classical Rankine earth pressure theory is predicated on the fact that the granular mass of soil, in-plane and section, is of infinite extent and therefore the failure surface propagates out the top of the soil mass. To study his theory Janssen used a circular bin that was filled with grain to a given height, h, that had a uniform surface area, A, and that had a uniform circumference, U (Figure 2-23).

Cross section   Plan section
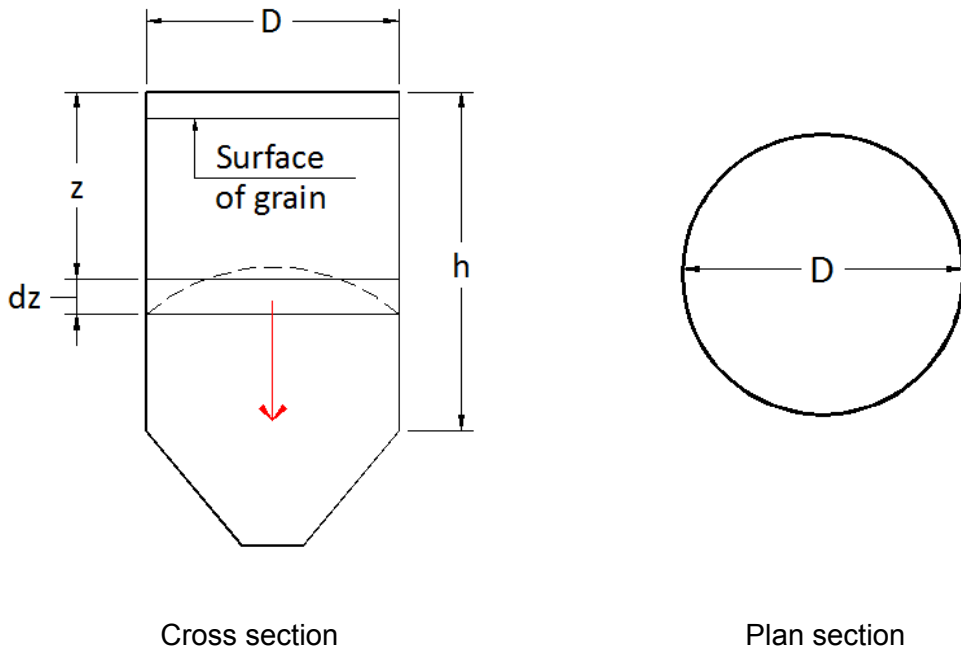
Figure 2-23   Janssen grain silo (Ketchum 1907)

Where: D   =   diameter of the bin (m)

              h   =   height of the vertical side wall of the bin (m)

              z   =   depth from the top of the bin to the top of the slice (m)

              dz   =   height of a slice (m)

Janssen assumed that a slice of grain stored in the circular bin was in static

equilibrium. Based on this, Janssen developed the free body diagram of the slice shown

in Figure 2-24.
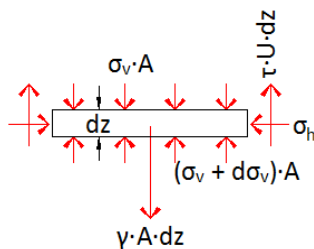
Figure 2-24   Janssen silo free body diagram (Janssen 1895)

By summing forces in the z direction he produced the following equation:

$$\sigma_v \cdot A + \gamma \cdot A \cdot dz = (\sigma_v + d\sigma_v) + \tau \cdot U \cdot dz \qquad \text{Equation 2-15}$$

Where: A   =   the area of the slice (m^2)

σ_v =   vertical pressure of the grain on the top of the slice (kPa)

σ_h =   normal pressure of grain on the side walls (kPa)

U   =   circumference of the silo (m)

τ =   shear stress on silo wall (kPa)

The shear on the side wall is equal to the horizontal force times the friction interface that develops between the grain and the side wall. Janssen assumed that the interface friction was approximately equal to the $\tan(\phi)$ where ϕ was set equal to the internal friction angle of the grain which he assumed to be equal to the angle of repose of the grain. By direct substitution into Equation 2-15 Janssen developed Equation 2-16.

$$\sigma_v \cdot A + \gamma \cdot A \cdot dz = (\sigma_v + d\sigma_v) + \sigma_h \cdot \tan(\phi) \cdot U \cdot dz \qquad \text{Equation 2-16}$$

As was explained in section 2.3.2 the lateral stress ratio is equal to K=$\dfrac{\sigma_h}{\sigma_v}$.

Janssen derived the lateral stress ratio K from experiments on different grains (Janssen 1895). Janssen applied the assumptions that the pressure is uniform across the surface of the slice, the lateral pressure coefficient is constant, the grain settles sufficiently to introduce shear at the interface of the wall, and that the grain is homogenous and isotropic. Based on these assumptions Janssen developed the differential equation shown in Equation 2-17.

$$\frac{d\sigma_v}{dz} + \frac{U \cdot K}{A} \cdot \tan(\phi) = \gamma \qquad\qquad \text{Equation 2-17}$$

To determine the lateral pressure σ_h Equation 2-17 can be algebraically manipulated to yield Equation 2-18 (Janssen 1895).

$$\sigma_h = \frac{\gamma \cdot A}{\tan(\phi) \cdot U}\left(1 - e^{\frac{-K \cdot \tan(\phi) \cdot U \cdot z}{A}}\right) + K \cdot \sigma_{v\_0} \cdot e^{\frac{-K \cdot \tan(\phi) \cdot U \cdot z}{A}} \qquad \text{Equation 2-18}$$

Where: σ_{v_0} = vertical pressure at the top of structure (kPa)

The vertical pressure, σ_{v_0}, is analogous to a surcharge load that is applied to the top of the grain mass as shown in Figure 2-24 and was considered a boundary condition.

Janssen's theory is a simple way to predict the horizontal pressure on grain silo walls and is widely accepted for determining the horizontal pressure when filling a grain silo however it is not used in determining the horizontal pressure when unloading the grain silo (Singh 1985). Because of Janssen's work Equation 2-18 is the basis of several standards for the calculation of stresses in silos including the AS 3774-1990 *Loads on Bulk Solids Containers,* Australian Standard, and the BMHB Code of Practice for the Design of Silos, Bins, Bunkers and Hoppers, British Material Handling Board.

2.4.4   Marston's Theory

In 1913 Marston extended the arching theory to soil mechanics by applying Janssen's theory to a buried conduit in an excavated ditch. Janssen used a finite slice that was bound by the walls of the bin whereas Marston used a two dimensional plane strain solution for a ditch of infinite length. Marston determined that the load above a conduit does not fully act on the conduit but is partially supported by the side material

through arching action. He developed an equation to determine the vertical force (V) and the corresponding horizontal stress (σ_h) in a ditch for a conduit that was filled with a non-cohesive backfill (Marston 1930).

$$V = \frac{\gamma \cdot w^2}{2 \cdot \mu \cdot K_a} \cdot \left[1 - e^{\left(-\frac{2 \cdot K_a \cdot \mu \cdot h}{w} \right)} \right]$$

Equation 2-19

$$\sigma_h = K_a \cdot \sigma_v \rightarrow \frac{\gamma \cdot w}{2 \cdot \mu} \cdot \left[1 - e^{\left(-2K_a \cdot \mu \cdot \frac{h}{w} \right)} \right]$$

Equation 2-20

$$K_a = \tan^2 \left(45° - \frac{\phi}{2} \right)$$

Equation 2-21

$$\mu = \tan(\delta)$$

Equation 2-22

Where:

σ_v = vertical stress (kPa)

σ_h = horizontal stress (kPa)

γ = unit weight of backfill (kN/m^3)

w = width of the ditch (m)

μ = interface friction boundary of the ditch (dim)

δ = interface friction angle (deg)

K_a = Rankine's active earth pressure coefficient (dim)

ϕ = internal friction angle of backfill (deg)

h = height of the ditch (m)

Marston's equation is for plane strain of a rectangular prism of width w. His equations therefore differ from Janssen, in that Janssen was considering a closed structure. Additionally, the Marston's equation differs from the Janssen equation through the introduction of the interface friction angle at the wall face, δ , and by equating the

lateral stress ratio to the principle stress ratio for a level ground surface in conformance

with the Rankine ratio $K_a = \dfrac{\sigma_1}{\sigma_3}$ (Handy 1985).

2.4.5 Arching Theory

Terzaghi's arching theory is based on his "trap door" experiment (Terzaghi 1936). This experiment is similar to the investigation that was performed by the French military engineers on magazine silos. Terzaghi's trap door experiment consisted of a box with a flush mounted trap door at the base. The box was filled with sand. The trap door was able to translate downward in controlled displacements while the remaining base of the box was fixed. The load and displacement on the door was monitored. In addition, indirect measurements of the vertical and horizontal stress above the door were measured using the friction tape method. In his experiment Terzaghi determined that as the door was displaced the force on the trap door decreased rapidly. The minimum vertical stress was less than 10% of the overburden and occurred at a vertical displacement that was approximately equal to 1% of the doors width. During displacement of the door it was observed that the sliding surfaces in the soil mass were curved and spaced greater than the width of the door.
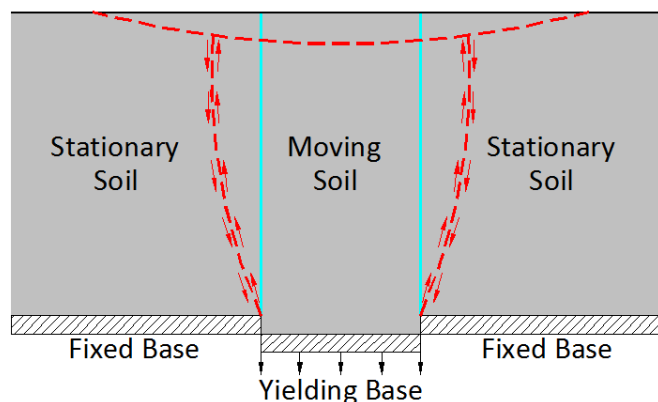
Figure 2-25   Terzaghi Trap Door – Redistribution of stresses

From his experiment Terzaghi determined that the movement in the soil is opposed by the shearing resistance within the contact zone of the yielding mass. The pressure transfer through the shear resistance is a key component to the arching theory. In order to solve the redistribution of the observed stresses as shown in Figure 2-25, Terzaghi made simplifying assumptions including (Tein 1990):

- the soil boundary was vertical

- the horizontal stress across the yielding soil mass was uniform

- cohesion existed along the vertical surface.

Based on these assumptions, Terzaghi developed the free body diagram shown in Figure 2-26.
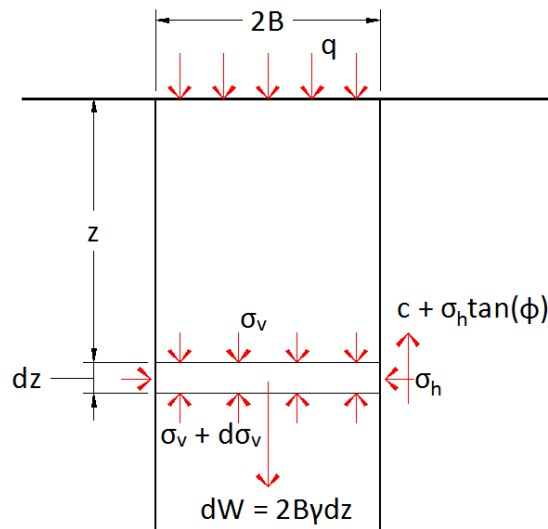
Figure 2-26   Slice of soil in yielding zone

By summing the forces in the vertical direction Terzaghi developed Equation 2-23:

$$2 \cdot B \cdot \gamma \cdot dz = 2 \cdot B\left(\sigma_v + d\sigma_v\right) - 2 \cdot B \cdot \sigma_v + 2 \cdot \left(c \cdot + \sigma_h \cdot \tan(\phi)\right) \cdot dz \qquad \text{Equation 2-23}$$

Where: 2B = width of the yielding mass (m)

z = depth (m)

γ = unit weight of soil (kN/m^3)

σ_v = vertical stress (kPa)

σ_h = horizontal stress = $K \cdot \sigma_v$ (kPa)

K = coefficient of lateral stress

c = cohesion (kPa)

ϕ = friction angle (deg)

Solving Equation 2-23 for σ_v and assuming a boundary condition that at a depth equal to zero, the overburden stress (σ_v) is equal to the surcharge at the soil surface, yields Equation 2-24 (Terzaghi 1943).

$$\sigma_v = \frac{B \cdot \left(\gamma - \dfrac{c}{B}\right)}{K \cdot \tan(\phi)} \left(1 - e^{-K \cdot \tan(\phi) \cdot \frac{z}{B}}\right) + q \cdot e^{-K \cdot \tan(\phi) \cdot \frac{z}{B}} \qquad \text{Equation 2-24}$$

Equation 2-24 is similar to the Marston Equation 2-19, with the addition of the cohesion term. By adding in the assumption of cohesion Terzaghi's theory could be applied to all soils not just granular soils. Further, in his experiments Terzaghi determined that the extent of the arching effect only occurred at a distance equal to 5B above the base of the trap door. Based on this Terzaghi treated the upper part of the soil prism as surcharge acting on the lower prism.

2.4.6   Handy Arching Theory

Handy described the soil arch in a silo or ditch as a continuous compression arch that dipped downward taking the shape of a catenary (Handy 1985). He noted that the "arch" is typically represented in the literature as being a flat "arch" (Janssen 1895, Marston 1930). Handy explained that when the material is loosely added to silos and ditches that it is partially supported by friction on the side walls. He demonstrated this by expanding on the Krynine-Mohr circle principle as shown in Figure 2-27 (Krynine 1945). Krynine demonstrated that a granular material could not be represented by the trajectory of the major principle stress because it was not a continuous curve since the center of the arch became vertical (Handy 1985). Further, since there is shear at the wall interface, the stress cannot be a principle stress and the shear is located at point P_A and not at point M. Handy suggested that using K_a as the pressure coefficient at the face of the wall is unsafe when no safety factor is applied.
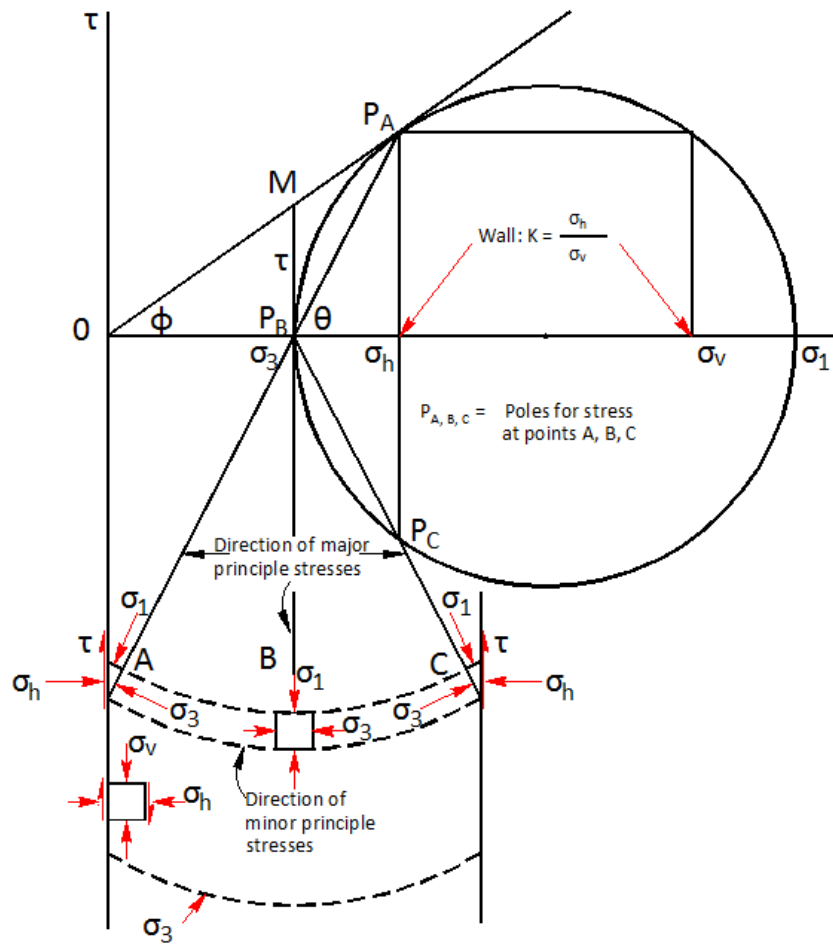
Figure 2-27 Krynine construction of Mohr circle

Krynine suggested using an earth pressure coefficient equal to that shown in Equation 2-25

$$K_K = \frac{1 - \sin(\phi)}{1 + \sin(\phi)}$$

Equation 2-25

Where: K_K =   Krynine earth pressure coefficient at wall interface (dim)

ϕ =   internal friction angle of backfill (deg)

Handy demonstrated that the principle stress at the face of the wall rotated by an angle θ. Using the equation of a catenary and the assumption that the vertical stress is

not equal to the average vertical stress at the face of the wall Handy derived the earth coefficient at the wall interface as shown in Equation 2-26. This yields a coefficient that is substantially greater than the active pressure coefficient and one that is slightly greater than the at-rest coefficient.

$$K_w = \frac{\cos^2\theta_w + K_a \cdot \sin^2\theta_w}{\sin^2\theta_w + K_a \cdot \cos^2\theta_w}$$

Equation 2-26

Where: K_w =   earth pressure coefficient at wall interface

             θ_w = $45° + \phi/2$

             K_a =   Rankine active earth pressure coefficient

In a silo, or ditch, the ends of the arch are supported by friction at the interface of the sidewalls as shown in Figure 2-28 and therefore cannot be a principle stress. Handy determined that the greater the magnitude of the wall friction the flatter the arch became.
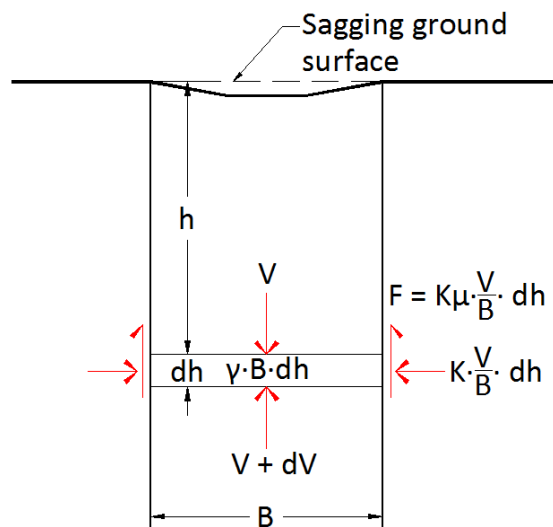
Figure 2-28   Differential element in classical representation of the flat soil arch

When the arch in Figure 2-28 is represented as being flat the frictional force (F) on the side wall is equal to the horizontal stress times a friction coefficient (μ). The

horizontal stress is the product of the vertical stress (V) times a lateral stress ratio (K). Based on the derivation of Equation 2-26 the lateral stress ratio is larger than the classical active pressure given by the ratio of the principle stresses σ_3/σ_1 and is due to the rotation of the principle stress at the wall interface.

The side force, F, acts to cumulatively reduce the total force, V, as the depth increases. This effect has been termed the "bin effect" (Ketchum 1919). Summation of the vertical force as a function of depth as shown in Figure 2-28 yields the following relationship (Handy 1985):

$$dV + 2 \cdot K \cdot \mu \cdot \frac{V}{B} \cdot dh = \gamma \cdot B \cdot dh \qquad \text{Equation 2-27}$$

Dividing by dh and integrating with respect to dV yields the Marston equation. The difference in the Marston equation is the application of a different value for K, e.g. K_w, as shown in Equation 2-28.

$$V = \gamma \cdot B^2 \cdot \frac{1 - e^{\left(-2 \cdot K_w \cdot \mu \frac{h}{B}\right)}}{2 \cdot K_w \cdot \mu} \qquad \text{Equation 2-28}$$

Where: V   =   total accumulated vertical force at depth h

              B   =   width of ditch

              K_w = σ_h/σ_{av}

              μ = $\tan(\phi)$

              σ_{av} = V/B

Substituting and rearranging Handy developed Equation 2-29 and is equal to the horizontal stress at depth h, for loading on a ditch conduit (Handy 1985).

$$\sigma_h = \frac{\gamma \cdot B}{2 \cdot \mu} \cdot \left[1 - e^{\left(-2 \cdot K_w \cdot \mu \frac{h}{B} \right)} \right]$$

Equation 2-29

2.4.7 Handy and Spangler Arching Theory

The theory prosed by Handy was expanded on by Handy and Spangler for fascia walls (Handy et. al. 2007). A fascia wall was defined by the authors as a wall that was close to, and approximately parallel to, a rock mass or resistant soil face. The distance between the fascia wall and the rock face is narrow as compared to the wall height.
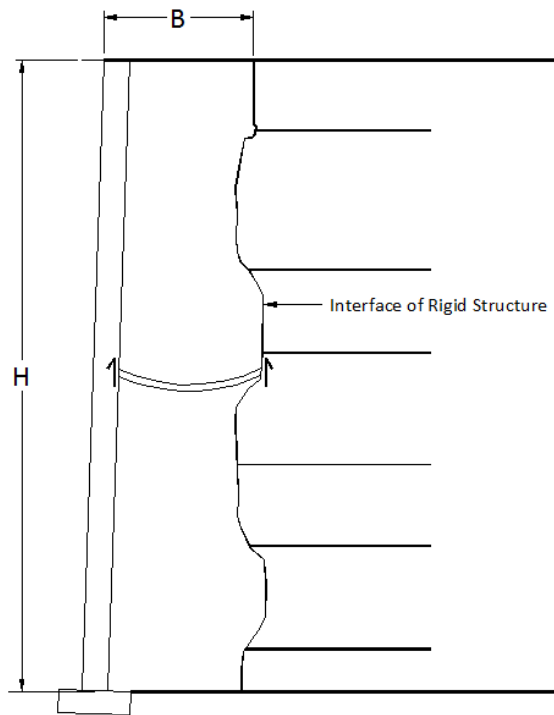
Figure 2-29   Handy and Spangler arching (Handy 2007)

Because of the narrow space the arching action would dominate the pressure distribution on the column of soil in the space. The lateral stress was defined in the equation provided by Handy as reproduced in Equation 2-29. It should be recognized that the term within the brackets in Equation 2-29 approaches 1 as the depth increases.

Based on this the maximum possible pressure in a fascia wall can be found by using Equation 2-30. Equation 2-30 is herein defined as the Handy Simplified Method.

$$\sigma_{h\_max} = \frac{\gamma \cdot B}{2 \cdot \tan(\delta)}$$

Equation 2-30

Where: σ_{h_max} = maximum horizontal pressure (kPa)

γ = unit weight of backfill (kN/m³)

B = width of silo (m)

δ = interface friction angle at wall face (dim)

The pressure at any depth can be found using Equation 2-31.

$$\sigma_h = \frac{\gamma \cdot B}{2 \cdot \tan(\delta)} \cdot \left(1 - e^{\left(-2K \cdot \tan(\delta) \cdot \left(\frac{z}{B}\right)\right)}\right)$$

Equation 2-31

Where: σ_h = horizontal pressure at depth z (kPa)

K = earth pressure coefficient (dim)

z = depth (m)

Handy(1985) demonstrated that the horizontal pressure follows the Rankine active earth pressure at the top of the structure to a shallow depth, then it rapidly decreases to a constant value that is substantially less than the equivalent Rankine active earth pressure.

Handy and Spangler (2007) proposed a simplified design method that used the maximum horizontal pressure at all depths (Equation 2-30). When the simplified method is used the fascia wall can be conservatively designed. When using this equation it is obvious that the choice of the earth pressure coefficient is therefore not important. The

controlling factor would be in the choice of the interface friction angle, δ. The Rankine active earth pressure is equal to Equation 2-32.

$$\sigma_h = K_a \cdot \gamma \cdot z$$
<div align="right">Equation 2-32</div>

Where: σ_h = horizontal pressure at depth z (kPa)

K_a = active earth pressure coefficient (dim)

γ = unit weight of cavity fill (kN/m^3)

z = depth (m)

Figure 2-30 is a plot of the Arching Equation (Equation 2-30) versus the Handy simplified equation (Equation 2-31) versus the common Rankine horizontal pressure (Equation 2-32). In this figure the structure height is assumed to be 15m and the width of the cavity is assumed to be equal to 1.8m for an aspect ratio equal to 0.12. The depth where the maximum pressure becomes constant is approximately equal to 4 times the width of the cavity or at a depth of 7.2m.
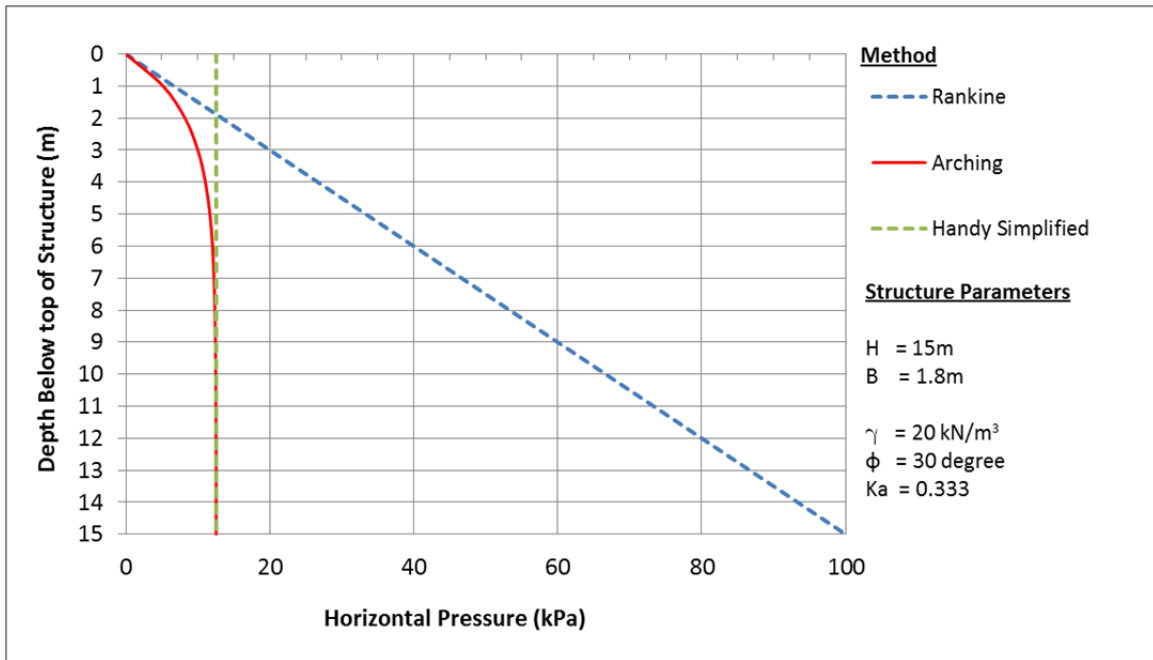
Figure 2-30   Graph depicting comparisons

2.5   Experimental Models

2.5.1   Introduction

As described in Section 2.4 arching theories are used to predict the reduction in lateral earth pressures for retaining structures in confined spaces. A search of the literature found two experimental models for retaining walls in confined spaces. These include work completed by Frydman and Keissar (1987) and Take and Valsangkar (2000). Both models were small-scale models that were placed in centrifuge systems. Frydman and Keissar tests were conducted on a wall that could rotate about its top and Take and Valsangkar tests were conducted on a wall that was fixed. These two models will be described and the findings reviewed in this section. The search of the literature did not find any full scale experimental models.

2.5.2   Frydman and Keissar (1987)

A series of centrifuge test were conducted to investigate the earth pressures on retaining walls in a confined space near rock. The aspect ratio was varied from 0.1 to 1.1. The Janssen arching theory for calculating silo pressure was used as the comparisons to the measured test pressures.

$$\sigma_x = \frac{\gamma \cdot b}{2 \cdot \tan(\delta)} \cdot \left(1 - e^{\left(-2K \cdot \left(\frac{z}{b} \right) \cdot \tan(\delta) \right)} \right)$$ Equation 2-33

Where: σ_x =   horizontal pressure at depth z (kPa)

b   =   distance between the walls (m)

z   =   depth form top of wall (m)

γ =   unit weight of backfill (kN/m^3)

K   =   earth pressure coefficient (dim)

δ =   interface shear (deg)

The model consisted of an aluminium box that contained an adjustable simulated rock face, a retaining wall that was capable of rotating about its base in controlled pulses using an electric motor-disk system, one LVDT to measure displacement, and two load cells to measure the pressure on the wall face. The backfill between the rock face and the retaining wall was sand with a maximum density of 16.4 kN/m^3, and uniformity coefficient (C_u) equal to 1.5 and an internal friction angle of 36 degrees. The sand was placed at a relative density equal to 70%. Direct shear test were performed on the interface of the wall face and the sand and were determined to range between 20-25 degrees.

Tests were performed at aspect ratios (b/H) equal to 1.1, 0.3, 0.22, 0.19 and

0.10. The model was spun to an initial acceleration corresponding to 43.7g which

simulated a wall height of 8.5m (Hu 2004). It was found that the use of the Janssen

Equation 2-33 could predict the lateral pressure on retaining walls with no movement,

e.g. K_o condition. However during movement it was determined that horizontal pressure

may be underestimated as progressive failure of the soil mass at the wall face

decreases the soil friction angle. It was proposed that a decreased friction angle value

be used in estimating K.

2.5.3   Take and Valsangkar (2000)

A series of centrifuge test were conducted to investigate the earth pressures on

unyielding retaining walls with narrow backfill widths. The aspect ratio was varied from

0.1 to 1.3. In this study the Janssen arching theory for calculating silo pressure was also

used as the comparisons to the measured test pressures (Equation 2-33).

The model consisted of an aluminium box that contained an adjustable simulated

rock face, a 140mm tall by 12.5mm thick retaining wall that was fixed, and six boundary

pressure cells that were evenly distributed over the height of the retaining wall to

measure the pressure on the wall face. The load cells were mounted in side individual

cavities using epoxy. The backfill between the simulated rock face and the retaining wall

was poorly graded sand with a maximum dry density of 15.7 kN/m^3, with a coefficient of

curvature equal to 1.0, and uniformity coefficient (C_u) equal to 2.2 and an internal friction

angle of 36 degrees. The sand was placed at a relative density equal to 79%. Direct

shear test were performed on the interface of the wall face and the sand for an

aluminium interface and 120A-grit sand paper interface. Test values were reported at the

peak and critical state.

Tests were performed at aspect ratios (b/H) equal to 1.31, 0.54, 0.27, and 0.11. Tests were performed at the prescribed aspect ratios for dense backfill and a smooth rock face $(\delta_{wall} = \delta_{rock})$, dense backfill and a rough rock face. Test for loose backfill were performed for aspect ratios equal to 0.27 and 0.11. The model was spun to an initial acceleration corresponding to 35.7g which simulated a wall height of 5m.

It was found that the use of the Janssen Equation 2-33 provides a good prediction of the lateral pressure on retaining walls with no movement, e.g. K_o condition. Further it was verified that it is reasonable to use an average interface friction angle for materials with dissimilar interface friction angles in the Janssen silo equation. The authors cautioned that although Janssen's equation is not complex for the case of unyielding retaining walls, the choice of the parameter K and the mobilized boundary friction angle δ-mob during the translation from at-rest to active conditions requires considerable engineering judgment. They stated that is safe to assume that neither the mobilized friction angle nor the lateral earth pressure coefficient will be constant with depth. During wall movement the soil will be in an intermediate state between at-rest and active conditions (Zhang et al. 1998).

2.6   Numerical Models

2.6.1   Introduction

Two numerical models that demonstrated soil arching were described in the literature. Both of these numerical model results were compared to experimental centrifuge models described in Section 2.5 as performed by Frydman and Keisser (1987) and Take and Valsngkar (2001).

2.6.2 Finite Element

A study titled, *Design Considerations for MSE Retaining Walls Constructed in Confined Spaces*, sponsored by the Texas Department of Transportation and performed by the Center for Transportation Research at the University of Texas at Austin performed numerical models on MSE walls in front of stable faces (Kniss et. al 2007). The two-dimensional FE program Plaxis was used to model a narrow cavity that was flanked by rigid, non-deformable walls. The FE model was then compared to experimental centrifuge model studies performed by Frydman and Keisser (1987) and Take and Valsngkar (2001). In the FE study a model structure was constructed that had three sides, e.g. left-side, right-side and base. In this study the base was completely fixed and the side fixity was varied from total fixity, to fixed in the horizontal direction and free in the vertical direction. Several parametric studies were introduced where the characteristics of the wall, backfill-wall interface, soil constitutive parameter, and the wall aspect ratio were varied.

Three soil models were investigated and include the Linear Elastic, Mohr-Coulomb and the Hardening-Soil models. Based on parametric studies it was determined that the Hardening-Soil constitutive model predicted horizontal pressures that were in agreement with experimental data and the Handy and Spangler arching equation (Equation 2-31). The liner elastic constitutive model did not properly capture plastic deformation that was occurring in the study and therefore was discounted as being a reasonable soil model. Based on parametric studies it was demonstrated that when the Mohr-Coulomb model was used that the selection of Poisson's ratio (ν) had a large influence on the equivalent earth pressure coefficient, K_{eq}. In a parametric study using the Hardening-Soil model it was determined that the internal friction angle (ϕ') of

the material had the most influence on the equivalent earth pressure coefficient, K_{eq}. Further, in the parametric studies it was demonstrated that the unit weight (γ) and Young's modulus (E) had little influence on the equivalent earth pressure coefficient, K_{eq}. Because of the difficulty in accurately predicting Poisson's ratio in soils, coupled with the fact that it is relatively easy to predict the internal friction angle of soils, it was determined that that the Hardening Soil model should be used in the FE model.

Also demonstrated in the parametric study it was shown that plate elements did not have to be used when defining the non-deformable wall. It was shown that using total fixity at the boundary of the wall sections had the same effect as using plates. In addition, it was determined that an interface element was required at the wall face and that it should include an interface reduction factor. In the study the interface reduction factor, R_{int}, was determined using Equation 2-34. In Equation 2-34 the interface friction angle (μ) was set equal to 2/3 of the internal friction angle of the soil based on recommendations of AASHTO 2012.

$$R_{int} = \frac{\tan(\mu)}{\tan(\phi')}$$
<div align="right">Equation 2-34</div>

Where: R_{int} =   interface reduction factor (dim)

                ϕ' =   internal friction angle of backfill (deg)

                μ =   interface friction angle equal to $\frac{2}{3} \cdot \phi'$

Based on the parametric studies it was determined that for non-deformable walls that arching was occurring in the confined space. It was demonstrated by parametric studies using the aspect ratio that as the confined space decreased the ability to predict

arching increased. It was concluded that the Handy and Spangler equation (Equation 2-31) could be used and was a reasonable method to predict the horizontal pressure in a confined space.

2.6.3   Limit Equilibrium

Leshchinsky and Hu. (2004) performed a study on limited backfill space in segmental retaining walls. This study used conventional slope stability analysis using a limit equilibrium (LE) approach to predict the total horizontal force that was required to support a soil mass in a confined space. The LE model results were then compared to a Finite-Difference (FD) procedure using the software program FLAC. The study determined that it was possible to use LE to accurately predict the force to be resisted in the confined space. From this study design charts were developed for designing MSE walls with various aspect ratios.

The model in the study consisted of a 5m tall wall that was off set from the retained fill comprising a sloping rock face. The wall was assumed to be supported on a rock foundation. The introduction of the rigid rock eliminated the effect of external stability and reduced the problem to purely an internal stability problem. A single layer of soil reinforcing was placed at a distance equal to 1/3 the height of the structure (Figure 2-31). In order to prevent a pullout mode of failure the soil reinforcing with a high pullout capacity was embed a large distance into the rock formation. This reduced the internal mode of failure to a single tensile resistance failure.
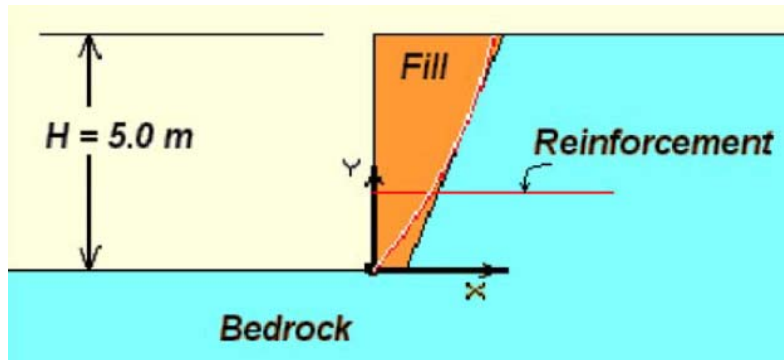
Figure 2-31   Limit equilibrium model structure (Leshchinsky et. al. 2004)

The software program ReSSA developed by Adama Engineering was used to perform the parametric study. ReSSA is an interactive program used to assess the rotational and translational stability of slopes. ReSSA allows for the introduction of soil reinforcing in the structure. A rotational failure mode using the Bishop method of analysis was specified. The soil reinforcing was given an initial tensile strength and the model was solved. The tensile strength of the soil reinforcing was reduced, or increased through trial and error until a state of equilibrium was reached; i.e. the computed factor of safety was equal to 1.0.

The structures aspect ratio (B/H), the rock face slope angle (m), and the internal friction angle of the soil was varied in a parametric study and compared with the results of the same models created in FLAC.
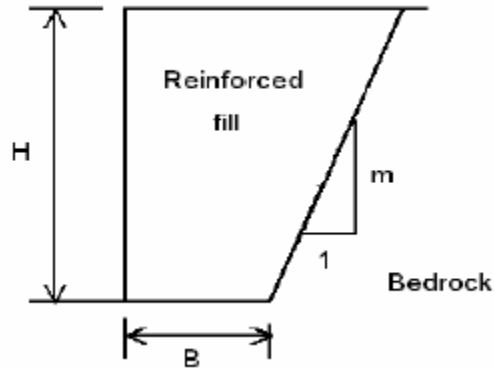
Figure 2-32   Limit equilibrium model structure parameters

In addition, and as verification, a model was constructed and compared to the experimental study performed by Frydman and Keissar (1987). A full treatment of the defined problems can be found in the reference by Hu (2004). Based on the parametric study it was concluded that it is possible to use a limit equilibrium analysis to determine the total force that is required to be resisted by the soil mass in a structure that is near a rigid face.

2.6.4   Summary

This chapter provided a literature review that was conducted on retaining structures, earth pressure theories, soil arching, experimental programs, and numerical modelling of retaining structures in confined spaces. The sections reviewed are required to fully understand how the horizontal pressure and the corresponding forces in a 2-Stage structure can be determined and how they relate to the fundamental earth pressure theory. The first section reviewed different types of retaining structures concluding with a description of the 2-Stage retaining structure. The second section provided general information on earth pressure theories and their influence on the design of MSE Structures. The third section reviewed how the forces in a 2-Stage MSE

can be correlated to, and determined from, the theory of soil arching. The fourth section reviewed experimental data that confirmed that the theory of arching equation proposed by Janssen and expanded on by Handy and Spangler is appropriate in predicting the horizontal pressure in a retaining structure in a confined space. The fifth and final section reviewed numerical modelling of structures in confined spaces, how the models were constructed and how the results were verified to experimental data in order to determine the horizontal pressure in a confined space.

Chapter 3

Large-Scale Test Program

3.1   Introduction

In a 2-Stage MSE structure the Veneer is attached to the Stage-1 flexible faced MSE using an adjustable connection element. One connection method that is used in 2-Stage structures allows the connector end that is attached to the Stage-1 facing to move in the vertical direction (Taylor 2000). Movement is allowed in order to prevent overstress of the connection in the event that some internal settlement of the cavity occurs. A large scale test structure was constructed in order to visually investigate the connector that attaches the Veneer to the Stage-1 facing during differential settlement of a 2-Stage wall (Figure 3-1).

A structural steel frame and platform was fabricated to support one panel of the 2-Stage structure. The steel frame and platform was used to place the segmental concrete panel, connect it to the Stage-1 MSE structure and to place cavity fill material. The steel platform combined with the panel and cavity fill could be raised and lowered using a hydraulic actuator. The 2-Stage structure was constructed and the platform was raised forcing the 2-Stage facing and cavity fill to move as a monolithic mass simulating settlement of the Stage-1 MSE. Four tests were conducted where the platform was raised 25mm, 50mm, 100mm and again at 100mm. After each test the cavity fill was exhumed and the condition and position of the turnbuckle connector was examined as well as the condition of the Stage-1 facing at the point of connection. In the final 100mm test the top-outside turnbuckle connector was left visible so the movement of the turnbuckle could be visually examined during the raising of the platform.

Figure 3-1 Test wall

3.2   Test Wall Components

The test wall was constructed in Mansfield, Texas, on the property of Big-R Bridge. The 2-Stage wall system was supplied by Atlantic Industries Ltd. (AIL) and represented their proprietary 2-Stage structure. The Stage-1 wall area was 150 square meters. The test frame consisted of structural steel tubing and was fabricated by Big-R Bridge of Mansfield, Texas. The test panels were fabricated by Speed Fab-Crete of Kennedale, Texas. The backfill was supplied by Vulcan Materials of Ft. Worth, Texas from their 342-Weatherford Quarry.

3.2.1   Stage-1 Wall System

The Stage-1 MSE wall consisted of a flexible welded wire wall (Figure 3-2, Figure 3-3 and Figure 3-4). The face panel and soil reinforcing were fabricated from a single sheet of welded wire mesh. The face panel was 0.762 meters tall and the soil reinforcing was 3.048 meters in length. The wall height was 3.0 meters. The aspect ratio was

therefore equal to 1.00. The wall length was 19.9 meters. The backfill consisted of non-cohesive manufactured sand with a unit weight of 18 kN/m^3 and an internal friction angle of 43 degrees. The optimum moisture content was 14.4%. At the front face of the MSE wall 19mm angular rock was placed for a width of 0.610 meters.
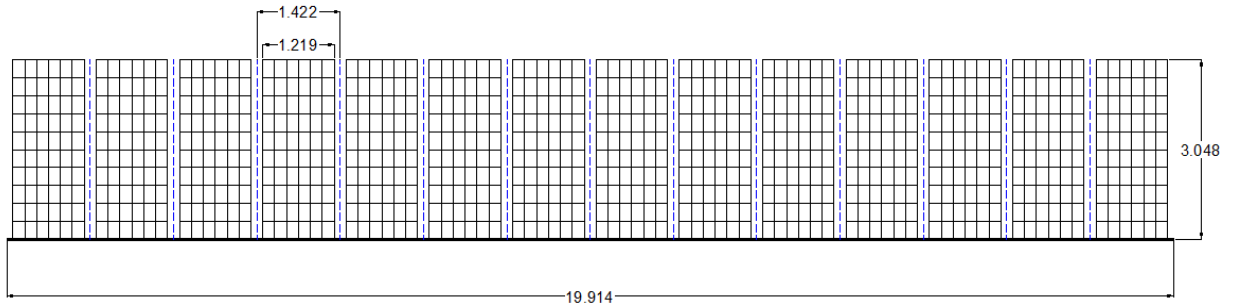
Figure 3-2   Plan view of test wall
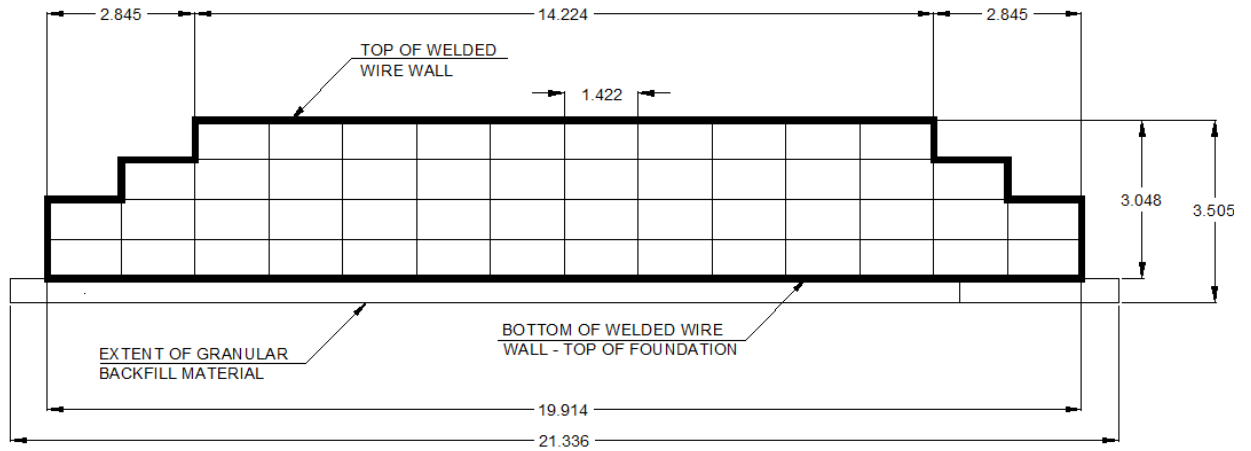
Figure 3-3   Elevation view of test wall
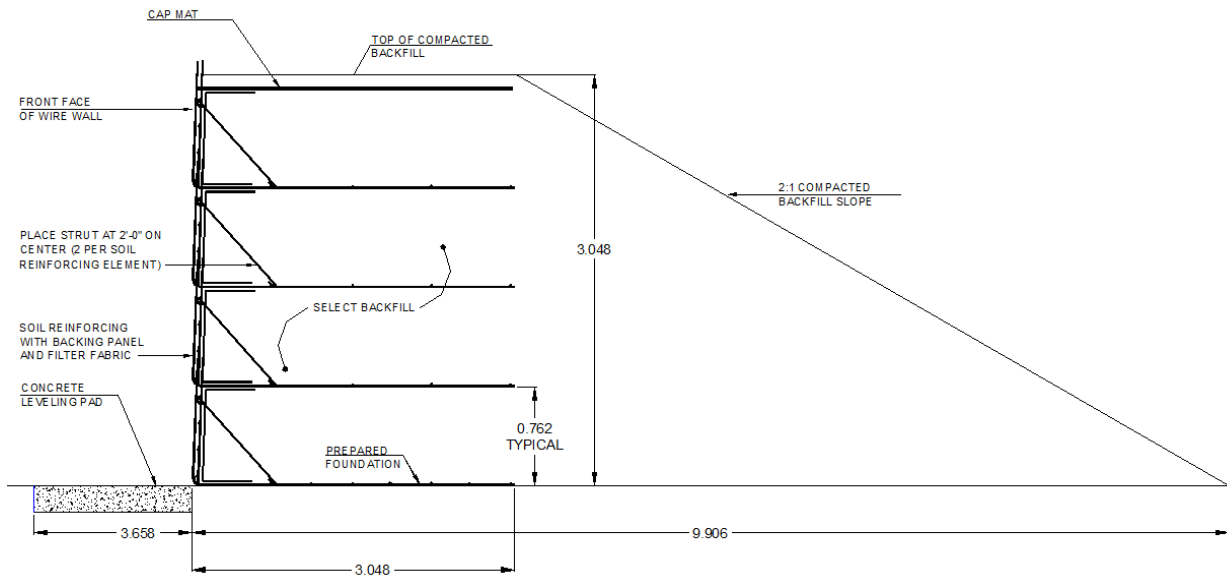
Figure 3-4   Cross section of test wall

The welded wire wall was constructed according to the recommendations of AIL.
The foundation was excavated to a depth of 0.610 m and at a distance 0.610 m past the
extent of the soil reinforcing and replaced with compacted backfill (Figure 3-5). The
facing panel, soil reinforcing and backing panel were placed on the prepared foundation
(Figure 3-6). To prevent the facing rock from sloughing out of the face of the wall a
geotextile filter fabric was placed (Figure 3-7). The sand backfill was installed in 0.250 m
compacted lifts (Figure 3-8). The backfill was compacted by the method of rolling wheel
(Figure 3-9) followed by 2 passes of a 10-ton vibratory roller (Figure 3-10). The backfill
density for each lift placement was determined by the Method of Sand Cone in
conformance with ASTM D1556. The backfill moisture content was determined using the
Speedy-Moisture Meter test procedure in conformance with ASTM D4944 (Figure 3-11).
At the interface of the sand backfill and the rock backfill a geotextile filter fabric was
placed (Figure 3-12). The face rock was compacted with the use of a light weight

74

mechanical plate compactor (Figure 3-13). The MSE wall was constructed to the required height and left undisturbed for 30 days (Figure 3-14).

Figure 3-5   Foundation preparation

Figure 3-6   Stage-1 MSE wall construction

Figure 3-7   Facing geotextile placement

Figure 3-8   Backfill placement

Figure 3-9   Sand backfill compaction – wheel rolling

Figure 3-10   Sand backfill compaction – smooth drum rolling
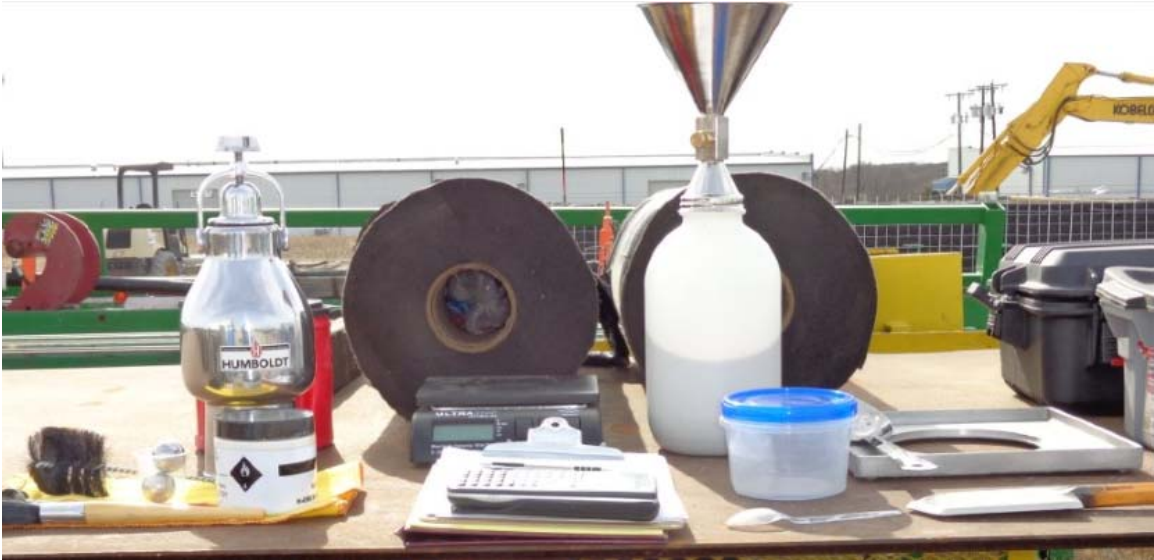
Figure 3-11   Backfill testing equipment

Figure 3-12   Interface geotextile separation

Figure 3-13   Facing rock compaction – plate compactor

Figure 3-14   Finished Stage-1 MSE wall

3.2.2   Test Frame

The test frame was fabricated from structural steel components (Figure 3-15). The frame was placed on a reinforced concrete slab that was cast in front of the Stage-1 wall. The frame was wide enough to fit the SCP panel in and deep enough to form a 0.456 meter wide cavity between the Stage-1 MSE wall and the back face of the SCP. The segmental concrete panels were attached to the Stage-1 MSE wall using turnbuckle connection components (Figure 3-14, Figure 3-19, Figure 3-20 and Figure 3-22). The frame was fitted with removable plywood bulkheads on each end. The bulkheads were necessary in order to remove the cavity fill material from within the cavity after each test. After placement of the bulkhead the cavity was filled with 19mm concrete aggregate. To secure the test frame from rotation it was tied back at the top of the frame using a chain that was fixed to an excavator positioned behind the MSE structure. Figure 3-16 and Figure 3-17 show the test frame setup.
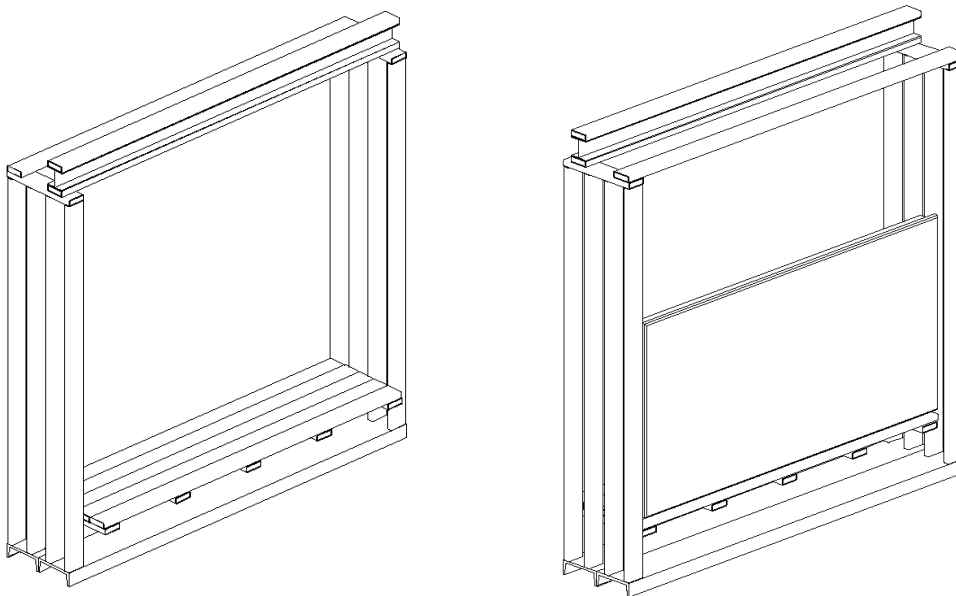
Figure 3-15   Isometric of test frame set-up
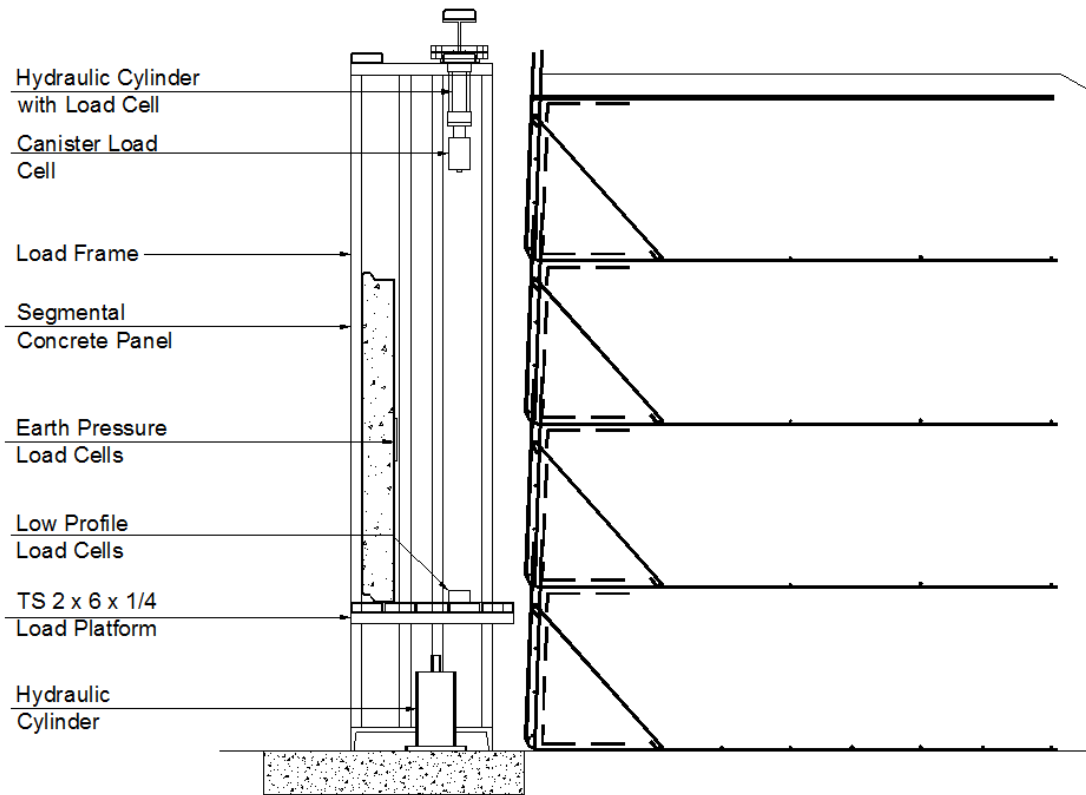
Figure 3-16   Cross section of test frame set-up

Figure 3-17   Frame Setup

3.2.3   Segmental Concrete Panel

The segmental concrete panel nominal dimensions were 1.524 m tall and 3.048 m in length (Figure 3-18). The thickness of the panel was 0.152 meters. The 28 day compressive strength (f'_c) of the concrete was equal to 35 MPa and had a modulus of elasticity (E_c) equal to 28 x 10^3 MPa. Cast integral to the panel and extending from the back face of the panel were wire loop anchors. There were two rows of two columns of six individual anchors that were spaced at 0.152 mm centers. The rows of panel anchors were spaced at 0.762 meters on center. The anchor extended from the back of the panel 0.150 meters and consisted of dual W11 wires. The panel was cast with a tongue and groove joint configuration.
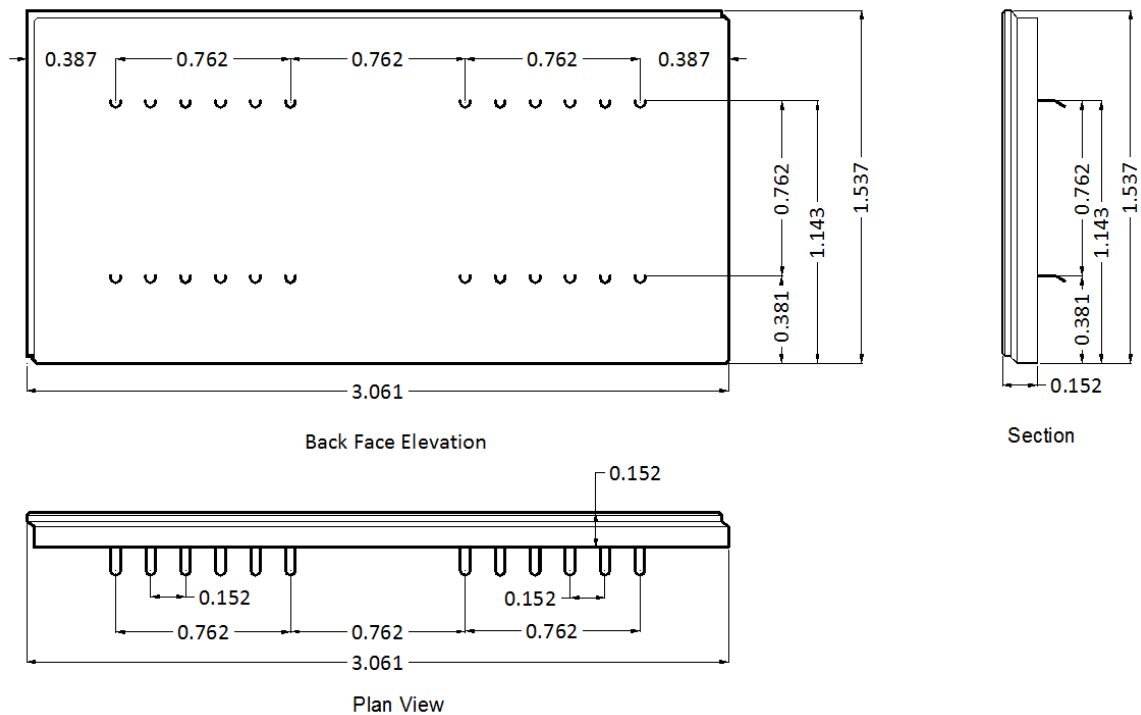
Figure 3-18   Segmental concrete panel dimensions

82

3.2.4   Turnbuckle

The Stage-2 concrete panels were attached to the Stage-1 welded wire wall face using a Jaw and Jaw Turnbuckle. The turnbuckle type was supplied by AIL and was fabricated by MacMor Industries of Winnipeg, Manitoba, Canada. The turnbuckle was 12mm diameter x 150mm drop forged steel component that was hot-dip galvanized. The peak load reported by the manufacturer was 65 kN. The turnbuckle Jaw was attached to the Stage-1 wall vertical facing wire so it was free to move in the vertical direction. The Jaw end that was attached to the segmental concrete panel was fixed in the horizontal and vertical direction but was free to rotate. There were a total of 6 turnbuckles attached to the SCP and the Stage-1 MSE wall. There were 3 turnbuckles in two rows.
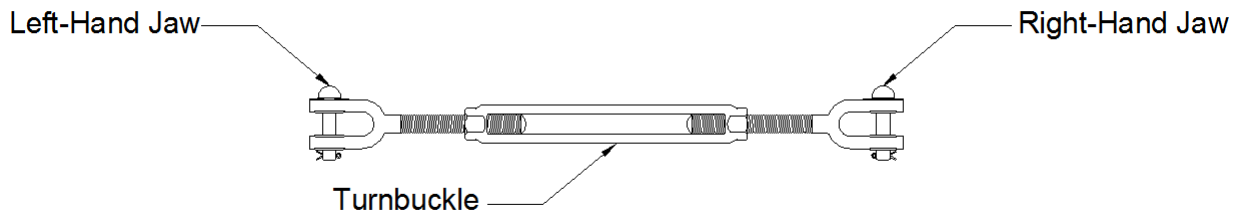
Figure 3-19   Side view of Jaw & Jaw turnbuckle

Figure 3-20   Jaw- & Jaw Turnbuckle attached to 2-Stage structure

83

3.3　Test Setup

The test frame was placed in front of the Stage-1 MSE and on the concrete levelling pad. The SCP was placed in the frame. As a safety measure to prevent the SCP from being able to dislodge from the steel frame, steel beams consisting of rectangular tubes were bolted to the front of the frame (Figure 3-21). Plywood bulkheads were then secured to the sides of the frame. The turnbuckles were connected to the SCP anchor and to the Stage-1 wall. At the Stage-1 wall face the turnbuckle was tied into position using low-strength tie wire. The turnbuckles were placed at a 3:1 angle (Figure 3-22). The angle sloped up from the Stage-1 wall face. Rock backfill was then dumped into the cavity using the method of free fall. The cavity fill was levelled as the material was placed using a shovel (Figure 3-23). Cavity fill placement continued until the fill was level with the top edge of the panel (Figure 3-25).

Figure 3-21　Placement of SCP with safety beams

Figure 3-22   Turnbuckle attached to Stage-1 and Stage-2

Figure 3-23   Placement of cavity fill

Figure 3-24   Top turnbuckle and cavity fill

Figure 3-25   Final level of cavity fill

3.4   Test Procedure

Four tests were performed. The tests consisted of displacing the platform that the panel and cavity fill were placed on upward using a hydraulic actuator (Figure 3-26). The platform was raised 25 millimeters (1 in.), 50 millimeters (2 in.) (Figure 3-27) and 100 millimeters (4 in.). The 100 millimeter test was performed twice. The platform was shimmed into the final displaced location and the hydraulic actuator load was released.

At the conclusion of each test the cavity fill was exhumed and the condition of the turnbuckle and Stage-1 wall face were inspected and documented.

Figure 3-26   Hydraulic actuator to raise and lower platform

Figure 3-27   Platform raised 50 millimetres

3.5 Test Results

All of the tests demonstrated that the turnbuckles were able to move up the Stage-1 wall vertical facing wire. Each of the 6 turnbuckles, 3 at the bottom, and 3 at the top, moved approximately the same distance during the application of each of the displacement loads. The tests at 25mm (Figure 3-28) and 50mm (Figure 3-29) showed no distortion of the Stage-1 facing wire. The 100mm test showed distortion of the Stage-1 facing wire (Figure 3-30) consisting of an outward bow, or pulling away from the Stage-1 face. On inspection of the facing wire at the 100mm displacement it was observed that the vertical facing wire below where the turnbuckle was attached developed a small crack at the interface of the weld between the horizontal wire and vertical wire (Figure 3-31). This crack occurred near the L-bend of the soil reinforcing and the facing panel. No cracks were observed in either the 25mm or the 50mm displacement.

Figure 3-28   Turnbuckle at 25mm displacement

Figure 3-29   Turnbuckle at 50mm displacement

Figure 3-30   Turnbuckle at 100mm displacement

Figure 3-31   Crack at Weld at 100mm Displacement

It was hypothesized that the distortion and subsequent crack at the interface of the weld at 100mm of displacement was due to the circular Jaw-Eye moving past the horizontal wire of the backing panel that was located in the face of the wall (Figure 3-32 and Figure 3-33). As the turnbuckle moved past the horizontal facing wire it would place a prying force on the vertical wire at the location of the weld.

To prove this theory the 100mm test was performed again. The turnbuckles were attached to vertical facing wires that had not been previously connected to the stage 2 face (i.e., virgin wires). In order to view the movement of the turnbuckle during application of the load to the platform, the outside top turnbuckle was left visible. This was accomplished by placing the bulkhead inside the cavity fill (Figure 3-34) in a manner that it was free to move up the wall face. The load to the hydraulic actuator was applied raising the platform 100mm. During application of the platform load the movement of the turnbuckle was observed and videotaped. During application of the displacement the Jaw did move out and past the horizontal wire as postulated (Figure 3-35).

Figure 3-32   Jaw-Eye

Figure 3-33   Interference of Jaw-Eye with horizontal wire at 50mm displacement

Figure 3-34   Isolated Top-Outside turnbuckle

Figure 3-35   Movement of turnbuckle Jaw-Eye past wire (videotape photo)

3.6   Test Conclusion

Based on the testing it was concluded that during settlement of the Stage-1 wall, and when the turnbuckle is connected to the facing vertical wire, that the turnbuckles were free to move vertically. Further, it was recognized that the configuration of the horizontal facing wires at the location were the turnbuckle is connected to the vertical wire are critical to allowing the turnbuckle to move without interference and distortion to the facing connection wire. Based on testing observations, it is recommended that 2-Stage structures include details for connections that allow for vertical unobstructed displacement at both connection elements. Further, it is recommended that the detail include limitations that prevent a horizontal wire from being welded near the bend of the L-Facing to prevent possible structural damage of the vertical facing wire.

Chapter 4

Numerical Model

4.1   Introduction

Numerical modeling (i.e., finite element FE method) was used to investigate the

structural capacity of the 2-Stage MSE structure. The computer program Plaxis 2DAE

(Plaxis 2014) that was developed at the Technical University of Delft in Delft,

Netherlands, will be used for the FE modelling. Plaxis was developed to model soil

interaction problems by the method of FE. The Plaxis software was selected to be used

base on the following:

1.   The large amount of literature that was found for modeling MSE

structures

2.   Ability to model staged construction

3.   Ability to model variable interface reactions of the Stage-1 MSE and the

Stage-2 SCP facing.

4.   Ability to model internal settlement of the Stage-1 wall by using a line

displacement.

5.   Ability to model the turnbuckle connectors that join the Stage-1 facing to

the Stage-2 facing

4.2   Numerical Model Objective

A control model that is considered the static case was constructed to compute

the horizontal stresses in the cavity and the forces in the turnbuckle connectors of a

stable 2-Stage Structure. The FE control model was constructed based on the results of the parametric studies that were conducted by Kniss et al. The results of the FE control model were compared to results from numerical (Kniss et al., 2007 and Leshchinsky et al., 2003) and analytical models (Handy and Spangler 2007) found in the literature. After the control model was established analysis was performed to determine the effects that internal settlement of the Stage-1 MSE structure has on the horizontal stresses in the cavity and on the turnbuckle forces of the 2-Stage structure. As validation of the 2D control model, and to understand the interaction of the turnbuckle with the cavity fill, a 3D model was created using the Plaxis 3D software (Plaxis 2013). A summary of the objectives of the numerical model is as follows:

1. Determine if arching occurs in the cavity of a static 2-Stage structure using the staged construction approach.

2. Determine the forces that are required to be resisted by the turnbuckles of the static 2-Stage structure.

3. Study the influence that internal settlement of the Stage-1 structure has on the horizontal stresses in the cavity and on the forces in the turnbuckle.

4. Study the influence that the interface friction angle of the Stage-1 and Stage-2 facing has on the horizontal stresses in the cavity and on the forces in the turnbuckle.

5. Study the influence that the internal friction angle of the cavity material has on the horizontal stresses in the cavity and on the forces in the turnbuckle.

6.   Study the influence that the fixity of the turnbuckle has on the forces in

the turnbuckle.

7.   Study the influence that modeling the turnbuckle as a node-to-node

anchor in the Plaxis 2D has when compared to a beam element in the

Plaxis 3D.

4.3   2D Control Model

The static 2D control model consisted of a 2-Stage MSE structure (Figure 4-1).

The physical space of the model was set up in the shape of "U". The left side of the U

defined the Stage-2 segmental concrete panel and the right side of the U defined the

Stage-1 MSE welded wire wall. The bottom of the U defined the base of the cavity, or

the foundation. The height of the model was set equal to 9.144 meters (30.00 feet) and

the width of the cavity was set equal to 0.457 meters (1.50 feet). The Stage-2 face

consisted of 6 segmental concrete panels (SCP) that were stacked one atop the other.

Each of the SCP height was equal to 1.524 meters (5.00 feet). Between each SCP an

interface plate was placed to model structures with and without bearing pads. Attached

to the top and bottom quarter points of each of the SCP and extending into the fill and

attached to the Stage-1 facing were turnbuckles for a total of 12 turnbuckles in the

model. Placed inside the cavity was a free flowing, non-cohesive, granular material.
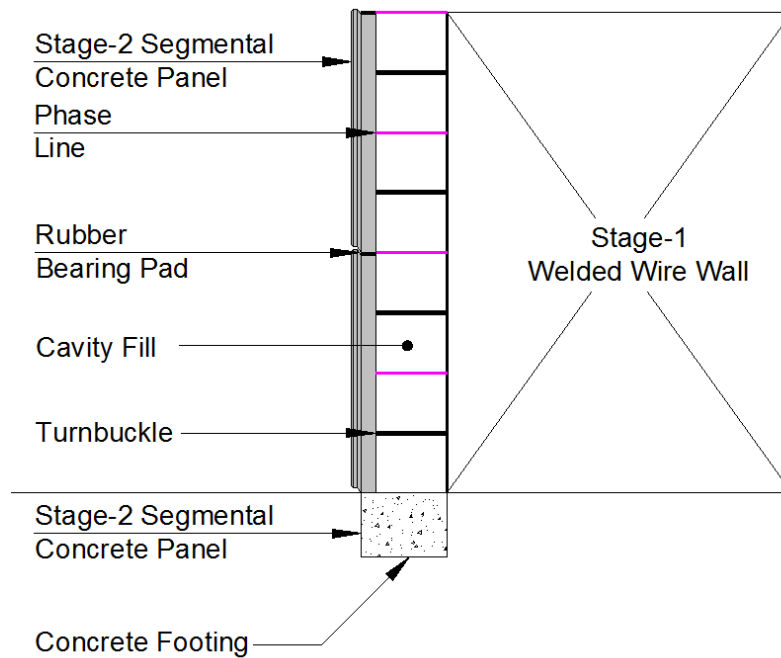
Figure 4-1 2-Stage MSE structure components

The 2-Stage components consisting of the SCP, interface plate, and welded wire wall were model as plate elements that had an axial stiffness (EA) and a bending stiffness (EI). Interface elements were applied at both the left and right side of the U and at the base of the U. In the 2D model the turnbuckle connector was modeled as a node-to-node anchor that was defined with an axial stiffness (EA). In the 3D model the turnbuckle connector was modeled as a beam element that was defined with an area (A), a Young's modulus (E) and a moment of inertia (I). Boundary conditions were defined for the right side, left side and base of the U-structure. The cavity space of the U-structure that was between the Stage-2 left side and the Stage-1 right side was filled with a non-cohesive backfill material (Figure 4-2). Staged construction that was similar to the construction practice used in the field was used to build the model.
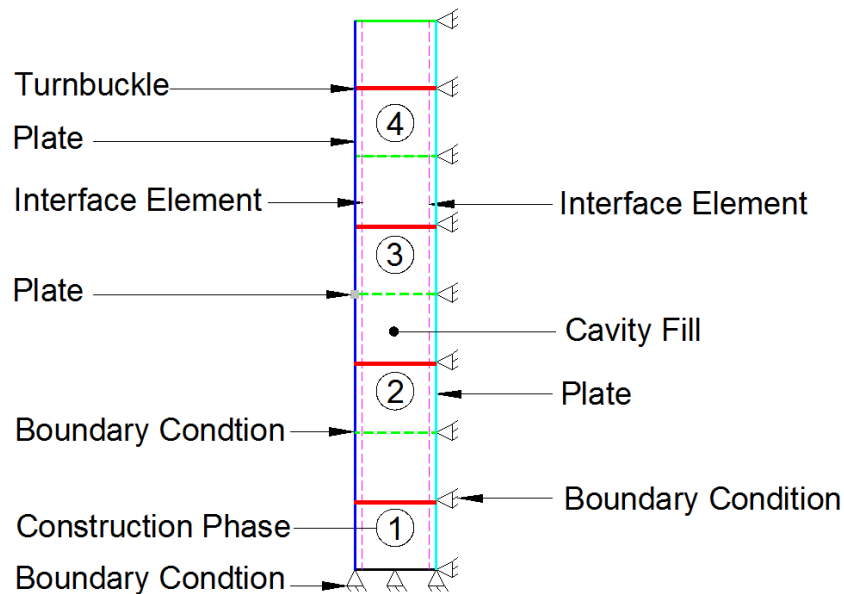
Figure 4-2 Control Model – Case 1

4.3.1 Segmental Concrete Panel (SCP)

The Stage-2 SCP were modelled as individual, isotropic plates. The SCP was located on the left side of the U. The SCP height was 1.524m (5.00 feet), the length (out of plane) was 1.524m (5.00 feet) and the thickness was 152mm (6 inches). The plate was modelled as a 5-node element in order to match the 15 node soil element (Plaxis 2014). In Plaxis 2D the plate's material parameters are modelled with a user input axial stiffness (EA) and bending stiffness (EI). From these inputs an equivalent plate thickness d_{eq}, was calculated. The equivalent plate thickness was required because the model is two-dimensional (2D plane strain) and the properties are smeared (out of plane) per meter of structure. The unit weight per meter of panel per meter of the structure was also input by the user.

The calculated area of panel per meter of wall per meter of height is given in Equation 4-1.

$$A_c = L \cdot b \rightarrow 1(m) \cdot 0.152(m) = 0.152 \cdot m^2 / m \qquad \text{Equation 4-1}$$

Where L is the out of plane length of the panel (assumed per meter of panel) and b is the width of the panel.

The concrete panel was assumed to have a 28 day compressive strength (f'_c) equal to 34.5 MPa with a modulus of elasticity (E_c) equal to 28 x 10^3 MPa. The axial stiffness per meter of panel per meter of wall was calculated using Equation 4-2. The bending stiffness per meter of wall was calculated using Equation 4-3. The equivalent plate thickness (d_{eq}) was calculated using Equation 4-4. Poisson's ratio was assumed to be equal to 0.20 and was the low end value for normal strength concrete (Nilson and Winter 1991).

$$E_c A_c = 0.152 \frac{m^2}{m} \cdot 28000 \text{ MPa} = 4.277 \text{ x } 10^6 \frac{kN}{m} \qquad \text{Equation 4-2}$$
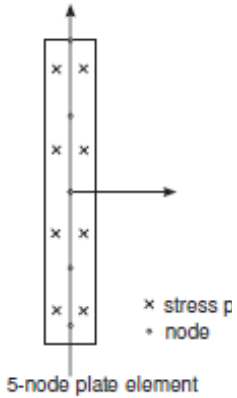
$$E_c I_c = E_c \cdot \frac{h \cdot b^3}{12} = E_c \cdot A_c \cdot \frac{b^2}{12} \rightarrow 28E3 \text{ MPa} \cdot \frac{0.152^2 \cdot m^2}{12} = 8.277E3 \frac{kN \cdot m^2}{m} \qquad \text{Equation 4-3}$$

$$d_{eq} = \sqrt{12 \cdot \frac{E_c \cdot I_c}{E_c}} \rightarrow \sqrt{12 \cdot \frac{8.277E3 \frac{kN \cdot m^2}{m}}{4.277 \text{ x } 10^6 \frac{kN}{m}}} = 0.152m \qquad \text{Equation 4-4}$$

Based on the above calculations the Stage-2 SCP plate element was modeled using the parameters given in Table 4-1.

Table 4-1 Plate model parameters for Stage-2 SCP

Properties	Variable	Value	
Isotropic		yes	
Axial Stiffness	EA1	4.277×10^6 kN/m	
Axil Stiffness	EA2	4.277×10^6 kN/m	
Bending Stiffness	EI	8.277×10^3 (kN·m2)/m	
Equivalent Plate Thickness	deq	0.152 m	
weight	w	3.591 kN/m/m	
Poisson's ratio	ν	0.200	

× stress p
• node
5-node plate element

4.3.2   Bearing Pad

At the interface between the horizontal joints of successive concrete panels neoprene bearing pads are placed. The neoprene bearing pad prevents direct concrete-to-concrete contact between the SCP. Based on research of varying MSE system details, for a structure height of 9.144m and a SCP with dimensions of 1.524m x 1.524m panel, 2 bearing pads are commonly used and are placed at the quarter points of the panel along the top edge. The bearing pads consist of discrete neoprene elements with dimensions equal to 75mm x 150mm x 19mm. The search of the literature did not find any FE models using the aching theory that included consideration of the bearing pads. The literature search did find a numerical analysis that considered the compressibility of the bearing pads in MSE. This study was undertaken to understand the effect that the facing vertical stiffness, that was assumed to be a function of the elastomeric bearing pads that were placed in the horizontal joints between panels, had on the load capacity of steel reinforced soil (Damians et. al., 2013).

The bearing pads are free to compress during placement of the panels. In order to model the compression of the bearing pad they are modelled as an isotropic plate. As

before, the plate is modeled as a 5-node element. In Plaxis 2D the plates are modeled with a user input axial stiffness (EA) and bending stiffness (EI). From these inputs an equivalent plate thickness d_{eq}, is calculated. As before, the equivalent plate thickness is required because the model is two-dimensional. The bearing pad is 75mm x 150mm x 19mm. From actual testing of the bearing pad in conformance with ASTM D575 – Rubber Properties in Compression, the modulus for the bearing pad for this model is specified as being equal to 13.8 MPa.

Based on the assumption that there are 2 bearing pads for every 1.524m panel there is one bearing pad placed every 0.762m on center. From this configuration the number of bearing pads per meter of wall is equal to 1.312 as calculated in Equation 4-5.

$$n = \frac{n_{bp}}{L_p} \to \frac{2}{1.524\,(m)} = 1.312 \frac{1}{m} \qquad \text{Equation 4-5}$$

Where n_{bp} is the number of bearing pads and L_p is the length of the segmental concrete panel. The area of the bearing pad per meter of wall is calculated using Equation 4-6.

$$A_{bp} = n \cdot b_{bp} \cdot L_{bp} \to 1.312 \cdot \left[0.075\,(m)\right] \cdot \left[0.150\,(m)\right] = 0.015 \frac{m^2}{m} \qquad \text{Equation 4-6}$$

Where b_{bp} is the width of the bearing pad and L_{bp} is the length of the bearing pad. The axial stiffness of the bearing pad is calculated using Equation 4-7 and the bending stiffness of the bearing pad is calculated using Equation 4-8. The equivalent width of the bearing pad is calculated using Equation 4-9.

$$E_{bp}A_{bp} \rightarrow = 13.8 \text{ MPa} \cdot 0.015\left(m^2\right) = 210\left(\frac{kN}{m}\right) \qquad \text{Equation 4-7}$$

$$E_{bp}I_{bp} = E_{bp} \cdot \frac{A_{bp} \cdot L_p^2}{12} \rightarrow 13.8 \cdot \text{MPa} \cdot \frac{0.015 \cdot \frac{m^2}{m} \cdot \left(0.075 \cdot m\right)^2}{12} = 0.097 \cdot \frac{kN \cdot m^2}{m} \qquad \text{Equation 4-8}$$

$$d_{eq} = \sqrt{12 \cdot \frac{E_{bp} \cdot I_{bp}}{E_{bp} \cdot A}} \rightarrow \sqrt{12 \cdot \frac{0.097 \frac{kN \cdot m^2}{m}}{210 \frac{kN}{m}}} = 0.075m \qquad \text{Equation 4-9}$$

One of the disadvantages of using the plate element in Plaxis is that it does not have a function that allows for the modulus to vary under loading. The bearing pad modulus increases under increasing compression and therefore is strain hardening. Therefore, the control model will first be constructed assuming that the bearing pad plate element has the same characteristics as the SCP plate element (Table 4-1) and in a subsequent model the bearing pad stiffness will be included and the results will be compared. When the bearing pad plate element is included it will be modeled using the parameters shown in Table 4-2.

Table 4-2   Plate model parameters for bearing pad

Properties	Variable	Value	
Isotropic		Yes	
Axial Stiffness	EA_1	210.2 kN/m	
Axil Stiffness	EA_2	210.2 kN/m	
Bending Stiffness	EI	0.407 (kN·m^2)/m	
Equivalent Plate Thickness	d_{eq}	0.152 m/m	
weight	w	0.000 kN/m/m	× stress point • node
Poison's ratio	ν	0.495	5-node plate element

4.3.3   Welded Wire Wall

The Stage-1 structure is a welded wire MSE system. As previously describe it is considered to be a flexible faced structure (Figure 2-15). It is the right side of the U in the control model. In the control model it was assumed that the MSE was constructed in accordance with state of practice methods and specifications and that the foundation soils that the 2-Stage structure was placed on had experienced all anticipated settlement. Based on these assumptions the Stage-1 MSE structure was assumed to be a rigid structure and it was not suspect to internal consolidation and bulging.

Bulging is a phenomenon that occurs in the construction of flexible faced MSE structures and that occurs as a result of poor compaction of the backfill material near the face of the MSE structure (Figure 4-3). As the backfill compresses under the self-weight of the placement of successive lifts of backfill, the face of the wall bulges outward between successive rows of soil reinforcing. Bulging typically occurs in lower sections of the wall face during construction. It can also occur as a result of hydrostatic compaction through the migration of fine backfill material by infiltration of water during and/or after construction. Bulging is controlled through the placement of free draining rock at the face of the structure, the use of a strut, control of compaction of the backfill at the face, and by preventing infiltration of water at the top of the structure.

Figure 4-3   Stage-1 bulging at face of welded wire wall

The 2-Stage structure requires a turnbuckle be attached to the Stage-1 MSE wire wall and then to the SCP panel of the Stage-2 facing. In order to attach the turnbuckle as a node-to-node anchor in Plaxis the Stage-1 welded wire wall is required to be modelled as a plate element. The welded wire wall is modelled as a plate with extremely low bending and axial stiffness and therefore can be considered a "dummy" plate that has no influence on the force distribution. The Stage-1 MSE wire wall plate element is modelled using the parameters shown in Table 4-3.

Table 4-3   Plate model parameters for welded wire wall

Properties	Variable	Value	
Isotropic		yes	
Axial Stiffness	EA1	4.277 kN/m	
Axil Stiffness	EA2	4.277 kN/m	
Bending Stiffness	EI	8.277 (kN·m2)/m	
Equivalent Plate Thickness	d_{eq}	0.152 m	
weight	w	3.582 kN/m/m	
Poisson's ratio	ν	0.200	

4.3.4   Turnbuckle

In the Plaxis 2D the turnbuckle is modeled as a node-to-node anchor. A node-to-node anchor is only able to sustain an axial force, therefore, no bending forces are considered. Further, in the 2D model because the turnbuckle properties are smeared, it can be considered to be equivalent to a sheet. Because it is a "sheet" the interaction of the slender turnbuckle with the cavity fill material cannot be truly modelled. In order to determine the effects of the interaction of the cavity fill and the turnbuckle a 3D model was constructed and compared to the 2D model.

The turnbuckle type for this model was classified as a type Jaw-&-Jaw that includes a housing consisting of a Dual-Coil turnbuckle and is shown in Figure 4-4. The Dual-Coil turnbuckle housing consists of wire coils with one of them configured with a right-hand thread pattern and the other one configured with a left-hand thread pattern. The Dual-Coils are separated by two 9.5mm diameter steel bars (W11.0 Wire) that are resistance welded to the outside periphery of each coil loop. The Jaw consists of forged steel with parallel plates that terminate into a round bar with a diameter equal to 12 mm. Coil threads are formed on the end of the round bar. In order to be attached to the housing one Jaw is formed with right hand threads and the other Jaw is formed with left hand threads. The Jaw coil threads are screwed into each end of the Dual-Coil housing. The length of the turnbuckle is adjusted by altering how much of the Jaw threaded end is screwed into the Dual-Coil housing.
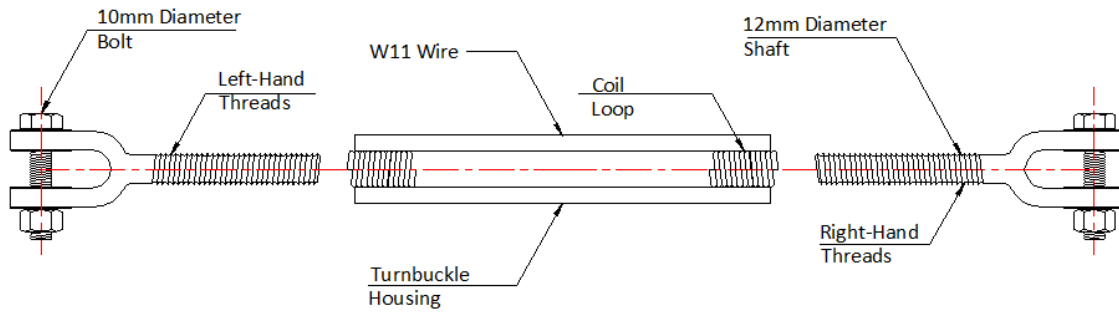
Figure 4-4   Turnbuckle detail

The turnbuckle is attached to the welded wire face of the Stage-1 structure and the back face of the Stage-2 SCP. At the Stage-1 structure the Jaw is hooked behind a vertical wire of the face element using the bolt. At the Stage-2 structure the Jaw is hooked into the anchor that is cast into and protrudes out of the SCP (Figure 4-5). The turnbuckle is tensioned by turning the Dual-Coil housing.

Figure 4-5   Jaw & Jaw turnbuckle installed in field

The turnbuckle components are manufactured from low carbon steel. The modulus of elasticity of low carbon steel (E_s) is 200 x 10^3 MPa and has a yield strength (F_y) equal to 450 MPa. The turnbuckle ultimate tensile capacity, based on information provided by the manufacture, is estimated to be equal to 65 kN. Based on the yield

strength and the ultimate tensile capacity of the turnbuckle the equivalent area of the

turnbuckle was back-calculated using Equation 4-10 and the axial stiffness of the

turnbuckle was calculated using Equation 4-11.

$$A_{tb} = \frac{T_u}{F_y} \rightarrow \frac{65 \cdot kN}{450 \cdot MPa} = 144E^- 6 \cdot m^2 \qquad \text{Equation 4-10}$$

$$E_s A_{tb} = 200E3 \cdot MPa \cdot 144E - 6\left(m^2\right) = 28.88E3\left(kN\right) \qquad \text{Equation 4-11}$$

The spacing of the turnbuckle was equal to 0.762m on center. The turnbuckle

node-to-node element is modelled using the parameters shown in Table 4-4.

Table 4-4   Plate Model parameters for turnbuckle

Properties	Variable	Value
Material		Elastic
Axial Stiffness	EA	28.88E3 kN
Turnbuckle Spacing	Ls	0.762 m

4.3.5   Cavity Fill

The cavity fill material in a 2-Stage structure typically consists of a non-cohesive,

granular material with a Unified Soil Classification type GW. The cavity fill is modelled in

Plaxis using the 15-node triangular, linear elastic non-porous element (Plaxis 2014). The

triangular element has 5 nodes along each edge and 3 nodes on the interior of the

triangle (Figure 4-6). The cavity fill is dissected and meshed automatically in Plaxis into

uninterrupted 15-node triangular elements.
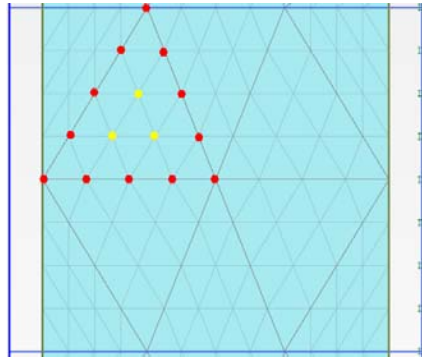
Figure 4-6 Cavity fill Plaxis model

4.3.5.1   Constitutive Soil Model

The Hardening-Soil (HS) model was used in the control model. This model was selected based on the parametric study performed by Kniss et. al., 2007. In the Kniss parametric study the soil constitutive parameters where varied in the Mohr-Coulomb model and in the HS model to determine the influence on the horizontal pressure when compared to the Handy-Spangler equation (Equation 2-31). The study found that the HS soil model produced results that were nearly identical to the arching equation proposed by Handy and Spangler. Further it was determined that the internal friction angle was the parameter that controlled the magnitude of the horizontal pressure when using the HS model. They also determined that the unit weight and Young's Modulus had little influence of the model (Kniss et al 2007).

The HS is an advance model that simulates soil behavior by accounting for the stress-dependency of the stiffness moduli (Plaxis 2012). The limiting states of stress are modelled using similar strength parameters defined by the Mohr-Coulomb constitutive soil model and include the friction angle (ϕ), the cohesion (c), and the dilatancy angle (ψ). The HS model describes the soil stiffness using three different soil moduli that include the triaxial loading stiffness $\left(E_{50}^{ref}\right)$, the triaxial unloading stiffness $\left(E_{ur}\right)$, and the

oedometer loading stiffness $\left(E_{oed}\right)$. Plaxis recommends that the default stiffness values be set equal to $E_{ur} \approx 3 \cdot E_{50}$ and $E_{oed} \approx E_{50}$. Therefore, the user only needs to define the secant stiffness modulus E_{50}.

4.3.5.2   Soil Modulus Parameters

The HS model is formulated based on the hyperbolic relationship that occurs between the vertical strain, ε_1, and the deviatoric stress, q, in a triaxial loading (Schanz 2000). It is based on the Duncan-Chang model (Duncan 1970) with the exception that the material is assumed to be elasto-plastic and not hypo-elastic (Plaxis 2014). In the HS model in primary loading the soil shows a decreasing stiffness and an irreversible plastic strain (Plaxis 2014). The stiffness values are based on a reference (ref) moduli value that is used to calculate the new moduli. This is based on the state of stress and the value of the minor principal stress $\left(\phi_3\right)$ or the confinement of the soil. The moduli change in accordance with the state of the minor principal stress creating a non-linear stress-strain curve as shown in Figure 4-7 (Kondor and Zelasko 1963).
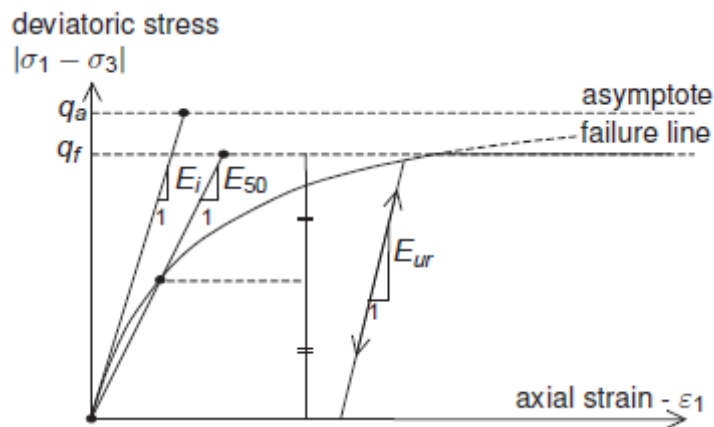
Figure 4-7   Hyperbolic stress-strain relationship (Plaxis 2014)

The strain can be determined based on the asymptotic shear stress and the deviatoric stress as demonstrated in Equation 4-12.

$$\varepsilon_1 = \frac{1}{E_i} \cdot \frac{q}{1 - \dfrac{q}{q_a}} \text{ for } q < q_f$$

Equation 4-12

Where q is the deviatoric stress in primary loading, q_a is the asymptotic value of the shear strength and E_i is the initial stiffness. The value q_f is based on the Mohr-Coulomb failure criteria and describes when perfectly plastic yielding occurs, or that yielding and failure coincide. The initial stiffness is calculated as shown in Equation 4-13.

$$E_i = \frac{2 \cdot E_{50}}{2 - R_f}$$

Equation 4-13

Where R_f is the failure ratio and E_{50} is the confining stress dependent stiffness modulus for primary loading. Plaxis recommends that the value of R_f be equal to 0.90 of the actual asymptotic failure. The failure deviatoric stress value is calculated as shown in Equation 4-14 (Duncan and Chang 1970)

$$q_f = \left(c \cdot \cot(\phi) - \sigma'_3 \right) \cdot \frac{2 \cdot \sin(\phi)}{1 - \sin(\phi)}$$

Equation 4-14
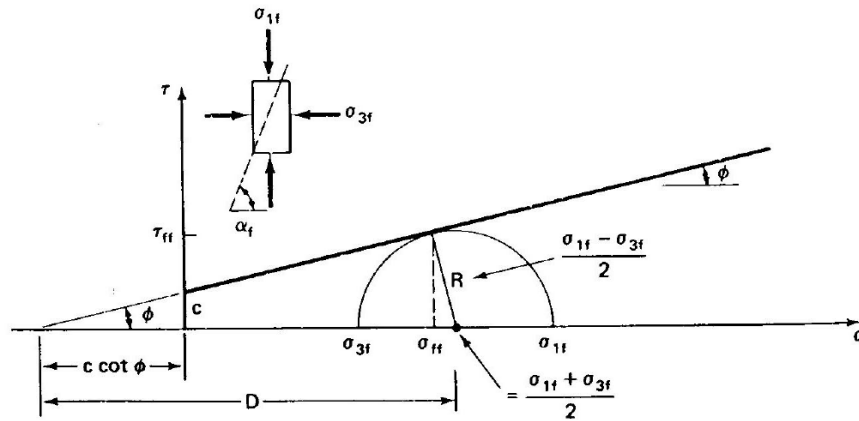
Figure 4-8 Mohr-Coulomb failure criteria (Duncan et. al. 1980)

Where q_f is the deviatoric stress at failure and is based on the Mohr-Coulomb failure criteria.
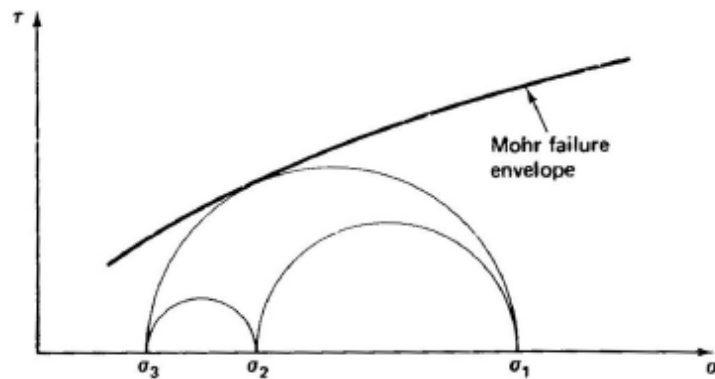
Figure 4-9 Mohr 3-Dimensional state of soil stress

4.3.5.3   Triaxial Loading Stiffness

The triaxial loading stiffness modulus parameter, E_{50}^{ref}, is characterized by plastic straining due to primary deviatoric loading. The parameter E_{50}^{ref} is represented by the secant stiffness within a drained triaxial test. A modulus, E_{50}, is calculated from the reference E_{50}^{ref} based on the minor principal stress. The units for E_{50}^{ref} are stress and are given in force per unit area (Plaxis, 2014).

$$E_{50} = E_{50}^{ref} \left(\frac{c \cdot \cos(\phi) - \sigma'_3 \cdot \sin(\phi)}{c \cdot \cos(\phi) + p^{ref} \cdot \sin(\phi)} \right)^m \qquad \text{Equation 4-15}$$

Where m is a power function and defines the amount of stress dependency and is simulated logarithmically. A value of m equal to 1.00 produces linear lines while values less than 1.00 produce slightly curved lines (Plaxis 2014).

4.3.5.4   Oedometer Stiffness

The oedometer stiffness modulus parameter, E_{oed}^{ref}, is characterized by plastic straining due to primary compression. The parameter E_{oed}^{ref} represents the tangent stiffness for primary oedometer loading. A stiffness modulus, E_{oed}, is calculated from the reference E_{oed}^{ref} based on the minor principal stress. The units for E_{oed}^{ref} are stress and are given in force per unit area (Plaxis, 2014).

4.3.5.5   Triaxial Unloading Stiffness

The triaxial unloading stiffness modulus parameter, E_{ur}^{ref}, measures the elastic unloading and reloading. The Plaxis documentation recommends using a value of E_{ur}^{ref} equal to three times E_{ref}. A modulus, E_{ur}, is calculated from the reference E_{ur}^{ref} and is based on the minor principal stress. The units for E_{ur}^{ref} are stress and are given in force per unit area (Plaxis, 2014).

4.3.5.6   Poisson's Ratio Unload-Reload

The unload-reload Poisson's Ratio (v_{ur}) is the parameter that captures the soil response to the unload-reload curve. Plaxis documentation suggests that a value equal

to 0.20 be used. It should be noted that this value is not related to the standard poisons ratio that is used in other elastic soil models (Plaxis 2014).

4.3.5.7   Unit Weight

The unit weight (γ') of semi-dense to dense gravel backfill ranges from approximately 15 kN/m^3 to 22 kN/m^3. A value equal to gravel that is compacted to 95% standard proctor and that has the UCS classification of GW will be used in the model and will be equal to 20 kN/m^3.

4.3.5.8   Angle of internal fiction

The cavity fill is classified by UCS as a free draining GW material. It is compacted by the method of gravity placement, i.e. it is dropped into the cavity from a height. Based on published soil correlations, the angle of internal friction (ϕ') of a semi-dense to dense gravel backfill is in the range of the lower bound value of 30° to an upper bound value of 45°. The lower bound value equal to 30° will be used in the control model. Based on the study performed by Kniss et al., 2007, this should provide the most conservative results.

4.3.5.9   Cohesion

The cavity fill is a granular non-cohesive material. To prevent errors from occurring in the analysis a small cohesion (c') value will be used. Plaxis recommends a value of 0.200 kPa for non-cohesive soils.

4.3.5.10 Dilatancy Angle

The cavity material is a classified as angular, well-graded gravel and will exhibit

dilatancy at a low confining pressure. Plaxis recommends using the Bolton method as

shown in Equation 4-16 to determine the dilatancy angle (ψ) (Plaxis 2014).

$$\psi = \phi' - 30°$$ Equation 4-16

4.3.5.11 Summary Backfill Constitutive Soil Parameters

The soil parameters as displayed in Table 4-6 were used in the control model.

Table 4-5   Backfill constitutive soil parameters

Strain Hardening Soil Model	
Variable	Value
Unit weight (kN/m^3)	20
Angle of internal friction (deg)	30.0
Cohesion (kN/m^2)	0.200
Dilatancy Angle (deg)	0.0
E_{50} (kN/m^2)	24.00E3
E_{oed} (kN/m^2)	24.00E3
E_{ur} (psf)	72.00E3
Power M (dim)	0.50
v_{ur} (dim)	0.20

4.3.6   Boundary Conditions

The choice of the fixity of each section of the structure is based on the work

completed by Kniss et. al, in 2007. The Stage-1 welded wire wall is considered to be the

right side of the model. The Stage-1 structure is a ridged mass of soil and is assumed to

be compacted backfill that has completely consolidated. By making this assumption

movement of the Stage-1 wall was not allowed to occur in either the horizontal or vertical direction.

A plate structure was required for the welded wire wall in order to allow for placement of a node and the attachment of the turnbuckle. The welded wire wall plate was assumed to have very low stiffness. The soil in the cavity was free to move up and down the Stage-1 wall face but not into the Stage-1 wall. Therefore, the right side of the U was fixed in both the horizontal (x) direction and the vertical (y) direction. The base of the structure was assumed to be placed on a soil that was consolidated and was modelled as a line. Therefore, the bottom of the U was also fixed in both the vertical (y) and horizontal (x) direction.

The Stage-2 segmental concrete panels were considered to be the left side of the model and were modelled as a series of plates that were defined with a bending stiffness and an axial stiffness. The SCP in an MSE structure is staggered in successive columns, e.g. there are no continuous horizontal joints. During placement of the panels the top corners are clamped to the adjacent panels to prevent outward displacement and the turnbuckle is tightened and the cavity fill is placed before the clamp is removed. Therefore, the left side of the U is modelled free to translate in the vertical direction but was fixed in and horizontal direction. The parallel set of U-faces are joined together with the turnbuckle and are modelled as a series of horizontal node-to-node anchors.

4.3.7 Interface

Friction develops between the boundary of the Stage-1 and Stage-2 facing and the cavity fill. The boundary locations are modelled using the interface option in Plaxis 2D. The interface strength parameters are a function of the friction angle of the cavity fill

material and the surface of the respective facing. The Stage-1 and Stage-2 facing

materials are different material and therefore the interfaces of the Stage-1 wire wall face

and the Stage-2 segmental concrete panel face could be modelled using different

interface strength parameter. The welded wire wall face is comprised of vertical and

horizontal wires that are bi-planar. The bi-planar configuration will allow the cavity soil to

"hang" up on the Stage-1 flexible wire wall face and the interface strength parameter

could be set equal to the friction angel of the cavity fill, however in the control model they

were set equal to the interface friction of the SCP. The back face of the SCP receives a

hand screed finish and the interface friction angel of soil-to-concrete is specified to be

equal to 2/3 of the friction angle of the cavity fill.

The interface reduction coefficients for the Stage-1 and Stage-2 interfaces in the

control model were therefore equal to:

$$R_{inter} = \frac{\tan(\delta)}{\tan(\phi^{'})} = 0.67 \qquad \text{Equation 4-17}$$

The interface reduction coefficient for the Stage-1 interface if modelled with the

friction angle equal to the soil is equal to:

$$R_{inter} = \frac{\tan(\phi^{'})}{\tan(\phi^{'})} = 1.00 \qquad \text{Equation 4-18}$$

In Plaxis the default interface is associated with the *Material* set and is set equal

to the *Cluster Material.* This indicates that the interface is associated with the cluster

material that borders the interface. The user must physically change the cluster material

to a defined material if invoking other interface parameters.

4.3.8   Stage Construction

The construction sequence for a 2-Stage structure is repetitive. The initial sequence assumes that the Stage-1 structure and the levelling pad that the concrete panel and the cavity fill are placed on has been constructed (Figure 4-10). The first stage of construction consists of installing the concrete panel, placing the bearing pad, attaching and tensioning the bottom turnbuckle. In the second stage of construction the first layer of cavity fill is placed to the mid-point of the concrete panel or for a total lift thickness equal to 0.762m (Figure 4-11). The third stage of construction consists of attaching and tensioning the second turnbuckle. The fourth stage of construction consists of placing the second layer of the cavity fill to the top of the first panel for a lift thickness equal to 0.762m (Figure 4-12). The combination of the construction stage 1 to 4 sequences represents the placement and the backfilling of one full sized panel equal to a panel height of 1.524m. This construction sequence was repeated for a model total of 24 stages. It should be noted that the appropriate interfaces are activated accordingly for each phase.
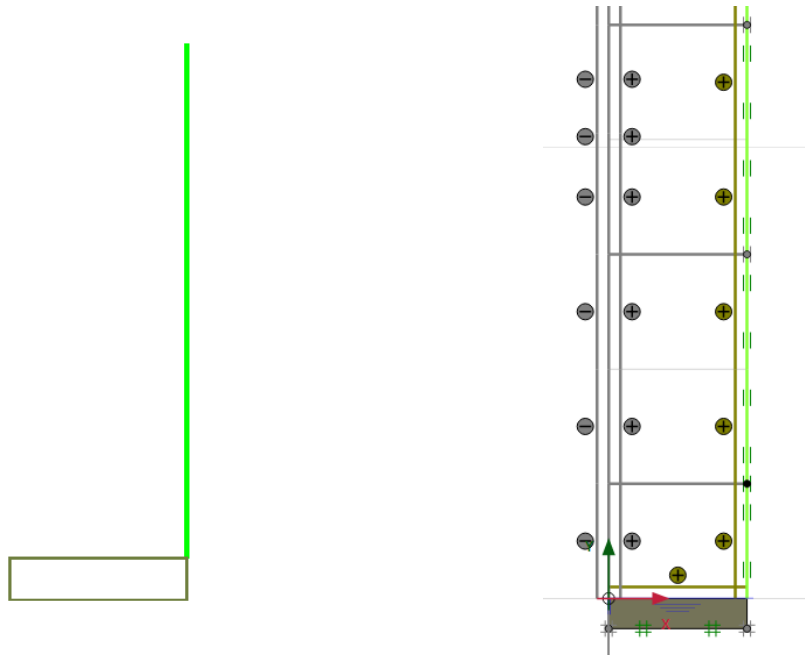
Figure 4-10   Phase-Initial
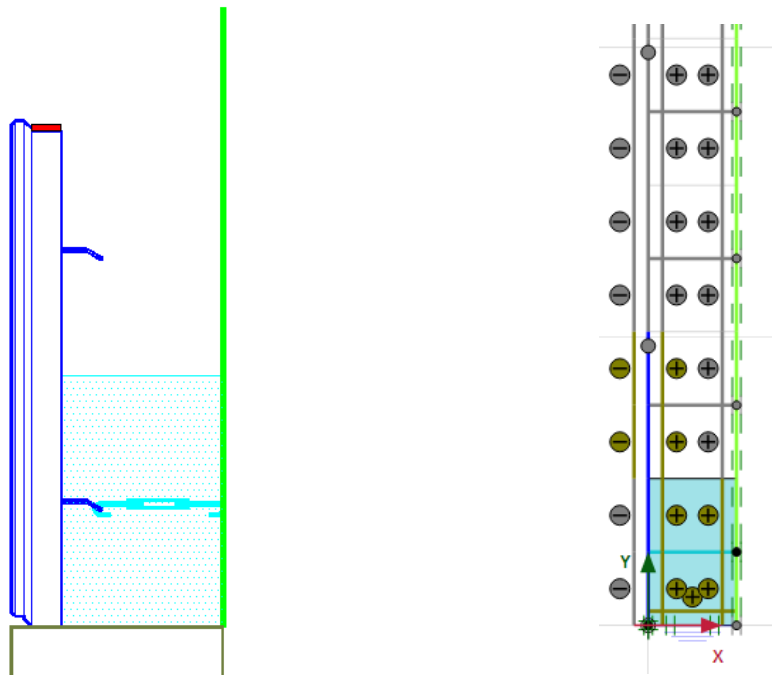
Figure 4-11   Stage 1 and stage 2 construction

118
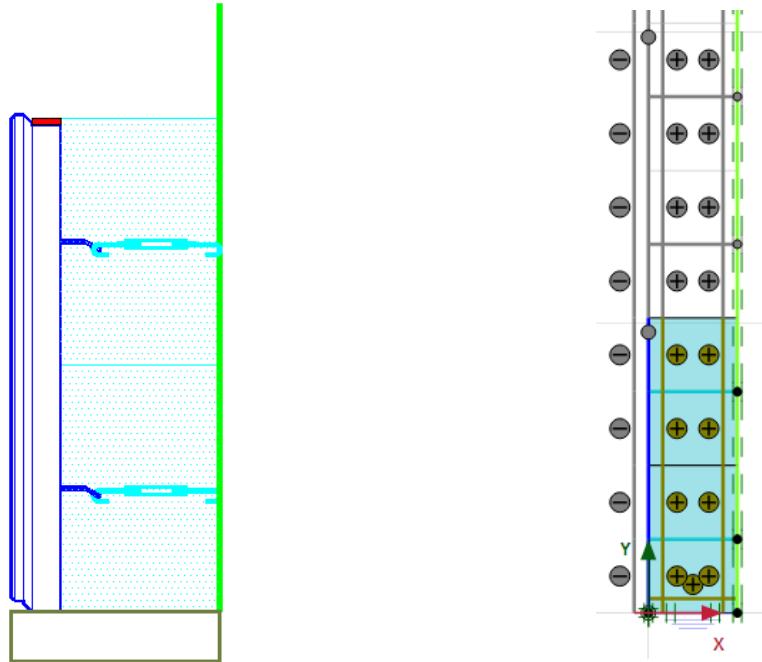
Figure 4-12   Stage 3 and stage 4 construction

4.4   2D Control Model Results

4.4.1   Cavity Horizontal Pressure

The Plaxis 2D control model results compared well with the Arching Theory proposed by Handy and Spangler for Fascia Structures as shown in the graph in Figure 4-13. As predicted by theory the horizontal pressure follows the Rankine pressure conditions (Equation 2-1 and Equation 2-4) then quickly dissipates to a constant value that is approximately equal to the maximum value of the arching theory (Equation 2-30). As predicted the horizontal pressure in the cavity is well below both the Rankine at-rest pressure and the Rankine active pressure cases.
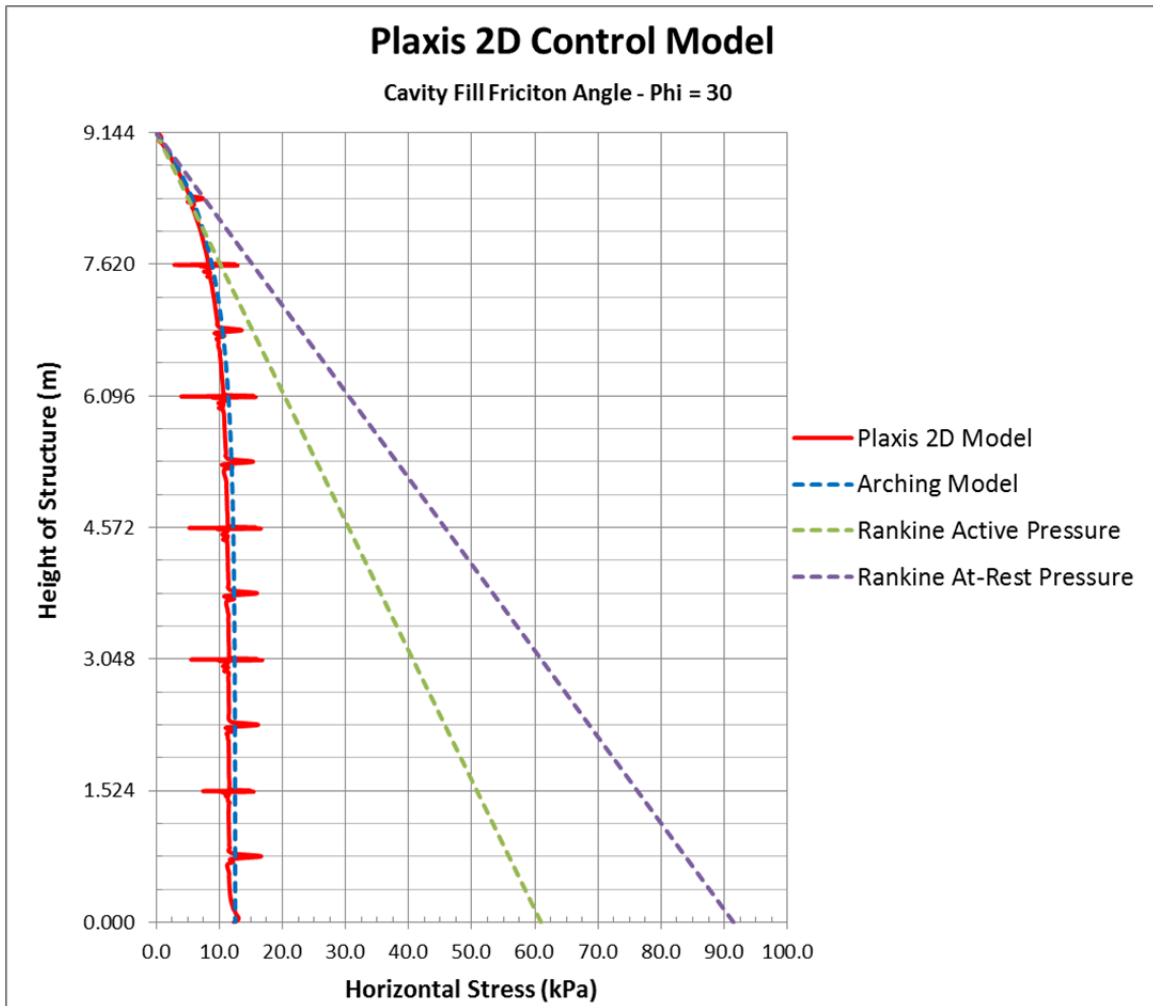
Figure 4-13   Graph of Plaxis 2D control model – horizontal pressure

The maximum arching pressure when utilizing Equation 2-30 and a unit weight of backfill equal to 20 kN/m^3, internal friction angle equal to 30 degrees, cavity width equal to 0.456m and an interface friction angle equal to 20 degrees, is equal to 12.53 kPa. The maximum Rankine Active pressure for the wall design height equal to 9.14m and with a Rankine active earth pressure coefficient equal to 0.33 for a 30 degree internal friction angle backfill material (Equation 2-4) is equal to 60.87 kPa. The arching maximum pressure is 21% of the Rankine active earth pressure. The maximum arching pressure in the Plaxis 2D model is more complex due to the use of staged construction. At the

120

location of each of the phases where the displacement is reset, which coincides with the

midpoint of each panel and the top of each panel there is a spike in the pressure. If the

spiked pressure points are removed the maximum pressure is equal to 12.1 kPa which is

3% less than the pressure calculated using the arching equation. This demonstrates that

for a static condition, e.g., no structure movement, that arching does occur in the 2-

Stage structure.

Table 4-6   Control model maximum horizontal pressure

Method	Pressure (kPa)	Difference from theoretical (Handy and Spangler)
Handy	12.53	-
Plaxis 2D	12.10	3%
Rankine Active	60.87	4.85%
Rankine At-Rest	91.40	7.29%

4.4.2   Turnbuckle Forces

The turnbuckle forces from the Plaxis 2D model, when compared to the design

forces that are based on the use of the maximum force from the arching theory, also

agreed well. The 2D model results were for a one meter section of the structure. There

were 2 turnbuckles per row for the 1.524m panel; therefore, each turnbuckle was

responsible for the forces for a tributary length out-of plane equal to 0.762m, or there are

1.31 turnbuckles per meter of structure. The turnbuckle graph that is shown in Figure 4-

14 includes the forces from the Plaxis 2D model, the turnbuckle ultimate tensile force,

the turnbuckle maximum design tensile force at the time of installation, and the

turnbuckle maximum tensile force at a design life of 75 and 100 years. The resistance

factor that is used for steel was in conformance with the AASHTO Bridge Design

Specification using the Allowable Stress Design (ASD) and was equal to 0.55.

It is a well-known fact that steel elements degrade over time when they are buried in soil. Based on prescribed design durations the designer can design the steel elements based on the degraded area of steel. This degraded area is sacrificed and the remaining steel area resists the loading. The amount of sacrificial steel is dependent on the prescribed design duration of the structure. Based on the AASHTO corrosion models for prescribed design durations equal to 75 years and 100 years the amount of sacrificial steel that is removed from the diameter of the steel elements are equal to 1.42mm at 2.00mm, respectively. Using the sacrificial thickness and calculating the remaining steel area, the allowable tensile force for given design duration can be determined using Equation 4-19. For the turnbuckle, the limiting component shown in Figure 4-4, are the dual wires that separate the coil connectors and their combined sacrificial area is used in the calculation.

$$T_{al} = \theta_y \cdot F_y \cdot A_c \qquad \text{Equation 4-19}$$

Where:

T_{al} = Allowable tensile force (kN)

θ_y = Resistance factor for yield equal to 0.55 (dim)

F_y = Yield strength of steel equal to 450 MPa (MPa)

A_c = Cross sectional area after corrosion (m^2)

The following Table 4-7 lists the maximum tensile capacity at design durations equal to 0, 75 and 100 years as calculated using Equation 4-19.

Table 4-7   Turnbuckle design forces

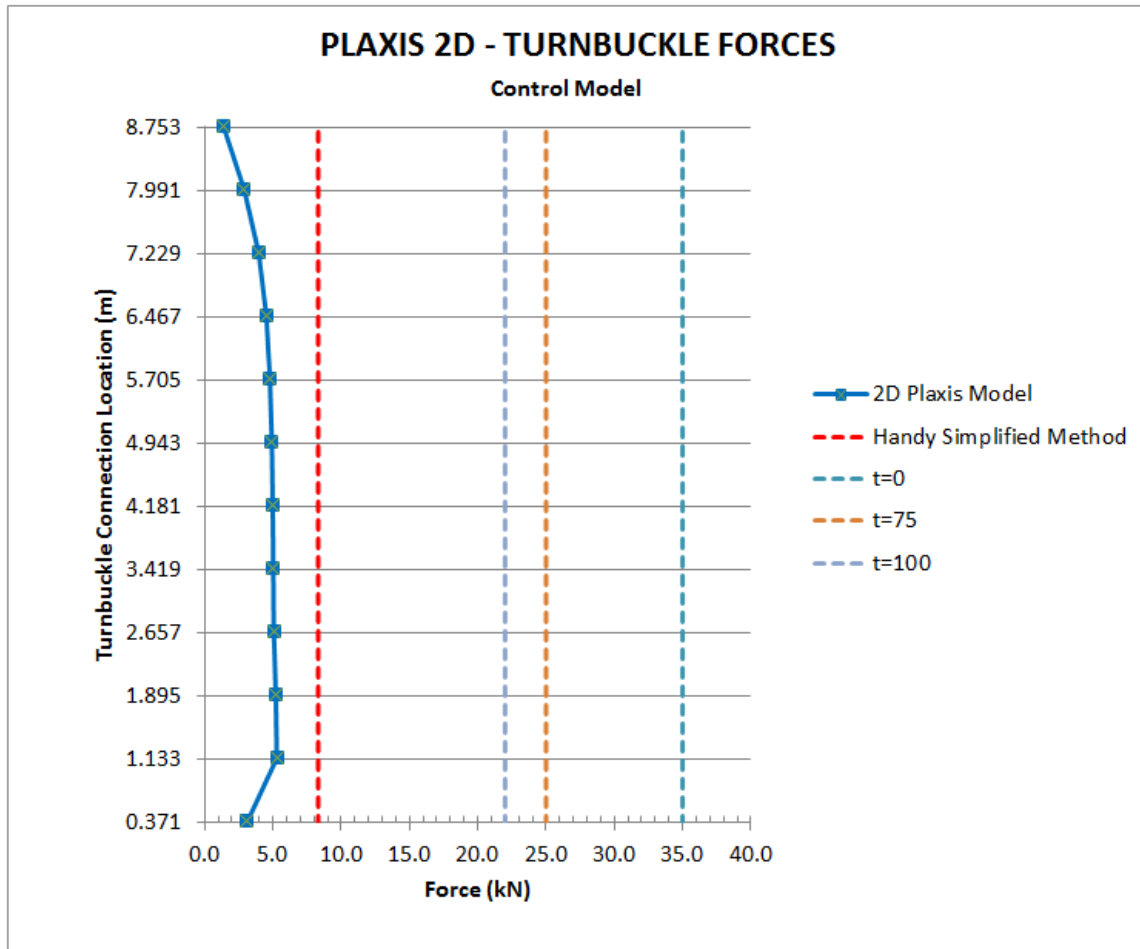| Design Life (yr)	Cross Sectional Area (m²)	Allowable Tensile Capacity (kN)
0	70.88 x 10^{-6}	34.94
75	51.24 x 10^{-6}	25.26
100	44.10 x 10^{-6}	21.74

Figure 4-14   Graph of Plaxis 2D control model – turnbuckle force

To determine the total force per meter in the 2-Stage cavity the area under the Plaxis diagram and the Arching Diagram was determined. The area is equal to the integration of the pressure function over the height of the structure and can be approximated using the trapezoidal rule shown in Equation 4-20.

123

$$F = \int_b^a f(x) \cdot dx \approx (b-a) \cdot \frac{f(a)+f(b)}{2} \qquad \text{Equation 4-20}$$

Where: F   =   total force in cavity (kN/m)

          f(x)   =   pressure function (KPa)

          b   =   depth to point on graph (m)

          a   =   depth to point on graph (m)

          f(a)   =   pressure at point a (kPa)

          f(b)   =   pressure at point b (kPa)

The total force per turnbuckle tributary area for the 2D Plaxis model is equal to 70.6 kN/m and for the Arching Method the total force per meter is equal to 75.4 KN/m. The difference between the two models is 7%. The Arching method predicts a higher total force per meter than the Plaxis model.

For the control model there were 12 turnbuckles in the 2-Stage cavity. Assuming that the turnbuckles are required to proportionally resist the total cavity force, the force that each turnbuckle will be required to resist is equal to 1/12 of the total load or 5.9 kN for the Plaxis model and 6.3 kN for the Arching model. These loads are well below the allowable tensile capacity of the turnbuckle for the 75 year and 100 year design duration.

The axial force of the turnbuckles from the Plaxis 2D control model are shown in Table 4-8. The factors of safety for design durations at the end of construction, 75 years and 100 years are shown in Table 4-9. The location is equal to the distance from the foundation.

Table 4-8   Turnbuckle forces from Plaxis 2D

Turnbuckle	Location [m]	2D [kN]
1	8.763	1.38
2	8.001	2.90
3	7.239	3.95
4	6.477	4.52
5	5.715	4.78
6	4.953	4.92
7	4.191	4.99
8	3.429	5.03
9	2.667	5.06
10	1.905	5.21
11	1.143	5.28
12	0.381	3.12

Table 4-9   Turnbuckle Factors of Safety

t = 0		t = 75 years		t = 100 years	
Plaxis	Arching	Plaxis	Arching	Plaxis	Arching
5.9	5.6	4.2	4.0	3.7	3.5

Based on the results of the Plaxis 2D control model, for the modeled 2-Stage structure under static conditions, e.g. no movement of the Stage-1 or Stage-2 structure, arching within the cavity is occurring and the turnbuckle design based on the prescribed turnbuckle configuration is conservative.

4.4.3   Control Model FE 3D Results

A 3D Plaxis control model was constructed and the results compared to the results from the 2D model. It is practical to assume that the difference in the stress distribution in the 2-Stage structure will not significantly vary between models. However, the forces in the turnbuckle may vary based on the 2D node-to-node element and the 3D

beam element. The 3D model is developed to understand the interaction of the

turnbuckle with the cavity fill. In the 3D model the turnbuckle is modelled as a beam

consisting of a slender element and therefore it can interact with the cavity fill material.

The beam can sustain axial forces and bending forces. In a 2D model the turnbuckle

properties are smeared out of plane into a sheet and therefore there is no out-of-plane

interaction and the node-to-node anchor can only sustain axial forces and no bending

forces.

For the 3D control model the panel length (out-of-plane in the 2D model) was set

equal to 0.762m. The 2D model is calculated based on a per meter of structure,

therefore, in order to compare the results of the 2D model the stresses and forces are

required to be adjusted by a factor 0.762. It should be noted that the 3D model also did

not use any bearing pads.

4.4.3.1   3D Control Model Horizontal Pressures

The results of the horizontal pressures for the 3D model are very similar to the

horizontal pressures from the 2D model. The stress on the wall face is slightly less than

the 2D model but agrees reasonably well with the theory of Arching. The lower stress

profile can be attributed to the interaction of the beam element model for the turnbuckle

in the 3D model when compared to the 2D smeared node-to-node anchor.
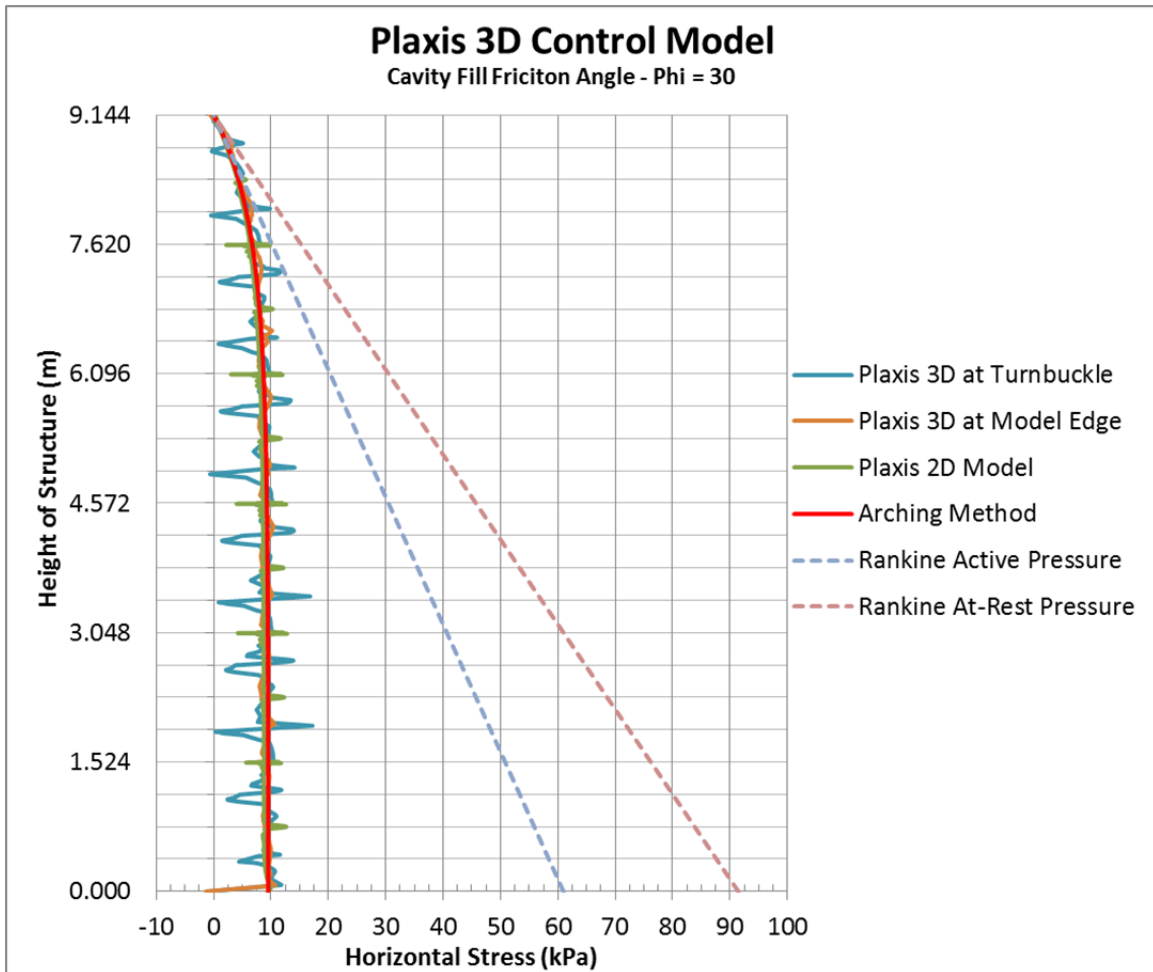
Figure 4-15 Graph of Plaxis 3D control model – horizontal pressure

4.4.3.2 3D Control Model Turnbuckle Forces

The forces in the turnbuckle from the 3D model were compared against the forces in the 2D model using the same methodology as defined in the 2D sections above. To be consistent with the fixity of the 2D mode the 3D model turnbuckle connection was considered fixed. Based on the results of the 3D model (Figure 4-16) the forces are slightly larger than the forces in the 2D model (Table 4-10). This demonstrates that modelling the turnbuckle as a beam allows for the slender element to interact with the cavity fill and that the bending increases the axial force.

127

Figure 4-16   Graph of Plaxis 3D control model – turnbuckle force

Table 4-10   2D & 3D turnbuckle force comparison

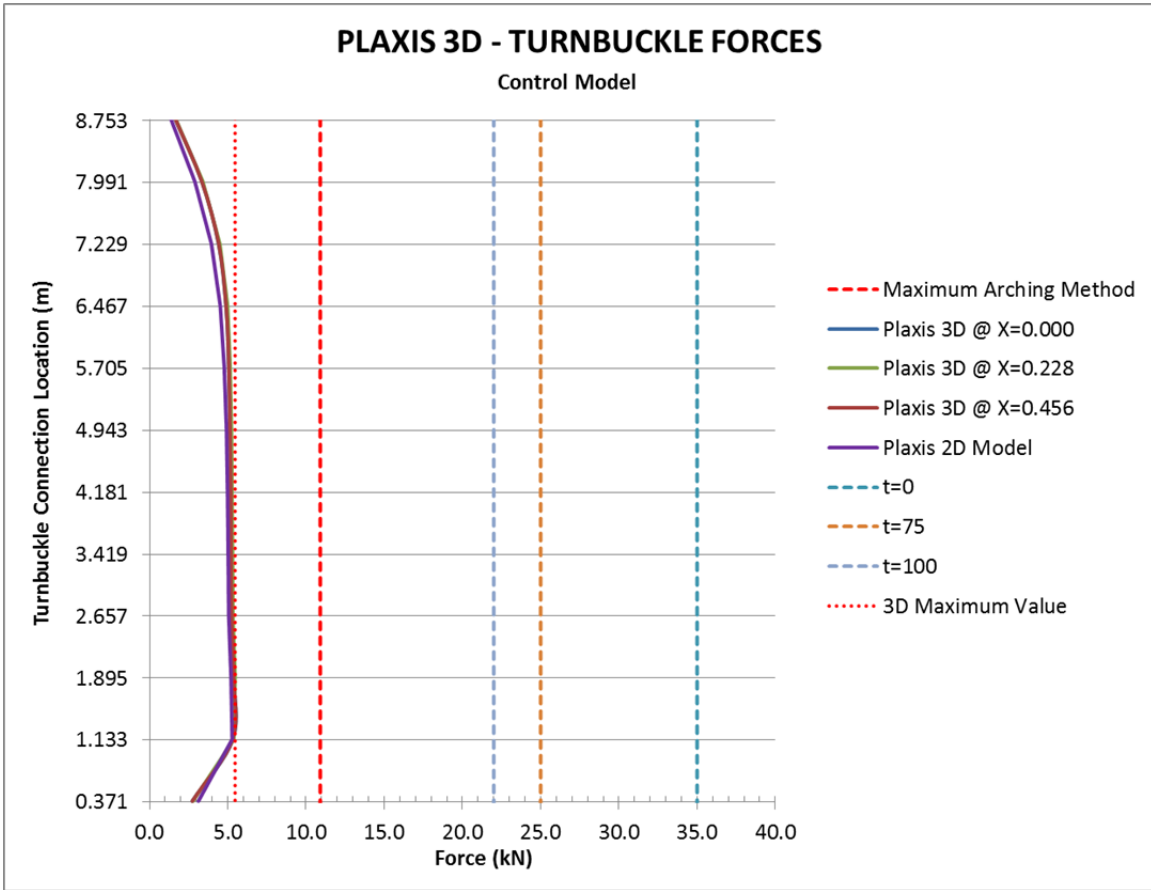| Turnbuckle	Location [m]	3D [kN]	2D [kN]	Difference
1	8.763	1.70	1.38	122.54%
2	8.001	3.41	2.90	117.56%
3	7.239	4.49	3.95	113.68%
4	6.477	4.99	4.52	110.37%
5	5.715	5.15	4.78	107.88%
6	4.953	5.24	4.92	106.46%
7	4.191	5.27	4.99	105.73%
8	3.429	5.30	5.03	105.49%
9	2.667	5.33	5.06	105.21%
10	1.905	5.47	5.21	104.97%
11	1.143	5.39	5.28	102.07%
12	0.381	2.77	3.12	88.89%

4.4.4   Control Model Limit Equilibrium Verification

As a check of the 2D-FE model a Limiting Equilibrium (LE) analysis in conformance with the procedures outlined by Leshchinsky and Hu (2004), was performed. The commercially available software program ReSSA (Reinforced Slope Stability Analysis) developed by Adama Engineering was used to perform a Bishop Failure Analysis. The model was constructed by assuming three different soil profiles (Figure 4-17). The foundation soil and the retained soil were modemed as a ridged mass by specifying a high friction angle and a high cohesion value. The cavity was modelled as a thin soil element with a height of 9.144 meters and a width of 0.456 meters. The soil parameters used in the LE model are shown in Table 4-11.

Table 4-11   ReSSA soil constitutive parameters

Soil	Unit Weight (kN/m^3)	Friction Angle (deg)	Cohesion (kPa)
Reinforced Soil	20	30	0
Retained Soil	20	50	40
Foundation Soil	20	50	40

A single soil reinforcing element was placed at a distance equal to 1/3 the height of the structure from the base, e.g. elevation 3.048m. The initial strength of the soil reinforcing was specified as having an ultimate tensile strength of 100 kN/m. The soil reinforcing was embedded into the retained soil mass 10 meters to prevent any possible pullout failure.
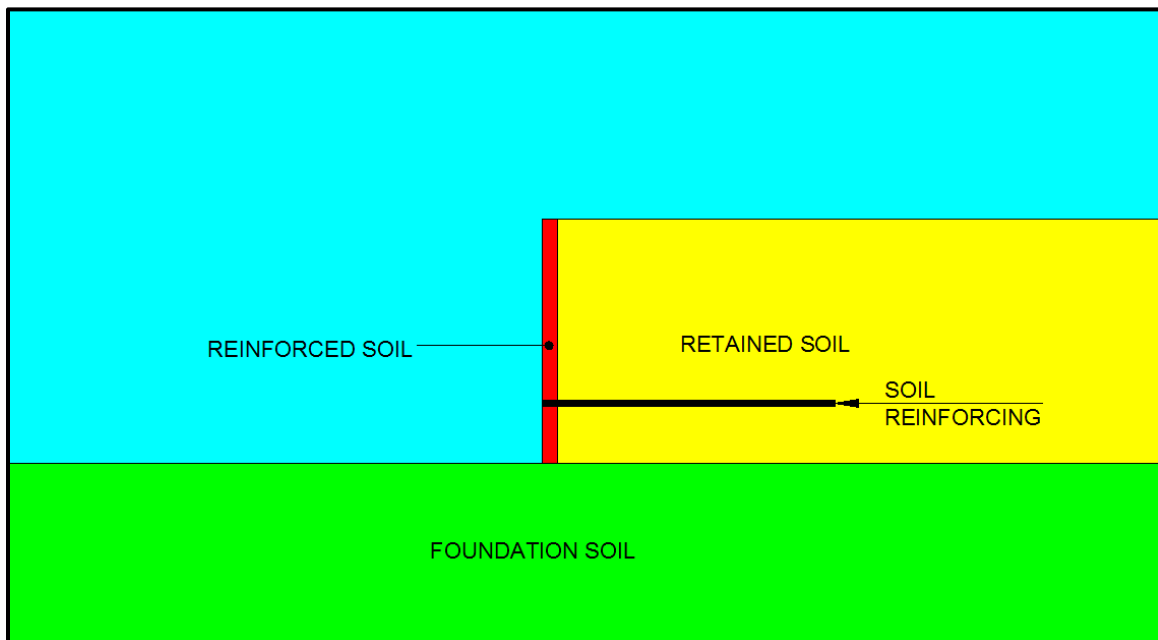

Figure 4-17   ReSSA model

A rotational failure mode was specified and run to determine an initial factor of safety and then the ultimate strength of the soil reinforcing was modified until a factor of safety of 1.00 was achieved. Based on the modification of the soil reinforcing an ultimate

strength of 94 kN/m was required to achieve the factor of safety of 1.00. Table 4-12 displays the comparison between the total cavity force per meter that was obtained using the Arching Method, Plaxis 2D, Plaxis 3D and the LE Models. The results are in good agreement using each method of analysis validating the control model (Hu 2007).

	Geosynthetic Designated Name	Geosynthetic Ultimate Strength, T ult [kN/m]	Reduction Factor for Installation Damage, RFid	Reduction Factor for Durability, RFd	Reduction Factor for Creep, RFc	Additional Reduction Factor, RFa	Coverage Ratio, Rc
1	Geosynthetic type #1	94.00	1.00	1.00	1.00	1.00	1.00

Figure 4-18   ReSSA reinforcing input parameters
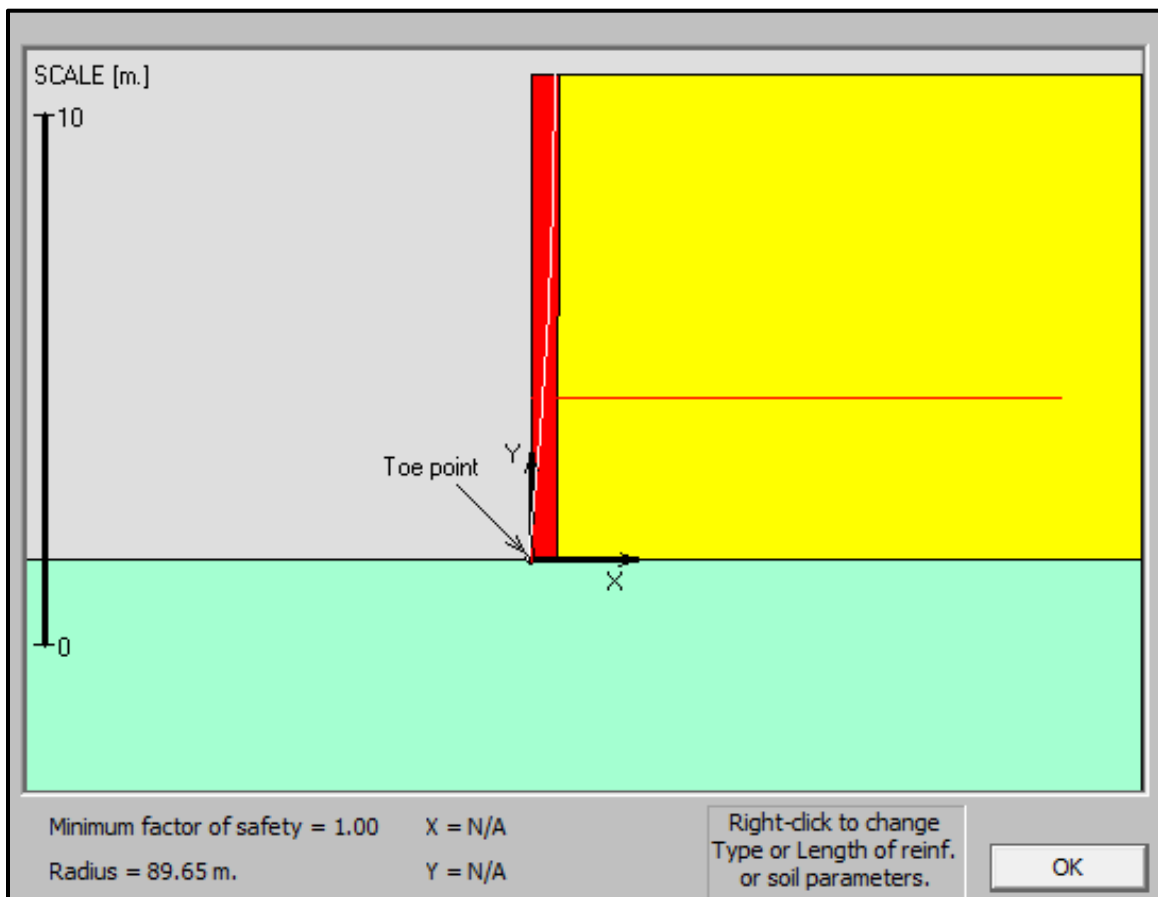
Figure 4-19   ReSSA results

Table 4-12   Total force comparison

Method	Total Force (kN/m)	Difference from Arching
Arching	98.9	-
Plaxis 2D	92.7	-7%
2D-LE	94.0	-5%
Plaxis 3D	97.4	-1%

4.5   Settlement of Stage-1 Structure FE 2D Results

As described in Section 2.2.5.3, the Stage-2 facing is not attached to the Stage-1 structure until all anticipated settlement has taken place. Settlement includes the foundation soils as well as the internal settlement of the Stage-1 structure. Based on performance of known 2-Stage structures this may be an unrealistic requirement. Therefore, to understand the effects that settlement of the Stage-1 structure has on the stress profile in the cavity and the forces in the turnbuckles the Plaxis 2D control model was modified to include a linearly decreasing line displacement on the Stage-1 wall face. The line displacement was included to simulate internal settlement of the Stage-1 structure after construction. The line displacement was prescribed to be the maximum at the top of the Stage-1 structure, linearly decreasing to no displacement at the base of the structure.

Three different line displacements were analyzed and include 25 mm, 50 mm, and 100 mm. The presentation of the results from each line displacement follows. The results include the interface stress and the turnbuckle forces. Based on the similarity of the numerical results from the 3D and the 2D control models only the 2D Plaxis results for the cavity pressure will be presented here.

The theory of arching is based on a static condition. Marston recognized that the forces in conduits changed when the sides of the ditch were more compressible than the fill material. Terzaghi also recognized that the arching theory was sensitive to outside external forces such as vibrations (Terzaghi 1945). The basis of placement of the 2-Stage structure is that the foundation soils and the Stage-1 MSE have experienced all predicated settlement and therefore can be considered ridged structures. This is typically verified through geotechnical instrumentation and though implementation of proper construction techniques. When this is the case the 2-Stage structure is static and can be assumed to behave as predicted by the 2D and 3D FE control models.

 Based on the results shown in Figure 4-20, Figure 4-22, and Figure 4-24, when the Stage-1 MSE settles internally the interface friction angle is trending to zero and the shear force is decreasing at the interface. This reduction in the interface friction angle is required for the Stage-1 structure to move during internal consolation. When the interface friction angle trends toward zero the horizontal pressure follows the Rankine at-rest condition. Depending on the magnitude of the prescribed displacement, the horizontal pressure follows the Rankine at-rest pressure condition than becomes constant. The at-rest condition is achieved because the turnbuckles prevent the wall from rotating, or moving outward. In fact the horizontal pressures are slightly larger than the at-rest values demonstrating that the turnbuckles are deflecting and pulling the wall in.

For the 25mm prescribed displacement (Figure 4-20) the depth where the horizontal pressure became constant was equal to 1.9m below the top of the structure. For the 50mm prescribed displacement (Figure 4-22) the depth where the horizontal pressure became constant was equal to 3.8m below the top of the structure. For the

100mm prescribed displacement (Figure 4-24) the depth where the horizontal pressure becomes constant was equal to 7.6m below the top of the structure. In each of the cases the soil is plastic and has fully mobilized and is sliding past the stage-1 wall.

The total idealized horizontal force, based on the respective pressure profile, can be calculated using Equation 4-21 and assumes that the pressure profile follows the Rankine at-rest pressure to the prescribed depth than becomes constant to the base of the cavity. As demonstrated in the figures (Figure 4-20, Figure 4-22, and Figure 4-24) the Plaxis 2D model predicts a pressure that is slightly larger than the Rankine at-rest pressure and therefore the idealized horizontal force shown in Equation 4-21 will be slightly less than the total force predicted in Plaxis.

$$F = \frac{1}{2} \cdot K_o \cdot \gamma \cdot (z)^2 \cdot \left(\frac{2 \cdot H}{z} - 1 \right) \qquad \text{Equation 4-21}$$

Where: F   =   total force in cavity (kN/m)

   K_o =   Rankine at-rest pressure coefficient (dim)

   γ =   unit weight of cavity fill (kN/m^3)

   z   =   depth to constant horizontal pressure (m)

   H   =   height of 2-Stage structure (m)

The total calculated forces using the idealized horizontal force from Equation 4-21 as compared to the Plaxis integrated total force are shown in Table 4-13.

Table 4-13   Total calculated force comparison

Settlement	Depth (m)	Plaxis Integrated Force (kN/m)	Calculated Force (kN/m)
1"	1.9	184	156
2"	3.8	301	276
4"	7.6	440	406

The maximum Rankine at-rest force is calculated using Equation 4-22 and is equal to 418 kN/m. As the internal settlement increases with depth the pressure follows the Rankine earth pressure and increases based on the internal settlement. For the control model condition and at 100mm of settlement the idealized calculated horizontal force is nearly equal to the Rankine at-rest horizontal force and therefore appears to be the limiting amount of internal settlement.

$$F_h = \frac{1}{2} \cdot K_o \cdot \gamma \cdot H^2 \qquad \text{Equation 4-22}$$

Where: F_h =   horizontal force (kN/m)

K_o =   Rankine at-rest earth pressure coefficient (dim)

γ =   unit weight of backfill (kN/m^3)
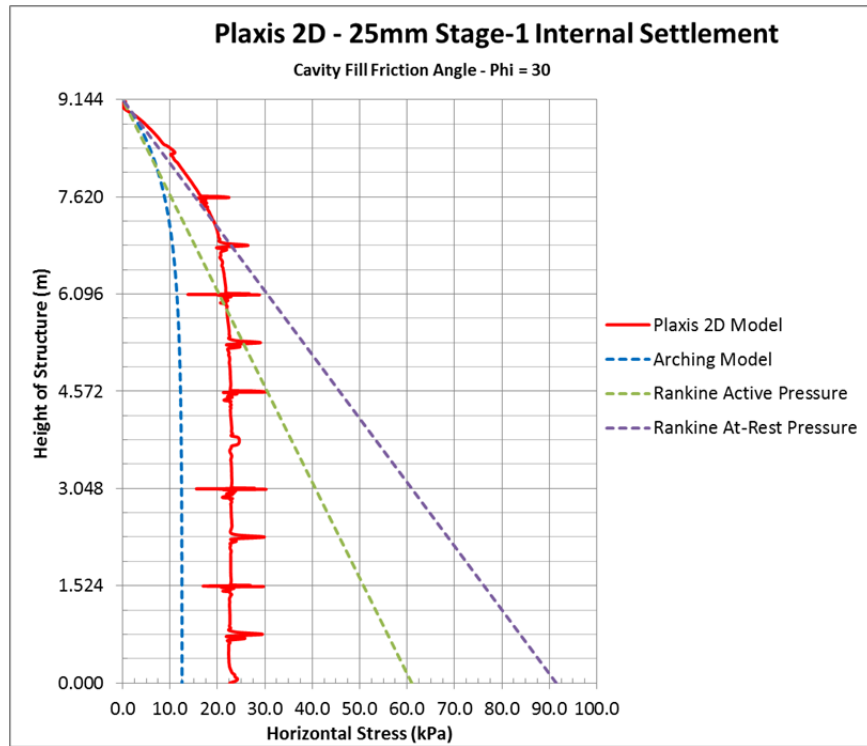
H   =   structure height (m)

Figure 4-20   Graph of Plaxis 2D 25mm Stage-1 internal settlement – horizontal pressure
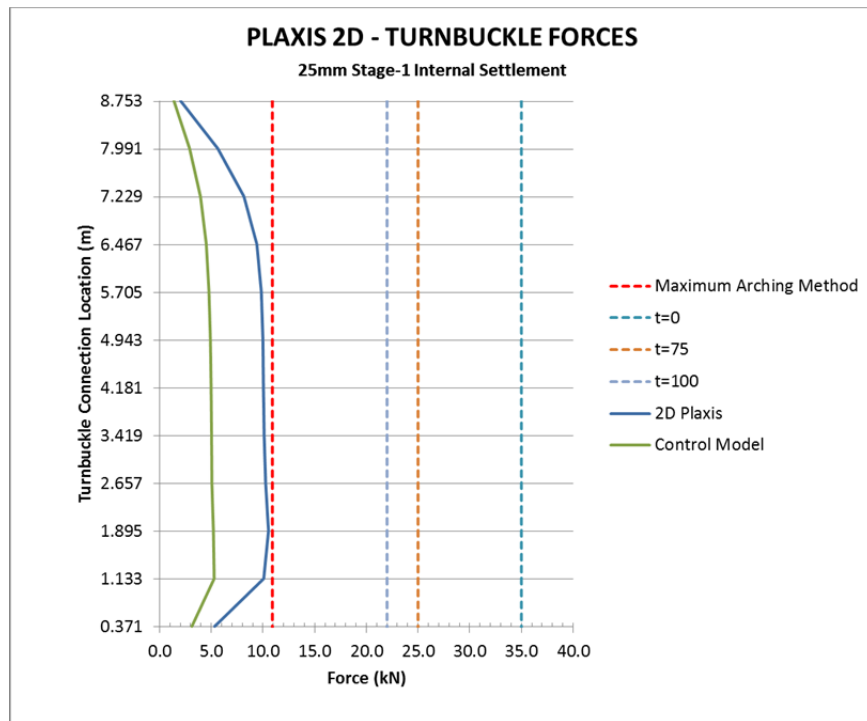

Figure 4-21   Graph of Plaxis 2D 25mm Stage-1 internal settlement – turnbuckle force

Figure 4-22   Plaxis 2D 50mm Stage-1 internal settlement – horizontal pressure

Figure 4-23   Plaxis 2D 50mm Stage-1 internal settlement – turnbuckle force

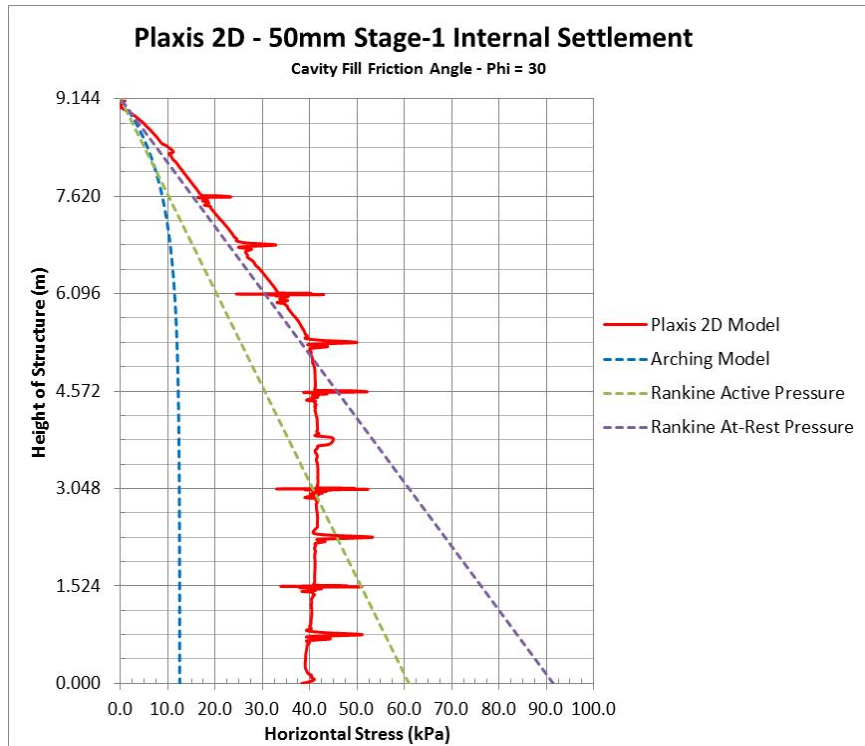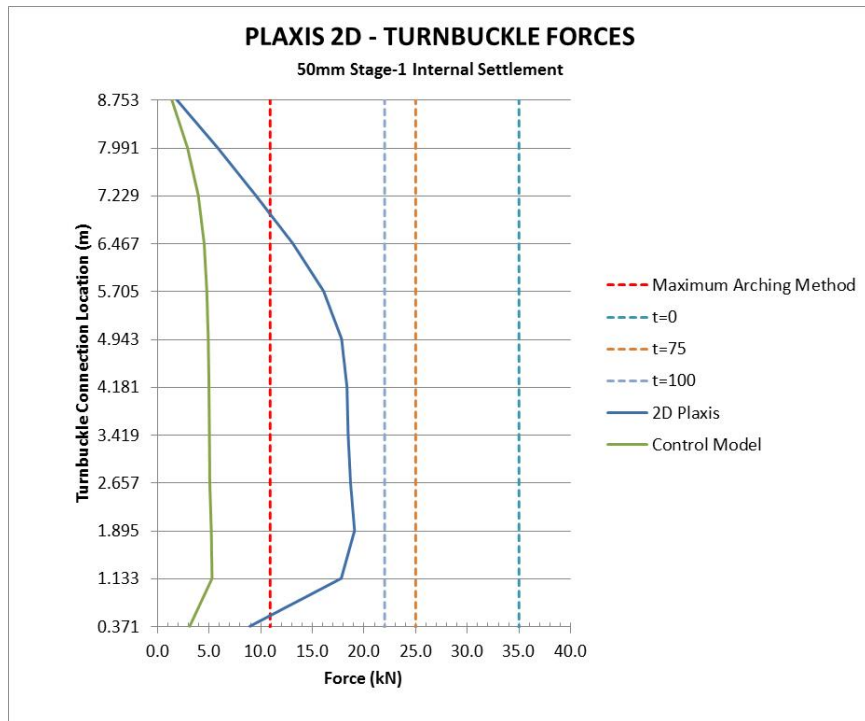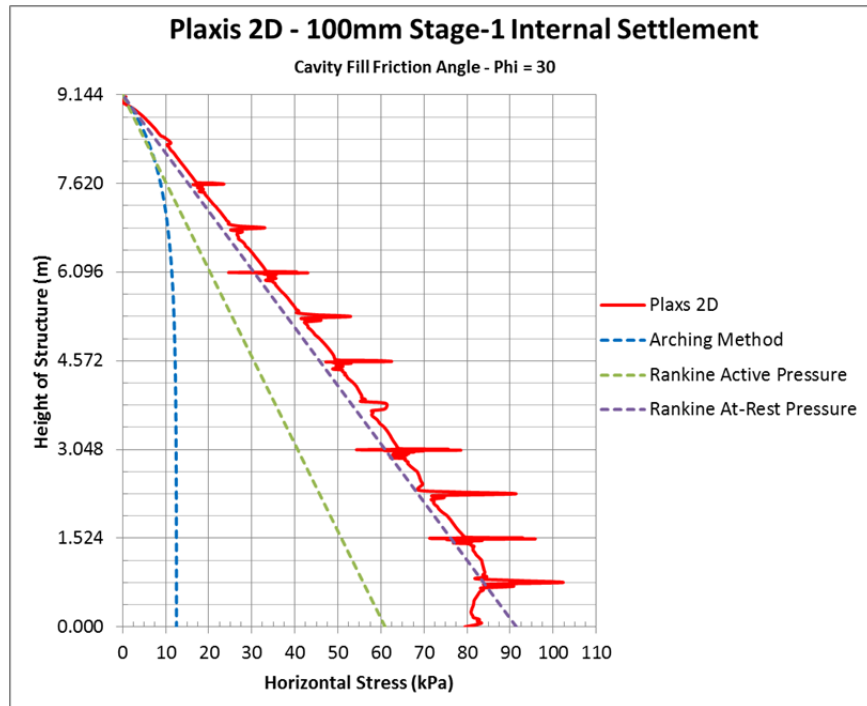Figure 4-24   Plaxis 2D 100mm Stage-1 internal settlement – horizontal pressure
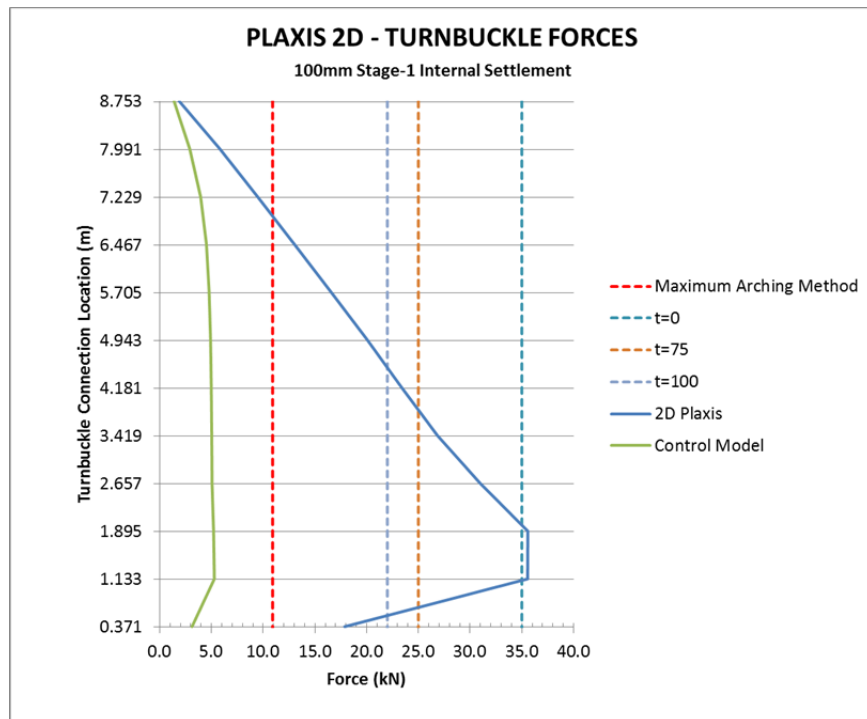
Figure 4-25   Plaxis 2D 100mm Stage-1 internal settlement – turnbuckle force

4.6   Horizontal Stress as a Function of Interface Friction Angle

In order to understand the effect the interface friction angle has on the pressure profile in the 2-Stage structure a parametric study was performed where the interface friction angle was varied using the Arching theory (Equation 2-31) and the Rankine internal earth pressure coefficient (Figure 4-26 to Figure 4-28). To understand the effect that the cavity backfill internal friction angle has on the horizontal pressure it was varied in combination with the interface friction angle.

Figure 4-26   Horizontal pressure as a function of interface friction angle – phi 30°

Figure 4-27   Horizontal pressure as a function of interface friction angle – phi 35°

Figure 4-28   Horizontal pressure as a function of interface friction angle – phi 40°

140

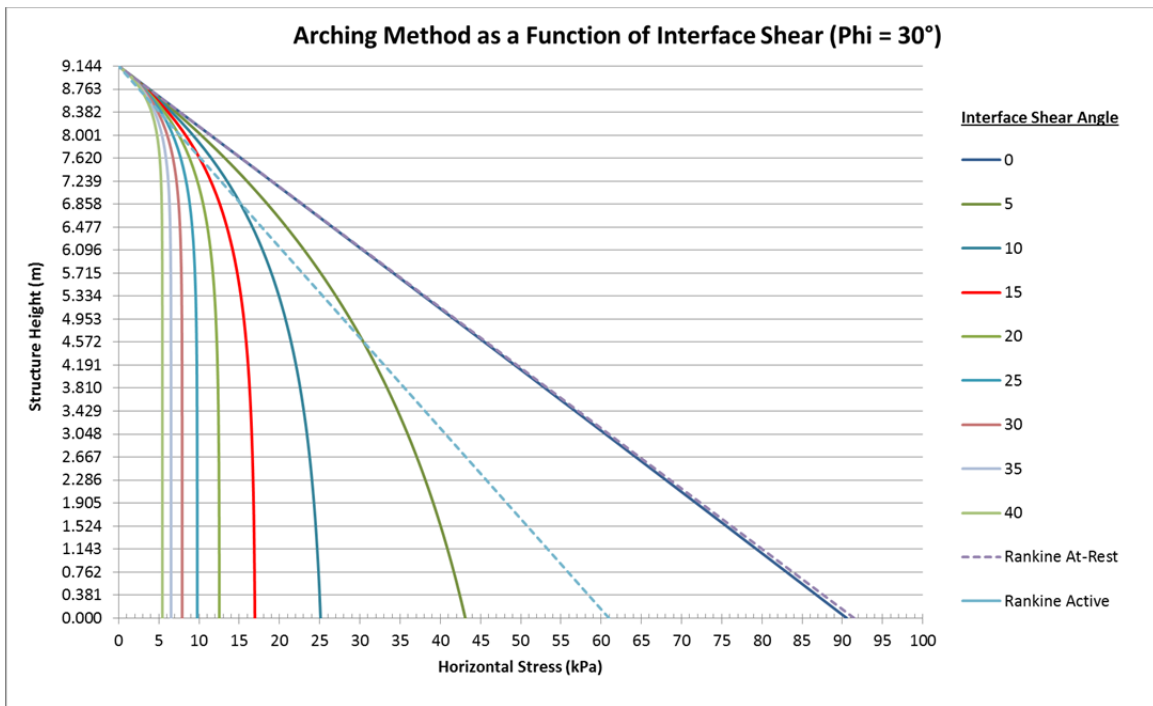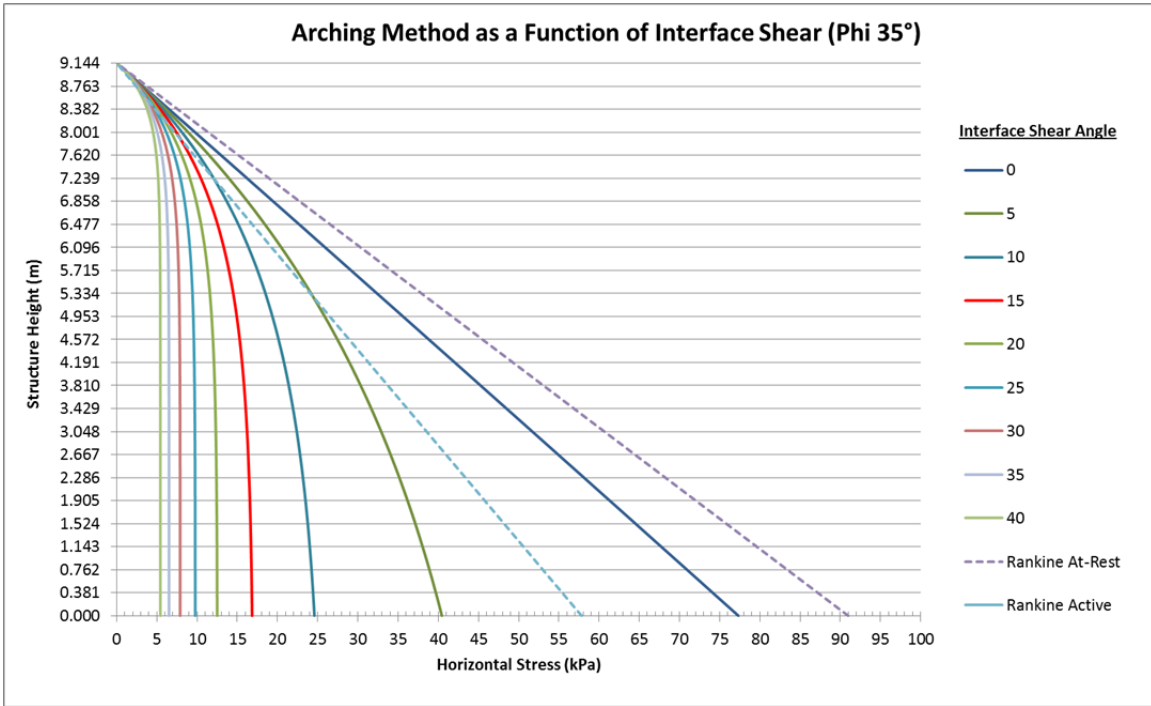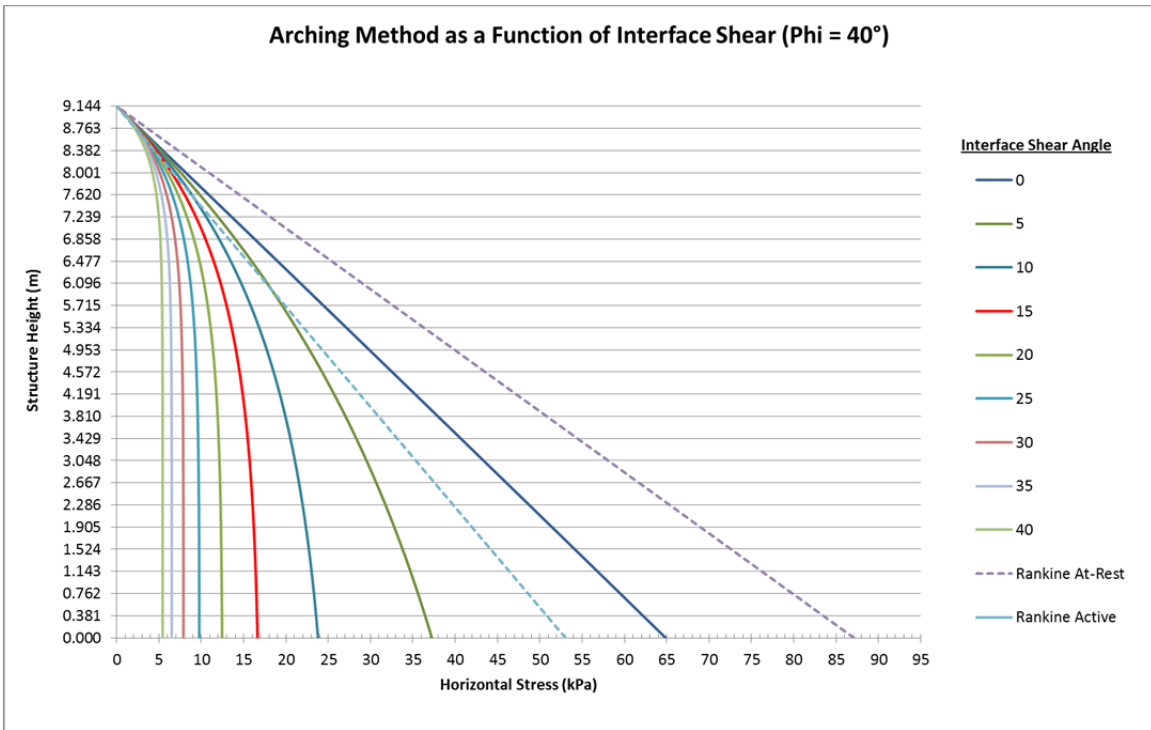Using the Arching theory and as is demonstrated by Figure 4-26 to Figure 4-28 as the interface friction angle decreases the horizontal pressure increases and trends toward the Rankine at-rest condition. The 2-Stage wall is restrained by the turnbuckles and is not free to rotate about its base and therefore cannot achieve the Rankine active case. This justifies the use of the Rankine at-rest pressure coefficient that is equal to the Jaky equation (Equation 2-3) in the Arching equation (Equation 2-31).

Also as demonstrated by Figure 4-26 to Figure 4-28, as the internal friction angle of the cavity fill increases the horizontal pressure decreases. The decrease is due to the use of the Rankine at-rest pressure coefficient in the arching equation. The Rankine at-rest pressure coefficient decreases with an increasing internal friction angle.

The Plaxis control model interface friction angle was then modified to compare the Plaxis 2D results to the Arching Equation. The interface coefficient R_{int} equates to interface friction angles shown in Table 4-14.

Table 4-14   Interface friction angle (δ) as a function of interface coefficient (R_{int})

R_{int}	φ	δ
1.00	30°	30°
0.67	30°	20°
0.33	30°	10°
0.17	30°	5°
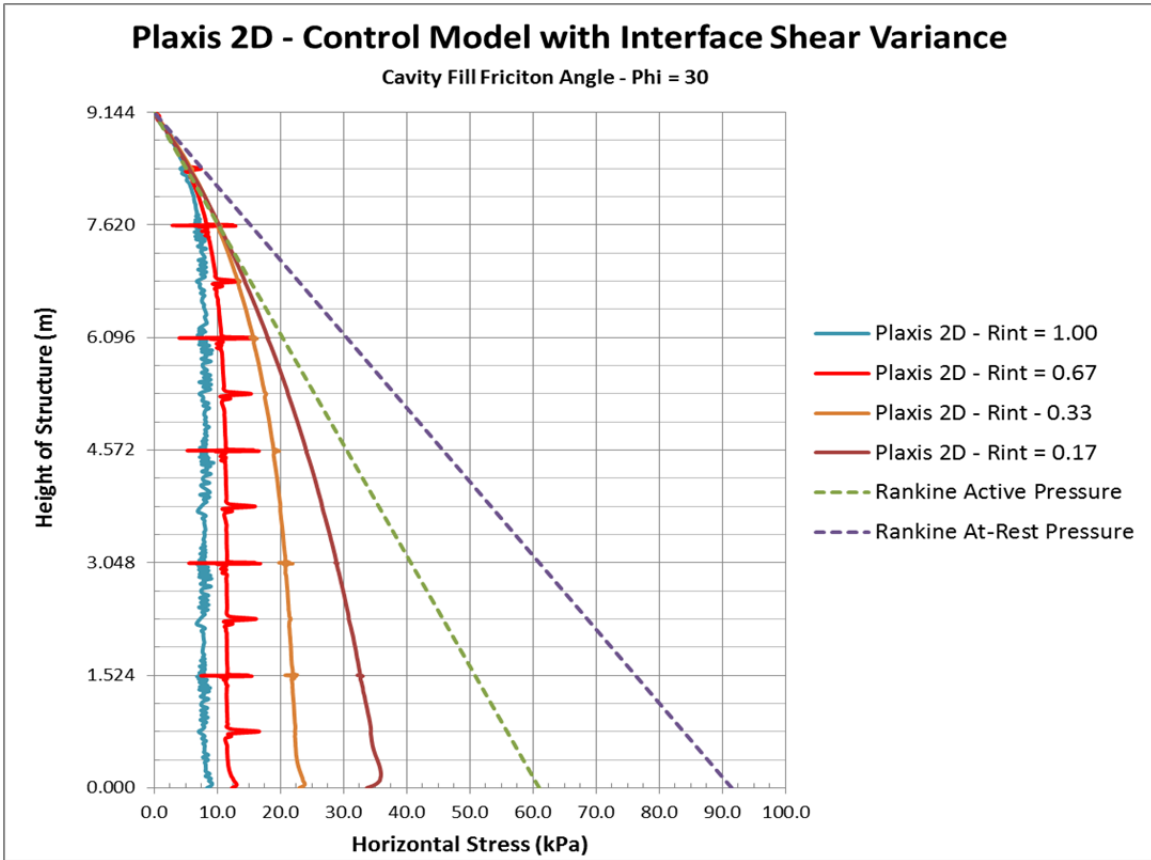
Figure 4-29 Horizontal pressure as a function of interface friction angle for control model
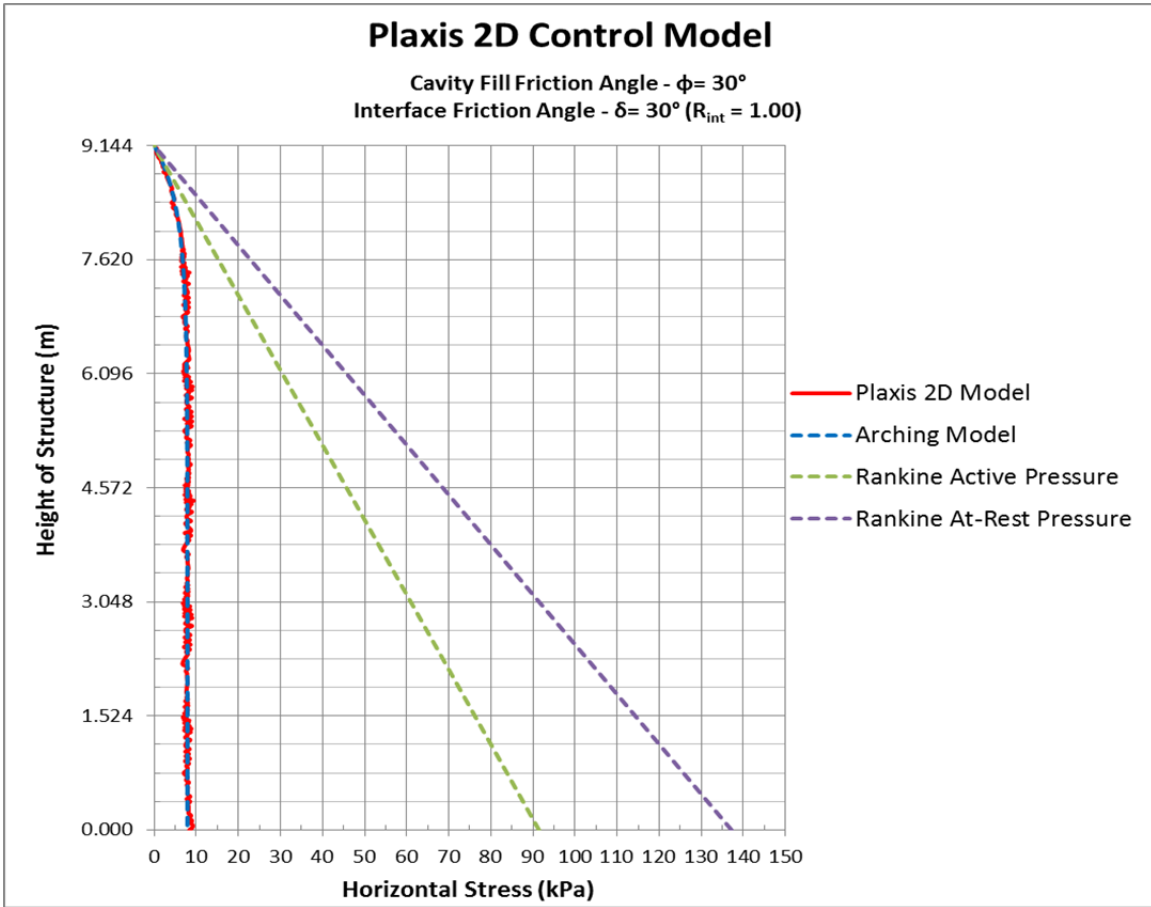
Figure 4-30 Horizontal pressure φ = 30° with δ = 30° (R_{int} = 1.00)
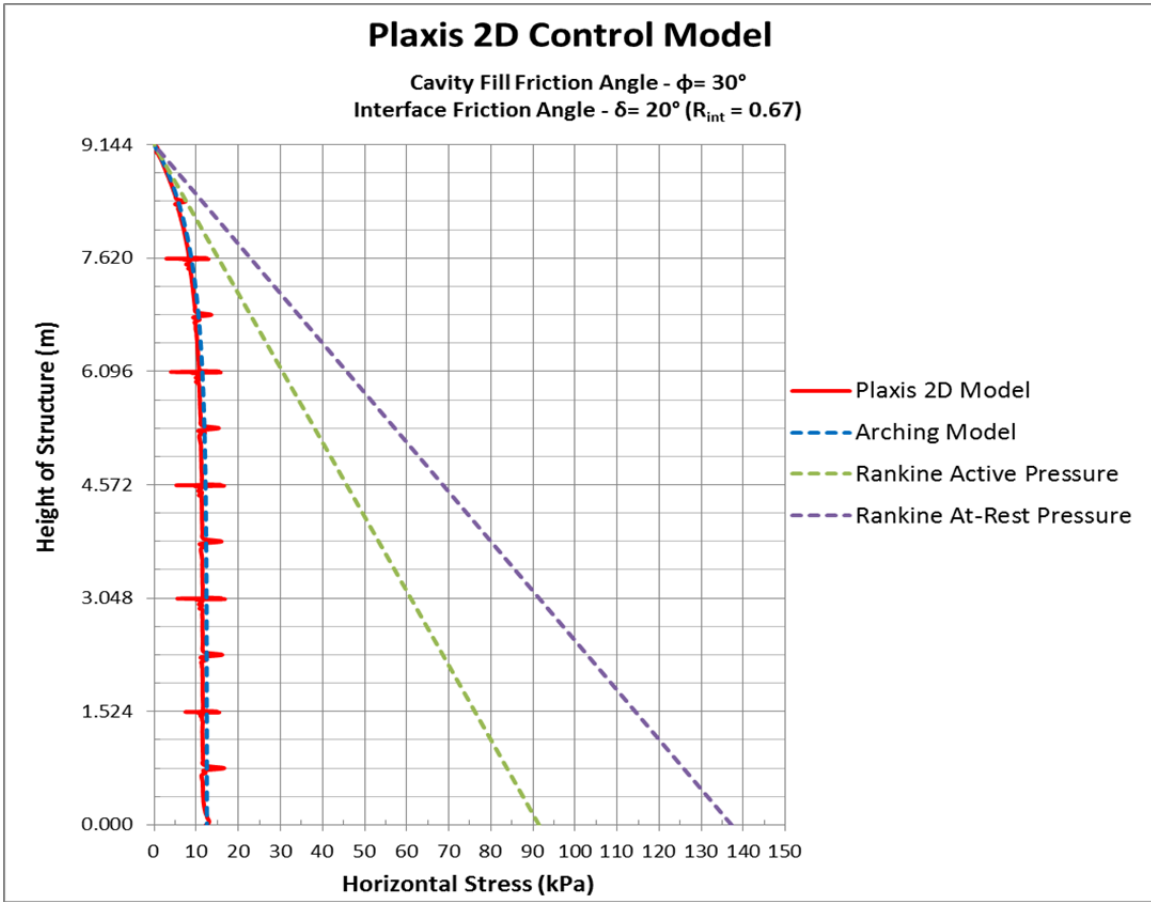
Figure 4-31   Horizontal pressure φ = 30° with δ = 20° (R_{int} = 0.67)
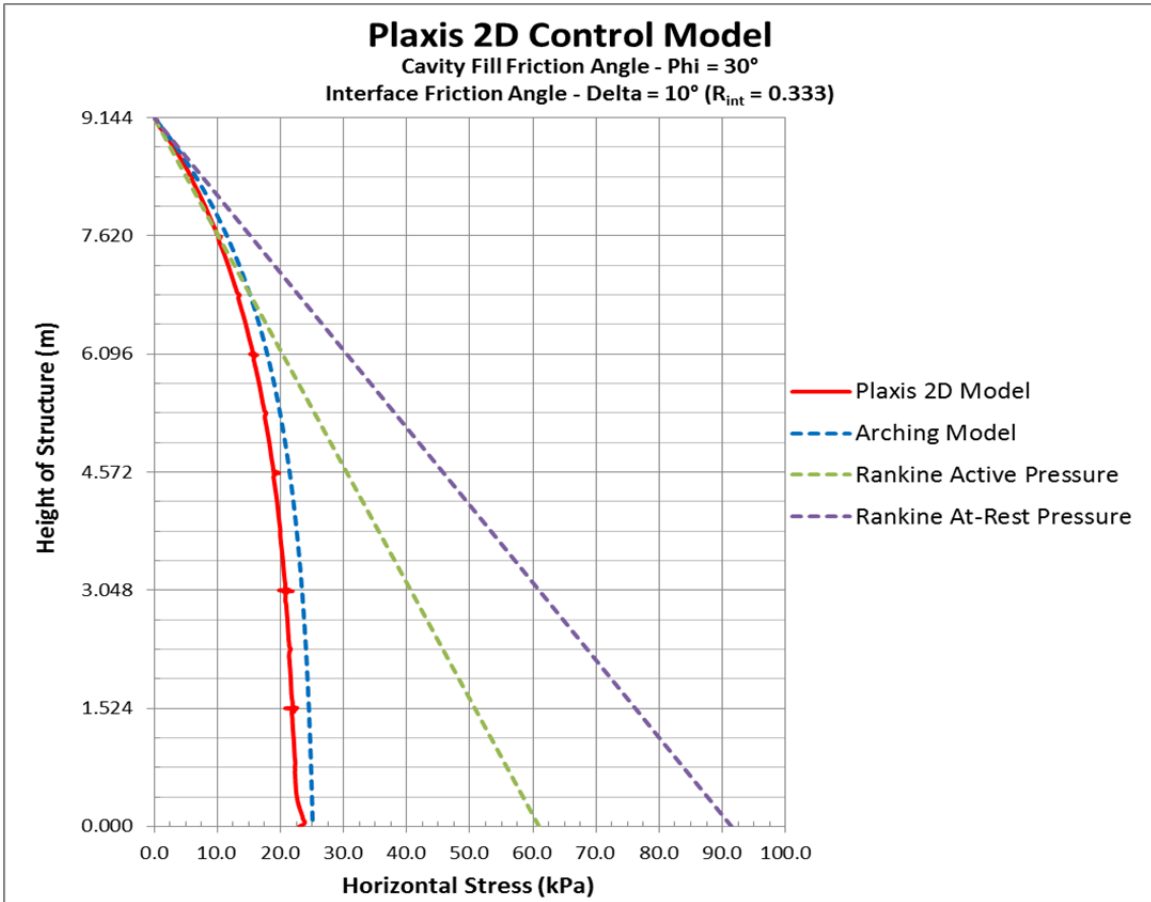
Figure 4-32   Horizontal pressure φ = 30° with δ = 10° (R$_{int}$ = 0.33)
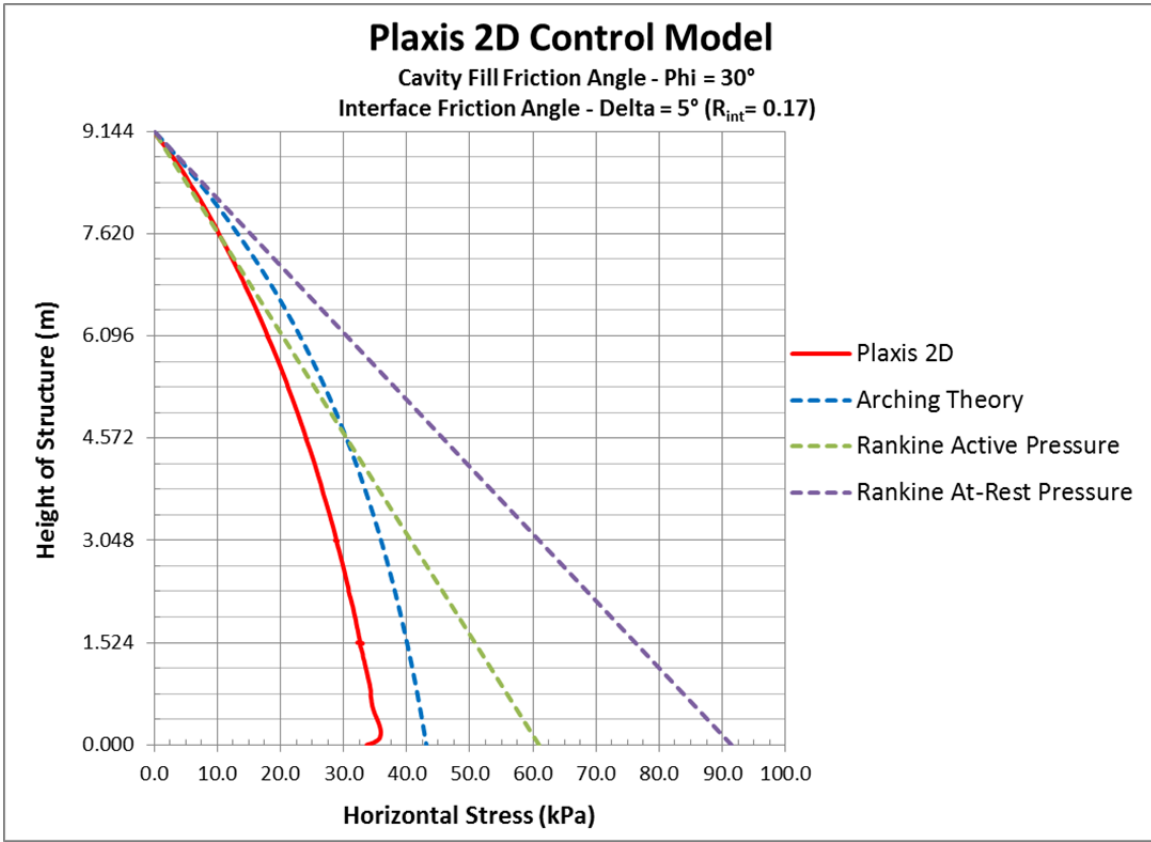
Figure 4-33   Horizontal pressure φ = 30° with δ = 5° (R_{int} = 0.17)

As the interface friction angle decreases the horizontal pressure increases. The Arching equation is a conservative approximation. Based on the figures as the interface friction angle decreases the Arching model predicts higher horizontal stress than the Plaxis 2D model.

At an interface friction angle equal to zero, the horizontal force is equal to the Rankine at-rest force and is calculated using Equation 4-23. This would be the limiting force in the 2-Stage cavity.

$$F = \frac{1}{2} \cdot K_o \cdot \gamma_c \cdot H^2 \qquad\qquad \text{Equation 4-23}$$

Where: F   =   Cavity total force (kN/m)

146

K_o =   Rankine at-rest pressure coefficient

γ_c =   Unit weight of cavity fill (kN/m^3)

H   =   Height of 2-Stage structure (m)

4.7   Horizontal Stress as a Function of Cavity Friction Angle

A study performed by Singh et. al., and Kniss et. al., demonstrated that soil arching is not sensitive to the internal friction angle of the cavity fill material. This relationship is demonstrated in Figure 4-34. As can be seen in this figure the horizontal force is more sensitive to a decrease in the interface friction angle than the increase in the internal friction angle of the cavity fill.
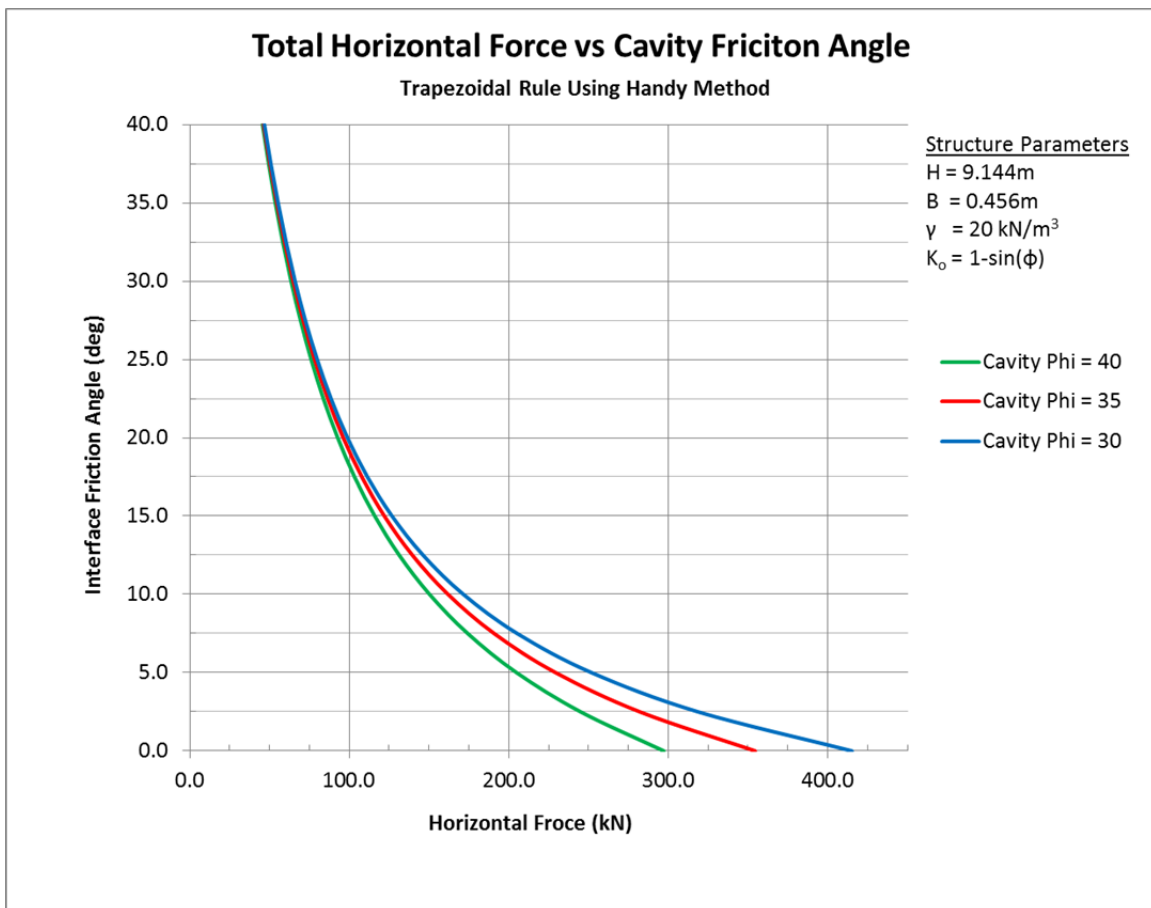
Figure 4-34   Horizontal pressure as a function of internal friction angle

4.8   Free VS Fixed Stage-1 Connection

To understand the implications of fixing the connection to the Stage-1 facing in order to prevent any vertical translation a parameter study was completed in the 3D Plaxis model. A model with the connection fixed in the Z-direction was compared to a model with the connection free in the Z-direction. Both results were compared to the 2D models.

The Static conditions results compared well as is demonstrated in Figure 4-35. This demonstrates that the node-to-node element of the 2D model behaves similarly to a beam element in the 3D model when no movement is occurring.
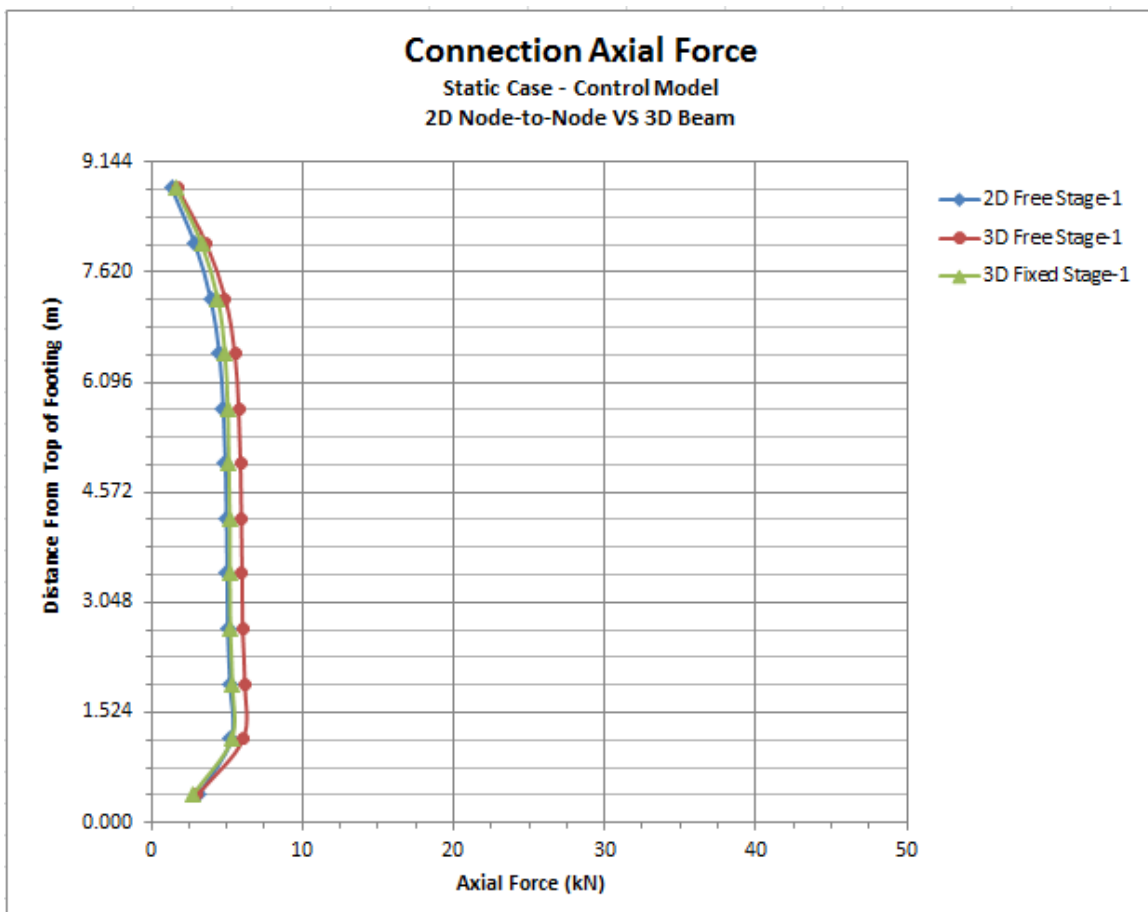
Figure 4-35   Connection axial force comparison for static condition

As movement is introduced the 3D model predicts axial forces that are greater than the forces predicted in the 2D model. There is virtually little difference in the axial force between the fixed and free condition until large settlements occur. At which time the force in the fixed connector increase while the load in the free connection decreases below the load predicted by the 2D case.
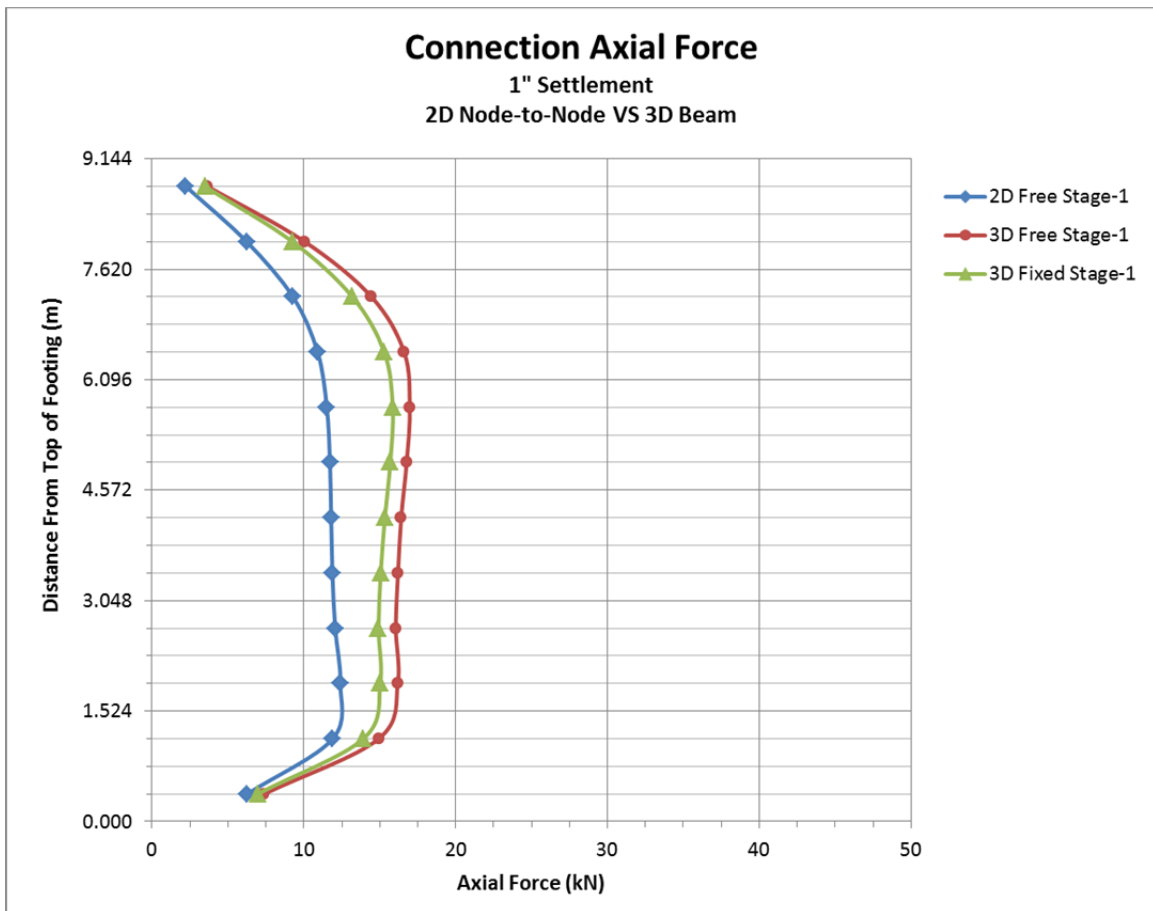
Figure 4-36   Connection axial force comparison for 1" settlement
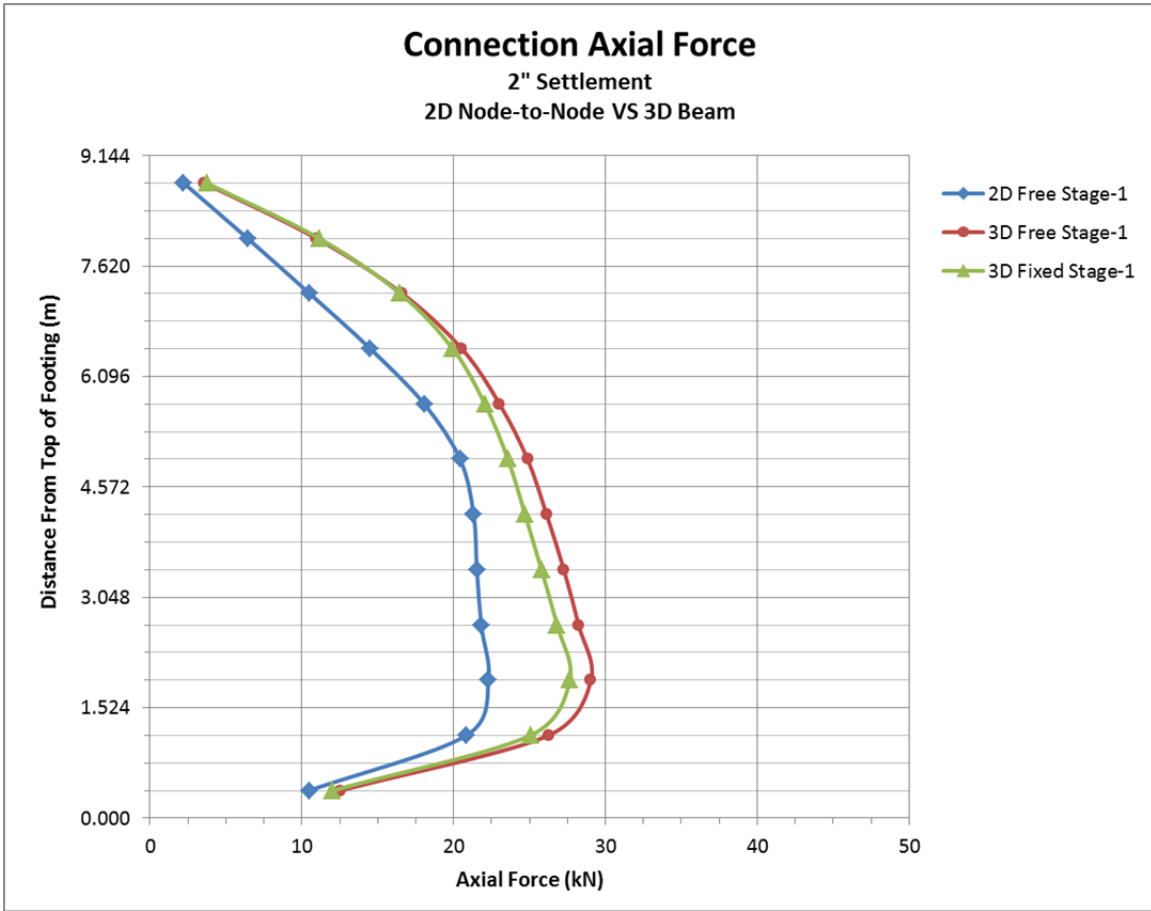
Figure 4-37   Connection axial force comparison for 2" settlement
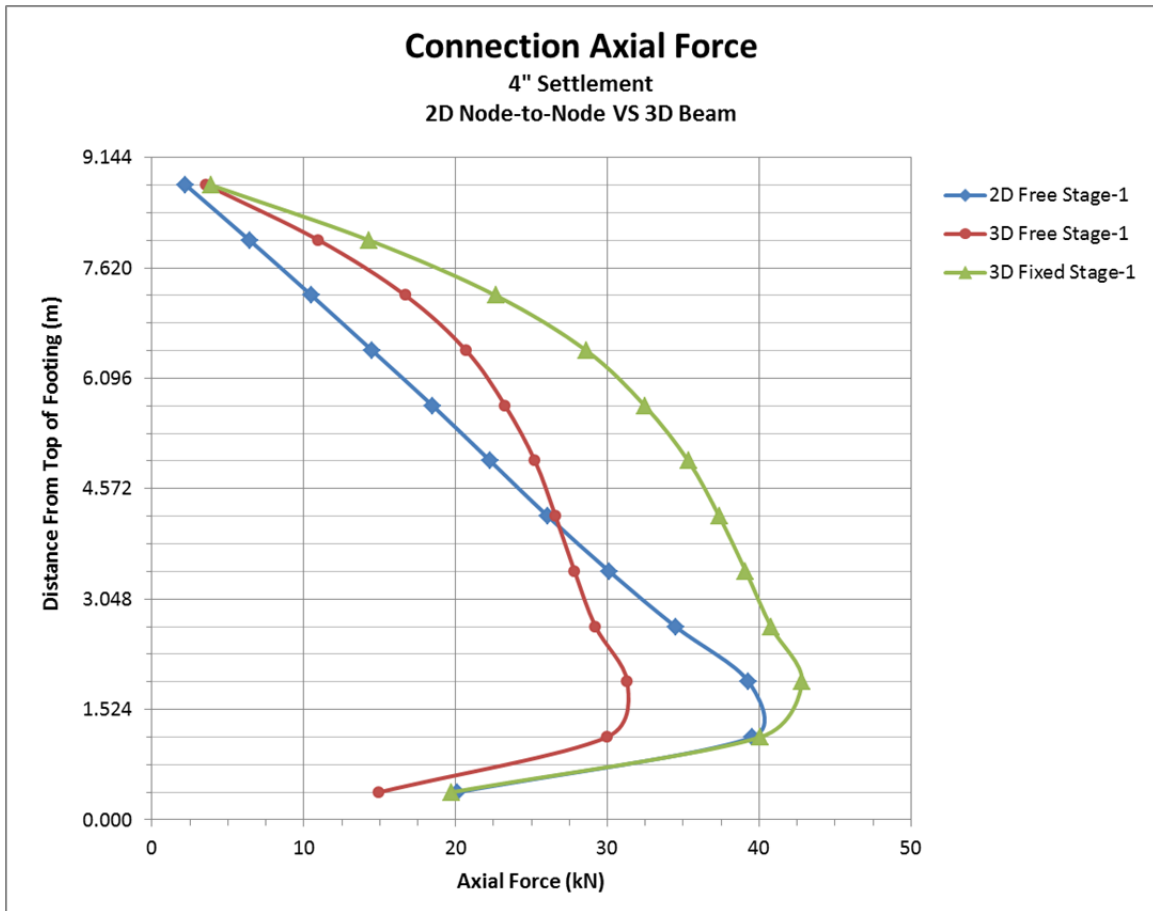
Figure 4-38   Connection axial force comparison for 4" settlement

Based on these results it is apparent that the interaction with the cavity is an important consideration. As the cavity material undergoes large displacement it fully mobilizes and slides by the connector. From this parametric study the following conclusions can be drawn:

1.   The use of a 2D FE or 3D FE with the connection fixed or free produces similar results under small settlement.

2.   When modeling settlement the interaction of the cavity fill and the modeling of the anchor as a beam element that allows for bending

produce higher axial forces than the 2D node-to-node anchor that only

allows axial forces and no bending.

3. Details that allow the connector the ability to freely move when attached

to the Stage-1 wall facing should be included in the design.
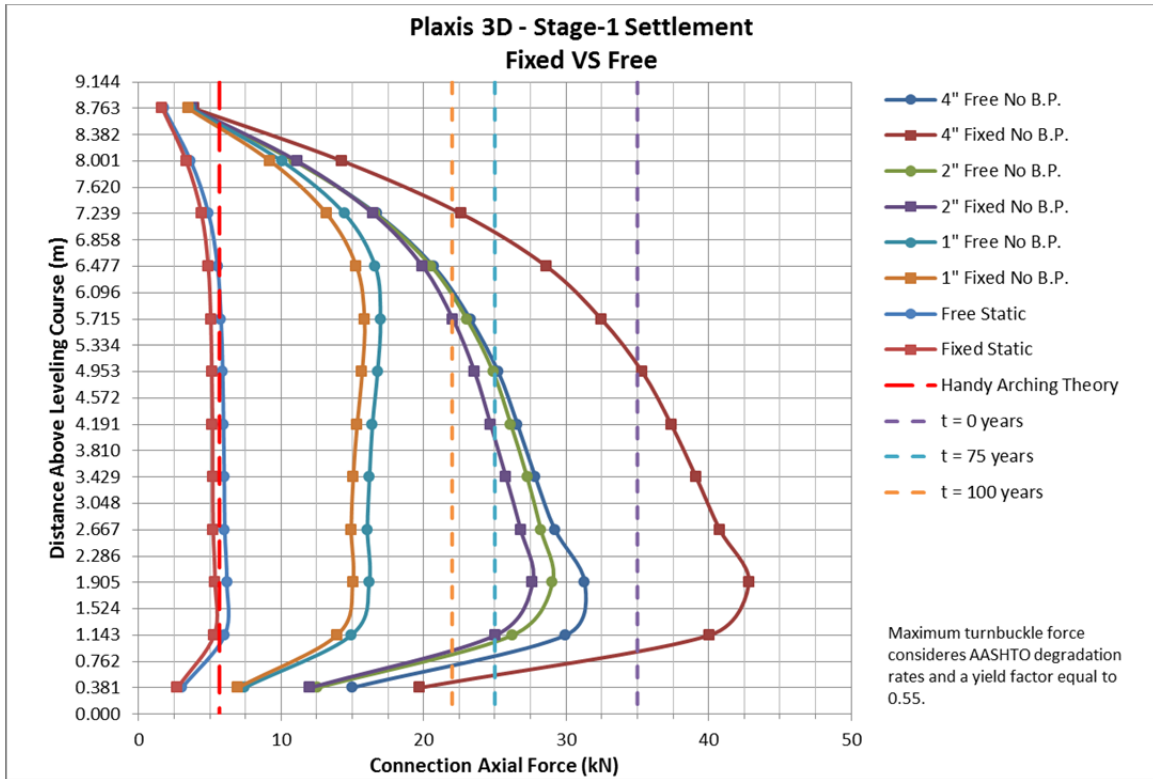
Figure 4-39   Summary of axial forces with settlement

4.9   Discussion of Inclusion of Bearing Pad in FE Model

The bearing pads were modeled in both the 2D and 3D models. Because Plaxis

cannot model the increase in strength of the bearing pad as a function in strain, it was

decided to not introduce the results into the thesis. The location of the bearing pad

created severe spikes in the horizontal pressure and appears to be a result of

compression introducing a similar condition equal to the decrease in the interface friction

angle. As the 2-Stage SCP are placed and the cavity is filled the bearing pads will compress and will increase in strength. Subsequent placement and filling will result in a decrease ability to compress.

Chapter 5

Summary, Conclusions and Recommendations

5.1   Summary

The purpose of the research study was to investigate the stress profile in the cavity and connection capacity for a 2-Stage MSE application. The specific objectives included:

1.   Investigate by using a full-scale structure the amount of settlement that the adjustable 2-Stage connector can tolerate.

2.   Develop 2D and 3D numerical control models to determine the stress profile in the cavity and the forces on the 2-Stage connector.

3.   Verify that the Arching theory is applicable to the design of 2-Stage MSE.

4.   Investigate the effects of post construction internal settlement of the Stage-1 MSE on the stress in the cavity and the forces on the 2-Stage connector.

5.2   Conclusions

The full-scale test structure demonstrated that as the cavity fill settles that the turnbuckle when connected to a vertical facing wire of the Stage-1 structure can slide up the wire in the facing. The ability of the connector to move will decrease the bending moment at the point of connection. It was demonstrated in the 2D numerical model by introducing fixed and unfixed connection points the axial force in the turnbuckle remains unchanged and therefore is a function of the cavity pressure.

Based on both 2D and 3D numerical models for the end of construction stage, e.g. no movement, soil arching is occurring in the 2-Stage structure. The magnitude of the horizontal soil pressure is nearly equivalent to the soil arching theory proposed by Janssen as modified by Handy and Spangler (Equation 2-31). The use of the Rankine at-rest earth pressure coefficient in the arching Equation 2-31 predicts the horizontal pressure that developed in the Plaxis 2D model. Therefore, in the design of a 2-Stage structure a constant pressure predicated by the maximum horizontal pressure that is calculated using the Handy Simplified method shown in Equation 2-30 should be used. Because of the likelihood that some settlement of the 2-Stage structure may occur a safety factor should be included and can be achieved by introducing a reduction factor that is then applied to the interface friction angle.

Based on both 2D and 3D numerical models the horizontal pressure increases as the interface friction angle decreases trending toward the Rankine at-rest condition. The forces in the turnbuckle increase proportionally to the increase in the horizontal pressure of the cavity. As the interface friction angle decreases the depth that the horizontal pressure follows the Rankine at-rest earth pressure condition increases.

The Rankine at-rest condition was reached at 100mm of settlement for the height of the structure modelled in this thesis. For the settlements that were in between this limiting value the Rankine at-rest condition was followed to a certain depth than the horizontal pressure became constant. The depth at which the pressure became constant increased with increasing settlement. Because settlement of the 2-Stage structure is not predictable due to the numerous factors that influence it, the interface friction angle should be decreased by a factor of 2.

Based on the findings in this thesis it is recommended that Equation 5-1 be used to determine the maximum force in the cavity for a 2-Stage structure and incudes the reduction factor for the interface friction angle.

$$F_{max} = \frac{\gamma_c \cdot B \cdot H}{2 \cdot \tan(\theta_f \cdot \delta)}$$

Equation 5-1

Where: F_{max} =   maximum cavity total force (kN/m)

γ_c =   unit weight of cavity fill (kN/m^3)

B   =   width of cavity (m)

H   =   height of cavity (m)

δ =   interface friction angle (deg)

θ_f =   reduction factor (dim)

5.3   Recommended 2-Stage Details

The details that are currently used by different MSE companies are proprietary and are covered by numerous US patents. Based on the review of the literature, experience with the design and construction of 2-Stage structures and this thesis the following recommend details should be included in all 2-Stage structures.

1   To induce settlement of the Stage-1 MSE, place a temporary surcharge at top of structure equal to 33% of the structure height or a minimum of 1.5m whichever is greater. The temporary surcharge structure should not be removed until all anticipated settlement has occurred.

2   In order to limit bulging of the Stage-1 face, a 610mm rock zone should be placed in the face area. In addition, the compaction requirements for

the face area (1m zone) should be increased and testing requirements incorporated into the specification.

3   To aid in construction in placement of the Veneer in the 2-Stage connector it is recommended that the following be included:

a.   The levelling pad that the panel bears on should be cast at an elevation that allows for placement of the 2-stage connectors as near to the horizontal as possible. This would require that the SCP panels be detailed and cast after all anticipated settlement has occurred.

b.   The cavity dimensions shall be verified after all anticipated settlement has occurred and the 2-stage connection element shall be fabricated to fit the as constructed conditions.

4   One end of the 2-Stage connection should be able to move in the vertical direction.

5   The bearing pad coverage area should be a minimum of 25% of the panel-to-panel interface area.

6   Steel alignment pins should be used at the panel-to-panel interface for all panels.

7   A minimum of one row of standard soil reinforcing should be attached to the top panel and extend a minimum of 70% of the structure height over the Stage-1 MSE.

5.4   Recommendations for Future Studies

Based on the numerical model and the test structure it is apparent that future study on a full height 2-Stage structure is warranted. Future test structures should be instrumented at varying heights and varying cavity widths. Different facing materials should be used to understand the effect varying interface friction angles have on the horizontal pressure profile.

It is recommended that instrumentation consist of the following:

- Strain gauge of the turnbuckles at different locations along its length to determine the axial force.

- Strain gauges at the connection points.

- Pressure cells at the base of the cavity to determine the vertical pressure at the base of the cavity.

- Pressure cells along the interface of the Stage-1 and Stage-2 structure to verify the horizontal pressure with depth.

Because of the continued use of the 2-Stage wall system on transportation structures a design manual and specification should be prepared.

References

[1]   AASHTO (2002). "Standard Specifications for Highway Bridges, 17th Edition", American Association of State Highway and Transportation Officials, Washington, DC

[2]   AASHTO (2009). "LRFD Bridge Design Specifications, 2009 Interims", American Association of State Highway and Transportation Officials, Washington, DC.

[3]   AASHTO (2010)." LRFD Bridge Design Specifications, 5th Edition", American Association of State Highway and Transportation Officials, Washington, DC.

[4]   AASHTO (2012). "LRFD Bridge Design Specifications, 6th Edition", American Association of State Highway and Transportation Officials, Washington, DC.

[5]   Adib, M. E., (1988)." Internal Lateral Earth Pressure In Earth Walls", Ph.D. Dissertation, University of California, Berkley, Civil Engineering Department..

[6]   Allen, T.M., Bathurst, R.J. (2001). "Application of the Ko-Stiffness Method to Reinforced Soil Limit States Design," Washington State Department of Transportation Report No. WA-RD 528.1, Olympia, WA.

[7]   Anderson, Loren R., et.al., (1985). "Performance of Rainier Avenue Welded Wire Wall", Seattle, Washington, Department of Civil and Environmental Engineering, Utah State University.

[8]   Anderson, P.L, (1991). "Subsurface Investigation and Improvements for MSE Structures Constructed on Poor Foundation Soils," 34th Annual Meeting, Association of Engineering Geologists," Environmental and Geological Challenges for the Decade, pp. 77-85

[9]   Anderson, P.L., and Brabant, K. (2005). "Increased Use of MSE Abutments," Proceedings of the 22nd Annual International Bridge Conference, Pittsburgh, PA, paper 5-10

[10] Anderson, P.L., Gladstone, R.A., and Withiam, J.L., (2010). "Coherent Gravity: The Correct Design Method for Steel-Reinforced MSE Walls," Proceedings of ER2010 Earth Retention Conference 3, ASCE, Bellevue, Washington

[11] Anderson, P.L., Gladstone, R.A., and Sankey, J.E., (2012). "State of the Practice of MSE Wall Design for Highway Structures," Geotechnical Engineering State of

the Art and Practice: Keynote Lectures from GeoCongress 2012, Oakland, California.

[12] Australian Standard AS 3774 (1996). "Loads on Bulk Solids Containers". Council of Standards Australia, Committee BD/65, October 1996.

[13] Bastick, M., Schlosser, F., Segrestin, P. Amar, S., and Canepa, Y. (1993). "Experimental Reinforced Earth Structure of Bourron Marlotte: Slender Wall and Abutment Test," Reinforcement Des Sols: Experimentations en Vraie Grandeur des Annees 80, Paris, pp. 201-228

[14] Bishop, Jerold A., (1980). "Evaluation of a Welded Wire Retaining Wall", M.S. Thesis, Utah State University, Civil and Environmental Engineering.

[15] Bloomfield, R. A., Soliman, A. F. & Abraham, A. (2001). Performance of mechanically stabilized earth walls over compressible soils. In Landmarks in Earth Reinforcement, Ochiai, H. and Yasufuku, N. (eds), Swets and Zeitlinger, Balkema, pp. 317–322

[16] Bonczkiewicz, C.B., (1990). "Evaluation of Soil-Reinforcement Parameters and Interaction by Large Scale Pullout Test, Masters of Science in Engineering Thesis submitted to Northwestern University, Evanston, Illinois.

[17] Bounaparte R., and Schmertmann, G (1987). "Reinforcement Extensibility in Reinforced Soil Wall Design". Nat Advanced Research Workshop, Application of Polymeric Reinforcement in Soil Retaining Structures, Royal Military College of Canada, Kingston, Ontario.

[18] Bowels, J.E. (1996). "Foundation Analysis and Design", 5th Edition. McGraw Hill Inc, Singapore.

[19] Christopher, B.R. and Bonczkiewicz, C.B., (1989). "Preliminary Results of Full Scale Field Test for Behavior of Reinforced Soil", Research Report to the U.S. Department of Transportation, Federal Highway Administration. FHWA Contract No. 61-84-C-00073.

[20] Christopher, B.R., Gill, S.A., Juran, I., Mitchell, J.K., (1990). "Reinforced Soil Structures, Vol. 1, Design and Construction Guidelines", FHWA-RD-89-043.

[21] Christopher, B.R., (1993). "Deformation Response and Wall Stiffness in relation to Reinforced Soil Wall Design", Ph.D. Dissertation, Purdue University

[22] Clayton, C. R. I., Woods, R. I., Bond, A. J. and Militisky, J (2013). "Earth Pressure and Earth-Retaining Structures", 3rd Edition. CRC Press, New York.

[23] Collin, J.G., "Earth Wall Design", 1988, Ph.D. Dissertation, University of California, Berkley, Civil Engineering Department.

[24] Coulomb C.A., (1776). Essai sur une application des regles des maximis et minimis a quelques problemes de statique relatifs a l'architecture. Memoires de l'Academie Royale pres Divers Savants, Vol. 7

[25] Crigler, J. R. (1999). "Mechanically Stabilized Retaining Wall System Having Adjustable Connection Means for Connecting Precast Concrete Facing Panels Thereto", U.S. Patent 5,971,669, October 22, 1999.

[26] Damians, I. P., Lloeret A., Josa A, and Bathurst R. J. (2013). "Influence Of Facing Vertical Stiffness On Reinforced Soil Wall Design", Proceedings of the 18th International Conference on Soil Mechanics and Geotechnical Engineering, Paris 2013

[27] Das, B. M. and Shukla, S. K. (2013). "Earth Anchors", 2nd Edition. J. Ross Publishing Inc., Plantation, Florida.

[28] Duncan, J. M. and Chang, C. Y. (1970). "Nonlinear Analysis of Stress and Strain in Soils", Journal of Soil Mechanics and Foundations Division, Proceedings of the American Society of Civil Engineers, September 1970.

[29] Duncan, J. M. and Seed, R. B. (1984). "SSCOMP: A Finite Element Analysis Program for Evaluation of Soil-Structure Interaction and Compaction Effects", Report No. UCB/GT/84-02, Department of Civil Engineering, University of California at Berkley.

[30] Duncan, J. M., Byrne, P., Wong, K. S. and Marby, P (1980). "Strength, Stress-Strain and Bulk Modulus Parameters for Finite Element Analyses of Stresses and Movements in Soil". Report No. UCB/GT/80-01 College of Engineering, Office of Research Services, University of California, Berkeley, California.

[31] Frydman, S. and Keissar, I (1987). "Earth Pressure on Retaining Walls Near Rock Faces". Journal of Geotechnical Engineering, ASCE 113 (6), 586-599.

[32] Ehrlich, M.E. and Mitchell J.K., (1994). "Working Stress Design Method for Reinforced Soil Walls", Journal of Geotechnical Engineering, Vol 120, No. 4, pp. 625-645.

[33] Gerber, T.M. (2011). "Observing and Improving the Performance of Two-stage Mechanically Stabilized Earth (MSE) Walls", Proceedings of Geo Frontiers, Dallas Texas, March 11-13, 2011, pg. 3459-3468.

[34] Handy, R. L. (1985). "The Arch in Soil Arching", Journal of Geotechnical Engineering, Volume III, No. 3, pages 302-317.

[35] Handy, R. L. and Spangler, M. G. (2007). "Geotechnical Engineering: Soil and Foundation Principles and Practice, Fifth Edition". McGraw-Hill Companies, New York, New York, pg. 544-555

[36] Hu, Y. (2004). "Design Implications of Limited Backfill Space in Retaining Walls". Master of Science Thesis, University of Delaware, Newark Delaware.

[37] Hunt, R. E., (1985). "Geotechnical Engineering Techniques and Practices". McGraw-Hill Inc.

[38] Huntington, W. C. (1957). "Earth Pressures and Retaining Walls". John Wiley and Sons, Inc. London.

[39] Jaber, M. (1989), "Behavior of Reinforced Soil Walls in Centrifuge Model Tests", Dissertation submitted in partial satisfaction of the requirements for the degree of Doctor of Philosophy, University of California, Berkeley, Department of Civil Engineering, March, 1989.

[40] Jaky, J. (1944). "The Coefficient of Earth Pressure at Rest", J. Soc. Hungarian Architects and Engineers (October), pp. 355-358.

[41] Janssen, H.A. (1895). "Tests On Grain Pressures In Silos", Zeitschrift des Vereines Deutscher Ingenieure, Band 39, No. 35, p 1045.

[42] Jewell, R.A., (1984). "Reinforcement Bond Capacity", Geotechnique 40, No. 3, 513-518.

[43] Jones, C. J. F. P. (1985). "Earth Reinforcement and Soil Structures", Butterworths Advance Series in Geotechnical Engineering.

[44] Juran, I. (1985). "Behavior of Reinforced Soil Structures", Research Report No. 1 to the U.S. Department of Transportation, Federal Highway Administration, FHWA No. 61-84-C-00072, 31 p.

[45] Juran, I., and Schlosser, F., (1978). "Theoretical Analysis of Failure in Reinforced Earth Structures", Proceedings, ASCE Symposium on Earth Reinforcement, Pittsburgh, pp. 528-555.

[46] Ketchum M. (1919). "The Design Of Walls, Bins And Grain Elevators", McGraw-Hill Book Comp. Inc., New York.

[47] Kniss, K. T., Wright S. G., Zornberg, J., and Yang, K (2007). "Design Considerations for MSE Retaining Walls Constructed in Confined Spaces", Center for Transportation Research, The University of Texas at Austin, 2007.

[48] Kondner, R.L. and Zelasko, J.S. (1963)," A Hyperbolic Stress-Strain Formulation of Sands", Proceedings of the 2nd Pan American Conference on Soil Mechanics and Foundation Engineering, Brazil, Vol 1, pp 289-324

[49] Krynine, J. J. (1945). "Discussion of Stability and Stiffness of Cellular Cofferdams", Transactions of the American Society of Civil Engineers, Volume 71, Issue 6, June 1945, pg. 996-996.

[50] Leshchinsky, D., Hu, Y and Han, J. (2004). "Limited Reinforced Space in Segmental Retaining Walls", Science Direct, Geotextiles and Geomembranes 22 (2004) 543-553.

[51] Macnab, A. (2002). "Earth Retention Systems Handbook". McGraw-Hill, New York.

[52] Marston, A. (1930). "The Theory Of External Loads On Closed Conduits In The Light Of Latest Experiments", Bulletin No. 96, Iowa Engineering Experiment Station, Ames, Iowa

[53] Meyerhof, G. G., 1953, "The Bearing Capacity of Foundations Under Eccentric and Inclined Loads", Proceedings of the Third International Conference of Soil Mechanics and Foundation Engineering, Vol. 1, pp. 225-244.

[54] Morrison, K F., Harrison E. F., Collin, J. G., Dodds, A., and Arndt, B. (2009). "Shored Mechanically Stabilized Earth (SMSE) Wall Systems Design Guidelines", FHWA-CFL/TD-06-001.

[55] Moradi, G., and Abbasnejad, A. (2013). "The State of the Art Report on Arching Effect", Journal of Civil Engineering Research 2013, 3(5), pg 148-161

[56] McKittrick, D.P. (1978). "Reinforced Earth: Application of Theory and Research to Practice", keynote paper, Symposium on Soil Reinforcing and Stabilizing Techniques, Sydney, Australia.

[57] Mitchel, J.K. and Villet, W.B.C., (1987), "Reinforcement of Earth Slopes and Embankments", NCHRP Report No. 290, Transportation Research Board, Washington D.C.

[58] Mitchel, R.J., (1983). "Earth Structures Engineering", Alan And Unwin, Inc., Pp. 39-61.

[59] NCHRP 290 (1987). "National Cooperative Highway Research Program Report 290, Reinforcement of Earth Slopes and Embankments," Transportation Research Board, Washington, D.C.

[60] National Highway Institute (2009). "Design and Construction of Mechanically Stabilized Earth Walls and Reinforced Soil Slopes", FHWA-NHI-10-024 and 025, Volumes I and II, NHI Course Nos. 132042 and 132043, November 2009.

[61] Neely, W. J., 1993, "Field Performance of a Retained Earth Wall", Reinforcement Des Sols: Experimentations en Vraie Grandeur des Annees 80, Paris, pp. 171-200.

[62] Nilson A.H. and Winter, G (1991). "Design of Concrete Structures". McGraw-Hill, Inc., New York.

[63] Nova, R (2004). "Development of Elastoplastic Strain Hardening Models of Soil Behavior", Degradations and Instabilities in Geomaterials, International Centre for Mechanical Sciences Volume 461, 2004, pp 35-76.

[64] Paik, K. H. And Salgado, R. (2003). "Estimation Of Active Earth Pressure Against Rigid Retaining Walls Considering Arching Effects", Geotechnique 53, No. 7, pg 643–653

[65] Plaxis 2D AE.02 (2014). "Reference Manual 2D" Plaxis B.V., Delft University of Technology, The Netherlands.

[66] Plaxis 3D (2013). "Reference Manual 3D" Plaxis B.V., Delft University of Technology, The Netherlands.

[67] Sampaoc, Casan L., (1994). "Behavior of Welded Wire Mesh Reinforced Soil Walls From Filed Evaluation and Finite Element Simulation", Ph.D. Thesis, Utah State University, Civil and Environmental Engineering

[68] Schanz, T. and Vermeer, P.A. (1996). "Angles of Friction and Dilatancy of Sand", Geotechnique 46, No. 1, pg. 145-151

[69] Schlosser, F., (1978). "History, Current Development, and Future Developments of Reinforced Earth", Symposium on Soil Reinforcing and Stabilizing Techniques, sponsored by New South Wales Institute of Technology and the university of Sidney, Australia.

[70]   Schmertmann, G., Chew, S.H., and Mitchell, J., "Finite Element Modelling of Reinforced Soil Wall Behavior," Geotechnical Engineering Report No. UCB/GT/89-01, University of California, Berkeley, September, 1989.

[71]   Segrestin, P. and Bastick, M. (1996). "Comparative Study and Measurement of the Pull-Out Capacity of Extensible and Inextensible Reinforcements," International Symposium on Earth Reinforcement, Fukuoka, Kyushu, Japan, A.A. Balkema, pp. 139-144.

[72]   Simac, M.R., Christopher, B.R., Bonczkiewicz, C. (1990). "Instrumented Field Performance of a 6-m Geogrid Soil Wall," Proceedings, 4th International Conference on Geotext.

[73]   Singh, D. and Moysey E. B. (1985). "Grain Bin Wall Pressures: Theoretical And Experimental", Canadian Agricultural Engineering 27, pg 43-48.

[74]   Take, W. A. and Valsangkar, A. L. (2001), "Earth Pressure on Unyielding Retaining Walls of Narrow Backfill Width". Can. Geotech Journal, 38: 1220-1230.

[75]   Tanyu, B. F., Sabatini, P. J., and Berg, R. R. (2007). "Earth Retaining Structures", FHWA-NHI-07-071. National Highway Institute, Washington D.C.

[76]   Taylor, T. P. and Hilfiker W. K. (2000). "System for Securing Face Panel to an Earthen Formation". U.S. Patent 6,024,516 A, February 15, 2000.

[77]   Taylor, T. P. and Bagwell, J. S. (2011). "Two Stage Mechanically Stabilized Earth Wall Systems", U.S. Patent 7,891,912 B2, February 22, 2011.

[78]   Taylor, T. P. (2013). "Two Stage Mechanically Stabilized Earth Wall Systems", U.S. Patent 8,496,411 B2, July 30, 2013.

[79]   Tein, H (1996). "A literature study of the arching effect" Master of Science Thesis, Massachusetts Institute of Technology, Cambridge, Massachusetts.

[80]   Terzaghi, K (1936). "A Fundamental Fallacy In Earth Pressure Computations". Journal Boston Society of Civil Engineers reprinted in Contributions to Soil Mechanism 1924-1940 by the Society, Boston, Massachusetts.

[81]   Terzaghi, K (1936). "Stress Distribution in Dry and in Saturated Sand Above a Yielding Trap-Door", Proceedings, Frist International conference on Soil Mechanics and Foundation Engineering, Cambridge, Massachusetts, pp. 307-311.

[82] Terzaghi, K (1943). "Theoretical Soil Mechanics". John Wiley and Sons, Inc., New York, New York.

[83] Terzaghi, K, Peck, R. A. and Gholamreza, M (1996). "Soil Mechanics in Engineering Practice – 3rd Edition". John Wiley and Sons, Inc., New York, New York.

[84] Timmons, M. and Bloomfield, R (2004). "Two Stage Wall Connector". U.S. Patent 6,802,675, October 12, 2004.

[85] Winkerton, Hans F. and Fang, Hsai-Yang, 1975. "Foundation Engineering Handbook", Van Nostrand Reinhold Company, Chapters 3, 5, and 7.

[86] Wong, Wing L., 1989. "Field Performance of Welded Wire Wall", M.S. Thesis, Utah State University, Civil and Environmental Engineering.

[87] Wright, E. J. (1994). "Development In Silo Design For The Safe And Efficient Storage And Handling Of Grain", Stored Product Protection, Proceedings of the 6th International Working Conference on Stored-Product Protection, 17-23 April 1994, Canberra, Australia. CAB International, Wallingford, United Kingdom, 1994.

[88] Wu, Y. H. (1990). "Static and Dynamic Analysis Of The Flow Of Bulk Materials Through Silo", PhD. Thesis, The University of Wollongong, Australia.

[89] Xanthakos, P. P. (1991). "Ground Anchors and Anchored Structures". John Wiley and Sons, New York.

[90] Zevgolis, I., and Bourdeau, P.L. (2007). "Mechanically Stabilized Earth and Wall Abutments for Bridge Support". FHWA/IN/JTRP-2006/38. Joint Transportation Research Program, Indiana Department of Transportation and Purdue University, West Lafayette Indiana.

[91] Zhang, J.-M., Shamoto, Y., and Tokimatsu, K. 1998. "Evaluation of Earth Pressure Under Any Lateral Deformation". Soils and Foundations, 38(1): 15–33.

Biographical Information

Thomas (Tom) Patrick Taylor received a Bachelor of Science degree in Architectural Engineering from the University of Wyoming in 1990. Tom worked as a design engineering until 1995. In February 1995 he started T&B Structural Systems LLC. In February of 2007 he sold T&B Structural Systems to the Atlantic Bridge Group and T&B Structural Systems became Vistawall Systems. Tom is presently Vice President Director of Research and Development for Vistawall Systems a division of Big-R Bridge. He is a registered professional engineer in 14 states and 2 Canadian provinces. Tom's research interests are in earth structures, ground improvements, and numerical modelling. He has 20 United States and Foreign patents and patents pending that deal primarily with Earth Structures. He has developed the proprietary software program MSE-Pro that is used in the design and analysis of Mechanically Stabilized Earth Structures.